

**Controlled Release Oral Dosage
Forms Using Functional Additives
in Hot Melt Extruded
Pharmaceuticals**

Fahad Jaloud S Alqahtani

Thesis submitted to the School of Pharmacy, University of East
Anglia for the Degree of Doctor of Philosophy in Pharmacy

December 2021

Acknowledgments

My gratitude to the following people who have helped me with this journey and writing cannot be adequately expressed.

I am eternally grateful to my supervisors Professor Sheng Qi and Professor Peter Belton for their guidance, vast knowledge, motivation, continued support and encouragement in all stages of my PhD. Honestly, there are not enough words to put in here to appreciate their help and support during this journey including my illness and Covid-19 pandemic. I would like to extend my thanks to professor Axel Zeitler and Mohammed Al-Sharabi (University of Cambridge, UK), Professor Dennis Douroumis (University of Greenwich, UK) and Dr Kofi Asare-Addo (University of Huddersfield, UK) for their honourable collaborations.

Special thanks to Dr. Muqdad Alhijjaj, Dr. Janine Wilkinson, Dr. Abdessamad Kaassis, Dr. Bin Zhang, Zuzana Hlaskova, Salman Rahman, Randa Ziqlam, Chak Tam, Sherif Ismail, Ibrahim Alshehri, Arwa Ahmed, Nada Lasllom, Huda Ibrahim and Bertrand leze. I would also like to extend my sincere thanks to my brother Dr Mohammed Akbar for his support. Deep thanks to Umm Al-Qura University thorough Saudi Arabia Cultural Bureau in London for granting me this opportunity and for their financial support.

I would like also to express my grateful thanks and love to my parents, Saif, Sultan and lovely sister ‘Toto’ for their support and love. I would have not been able to complete this thesis without your unconditional support.

Declaration of authorship

I declare that the work in this thesis submitted by me for the degree of Doctor of Philosophy is my work and it is original, to the best of my knowledge, except where stated, referenced and acknowledged.

Fahad Alqahtani

Abstract

Hot melt extrusion (HME) has been widely used for producing amorphous solid dispersions (ASD). There is an extensive body of literature on the pharmaceutical applications of solid dispersions produced by HME for improving the dissolution rates of poorly soluble drugs, but most systems are either binary polymer-drug or ternary polymer-drug-surfactant mixtures. There is still limited number of studies exploring the use of low quantities of functional additives in hot melt extruded solid dispersions to (1) tune the drug release rate from the formulations (for either immediate release or controlled release applications) and (2) to increase the drug loading capacity. The aim of this project is to develop fundamental understanding and formulation strategies in order to achieve these two new capabilities. Such knowledge has excellent potential to extend the application of solid dispersions for a much wider range of products.

Firstly, to develop tuneable drug release capability of ASD produced via HME, this project used carbamazepine as the model drug and HPMCAS as the base formulation and a range of low-quantity functional additives to investigate for their abilities to alter the drug release rate of the extrudates. We developed in depth understanding of the effects of these additives on the control of internal microstructure of HME extrudates. Secondly, to develop innovative approaches to increase the drug loading of ASD without compromising physical stability, we used tolbutamide as the model drug and Soluplus as the base formulation and mesoporous silica (MPS) as the functional additive. The results indicated the potential and limitations of MPS as a functional excipient for increasing drug loading in ASD prepared by HME. In this project, all hot melt extruded ASDs were characterised using conventional techniques including DSC, MTDSC, TGA, ATR-FTIR, PXRD, SEM, EDS, X μ CT, *in-vitro* dissolution testing. Novel UV-imaging methodology was developed and performed on carbamazepine-loaded ASDs which facilitated the understand of the *in-vitro* dissolution behaviour of the ASDs.

The results of this project demonstrate the practicality of using low-quality functional additives in a single-step hot melt extrusion (HME) process to tune drug release behaviour and drug loading of ASDs which can bring new insights into the industrial applications of HME and ASDs.

Access Condition and Agreement

Each deposit in UEA Digital Repository is protected by copyright and other intellectual property rights, and duplication or sale of all or part of any of the Data Collections is not permitted, except that material may be duplicated by you for your research use or for educational purposes in electronic or print form. You must obtain permission from the copyright holder, usually the author, for any other use. Exceptions only apply where a deposit may be explicitly provided under a stated licence, such as a Creative Commons licence or Open Government licence.

Electronic or print copies may not be offered, whether for sale or otherwise to anyone, unless explicitly stated under a Creative Commons or Open Government license. Unauthorised reproduction, editing or reformatting for resale purposes is explicitly prohibited (except where approved by the copyright holder themselves) and UEA reserves the right to take immediate 'take down' action on behalf of the copyright and/or rights holder if this Access condition of the UEA Digital Repository is breached. Any material in this database has been supplied on the understanding that it is copyright material and that no quotation from the material may be published without proper acknowledgement.

Table of contents

Acknowledgments	II
Declaration of authorship	III
Abstract	IV
List of Figures	IX
List of Tables	XII
List of Abbreviations	XIII
List of Publications	XIV
Chapter 1: General introduction	1
1.1 Pharmaceutical Solid dispersion	2
1.1.1 Amorphous materials	3
1.1.2 Solid dispersion system.....	4
1.1.3 Solid dispersion preparation methods.....	8
1.1.3.1 Solvent based method	8
1.1.3.1.1 Solvent evaporation	8
1.1.3.1.2 Spray drying.....	9
1.1.3.1.3 Freeze drying	9
1.1.3.1.4 Electrospinning	10
1.1.3.2 Melting based methods	10
1.1.3.2.1 Hot melt extrusion (HME).....	10
1.1.3.2.1.1 Types of extruders.....	13
1.1.3.2.1.2 Successful extrusion requirements.....	14
1.1.3.2.1.3 Suitable materials for HME	15
1.2 Drug release approaches via HME	18
1.2.1 Immediate drug release	18
1.2.2 Modified drug release	19
1.3 Mesoporous silica applications in drug delivery	21
1.3.1 Dissolution rate enhancement	22
1.3.2 Controlled drug release via MPS	23

1.3.3 Drug loading method into MPS	24
1.3.3.1 Solvent immersion	24
1.3.3.2 Melt mixing.....	24
1.4 Objectives	25

Chapter 2: Materials and methods **26**

2.1 Materials and methods	27
2.1.1 Materials	27
2.1.1.1 Model drugs	27
2.1.1.1.1 Carbamazepine.....	27
2.1.1.1.2 Tolbutamide	27
2.1.2 Polymeric carriers	29
2.1.2.1 HMPCAS	29
2.1.2.2 Soluplus.....	31
2.1.3 Additives	32
2.1.3.1 Croscarmellose sodium.....	32
2.1.3.2 Sodium starch glycolate.....	32
2.1.3.3 Crospovidone	33
2.1.3.4 Gelucire.....	33
2.1.3.5 Maltodextrin.....	34
2.1.3.6 α -Lactose monohydrate.....	34
2.1.3.7 Mesoporous Silica.....	34
2.2 Methods	35
2.2.1 Hot melt extrusion.....	35
2.2.2 Drug loading into MPS:	36

Chapter 3: An investigation into the use of low quantities of functional additives to control drug release from hot melt extruded solid dispersions for poorly soluble drug delivery..38

3.1 Introduction	39
3.2 Materials and Methods	41
3.2.1 Materials	41
3.2.2 Preparation of hot-melt extruded (HME) filaments	41
3.2.3 Materials characterisation	43
3.2.3.1 Attenuated total reflection-Fourier transform Infrared (ATR-FTIR) Spectroscopy	43
3.2.3.2 Powder X-ray diffraction (PXRD).....	43
3.2.3.3 Differential scanning calorimetry (DSC).....	43

3.2.4 Swelling/erosion measurement of the HME extrudates during dissolution testing	43
3.2.5 UV and visible imaging of HME extrudates.....	44
3.2.6 <i>In vitro</i> drug release studies	46
3.2.7 Dissolution kinetics model fitting	47
3.3 Results and Discussion	49
3.3.1 Characterisation of binary CBZ-HPMCAS extrudates	49
3.3.2 Accelerating the drug release using low quantity additives	54
3.3.3 Sustaining the drug release using lipid additives	63
3.4 Conclusion	68

Chapter 4: An investigation into the formations of the internal microstructures of solid dispersions prepared by hot melt extrusion **69**

4.1 Introduction	70
4.2 Materials and methods	71
4.2.1 Materials	71
4.2.2 Preparation of HME filaments	71
4.2.3 Materials characterisation	73
4.2.3.1 Thermogravimetric analysis (TGA).....	73
4.2.3.2 Powder X-ray diffraction (PXRD).....	73
4.2.3.3 Differential scanning calorimetry (DSC).....	73
4.2.3.4 Scanning electron microscopy (SEM)	74
4.2.3.5 X-ray microcomputed tomography (X μ CT)	74
4.2.3.6 <i>In vitro</i> drug release studies	74
4.2.3.7 Statistical analysis	75
4.3 Results and Discussion	75
4.3.1 The formation of the interior void structure in HME extrudates	75
4.3.2 Effect of moisture contents of the raw materials	78
4.3.3 Effect of Viscosity	81
4.3.4 Effect of process parameters	89
4.3.5 Effect of porosity on drug release	92
4.4 Conclusion	95

Chapter 5: An investigation into the use of mesoporous silica for improving physical stability of amorphous solid dispersion with high drug loading **96**

5.1 Introduction	97
5.2 Materials and methods	98

5.2.1 Materials	98
5.2.2 TBA loading by MPS alone	98
5.2.3 Preparation of ASD using HME	99
5.2.4 Materials characterisation	100
5.2.4.1 Powder X-ray diffraction (PXRD).....	100
5.2.4.2 Differential scanning calorimetry (DSC).....	100
5.2.4.3 Scanning electron microscopy (SEM)	100
5.2.5 <i>In vitro</i> drug release studies	100
5.3 Results and discussion	102
5.3.1 Investigation into MPS loading capacity of amorphous TBA	102
5.3.2 Low drug loading ASDs (LD) containing TBA-MPS prepared by HME.....	105
5.3.3 High drug loading ASD containing TBA-MPS and free TBA	108
5.4 Conclusion	112

Chapter 6: Conclusion and Future Outlook **114**

6.1 General Conclusion	115
6.1.1 Using functional additives as strategy to manipulate drug release from hot melt extruded solid dispersions.....	115
6.1.2 Investigating the parameters that control and adjust void formations	117
6.1.3 Using mesoporous silica to improve the stability of amorphous solid dispersion with high drug loading	119
6.2 Future outlook	121

Bibliography **122**

List of Figures

Figure 1.1: Volume and enthalpy of the amorphous state compared to a crystal, including glassy and rubbery regions [6]	4
Figure 1.2: Illustration of SD classes based on physical structure, where C, A and M represent crystalline, amorphous and molecularly dispersed, respectively [20].....	5
Figure 1.3: Schematic representation of the HME process and feedstock transfer.....	13
Figure 1.4: Different types of HMEs. A and B are single and twin screw extruders; C and D represent the co-rotating and counter-rotating screw movement [47].....	14
Figure 1.5: Schematic representation showing the bioavailability enhancement of API using mesoporous silica.	21
Figure 2.1: DSC thermogram of (a) crystalline and (b) amorphous carbamazepine.	27
Figure 2.2: DSC thermogram of (a) crystalline and (b) amorphous tolbutamide.	28
Figure 2.3: DSC thermogram showing the glass transition of HPMCAS.....	30
Figure 2.4: Chemical structure of HPMCAS [74]	30
Figure 2.5: Chemical structure of Soluplus [124].....	31
Figure 2.6: DSC thermogram showing the glass transition of soluplus.....	32
Figure 2.7: Hot Melt Extruder of Thermo Scientific HAAKE MiniLab II.....	35
Figure 3.1: Set-up of the SDI2 for the assessment of HME filaments for the measurement of CBZ release (a), width growth (swelling) (b), custom stainless steel holder to mount HME filaments in the whole dosage cell (c).....	45
Figure 3.2: A schematic representation of the dual closed loop method for the assessment of the HME filaments in both pH 1.2 and pH 6.8 media.....	46
Figure 3.3: Calibration curves of CBZ in HCl buffer (pH=1.2) and phosphate buffer solution (pH = 6.8), respectively.....	47
Figure 3.4: DSC results of (a) the main ingredients and (b) the additives.....	50
Figure 3.5: (a) DSC; (b) PXRD; partial ATR-FTIR data within the wavenumbers of (c) 3600-2600 cm ⁻¹ and (d) 1800-600 cm ⁻¹ of the crystalline, amorphous CBZ and extrudates of CBZ-HPMCAS binary formulation.	51
Figure 3.6: The 24-hour in vitro drug release of (a) CBZ-HPMCAS-additive ternary extrudates and (b) Gelucire-containing extrudates.	52
Figure 3.7: Swelling behaviour of the extrudates in pH 6.8 buffer measured in (a) weight and (b) volume.....	53
Figure 3.8: DSC thermograms of the (a) physical mixes and (b) HME extrudates of the CBZ-HPMCAS-additive ternary formulations; (c) physical mixtures and (d) HME extrudates of Gelucire-containing formulations.....	55
Figure 3.9: PXRD patterns of (a) the CBZ-HPMCAS-additive ternary extrudates and (b) the Gelucire-containing extrudates; the partial ATR-FTIR spectra of (c) the CBZ-HPMCAS-additive ternary extrudates and (d) the Gelucire-containing extrudates.....	56

Figure 3.10: SEM images of the comparison of the cross-sections of the CBZ-HPMCAS-additive ternary extrudates and Gelucire-containing extrudates (freshly prepared by HME).	57
Figure 3.11: False coloured SDI2 images for the HME extrudates (H, H-NaSG, and HG-NaSG) obtained from the SDI2 instrument when the dissolution tests were performed in pH 1.2 for the first 2 hours and in pH 6.8 from 2-6 hours. Images depict CBZ release and swelling using UV and Vis wavelengths at 280 nm and at 520 nm, respectively.	61
Figure 3.12: Normalised swelling measurements for the HME extrudates (H, H-NaSG and HG-NaSG) in (a) pH 1.2 with a pH shift to pH 6.8 obtained from the SDI instrument at 520 nm.	62
Figure 3.13: Examples of the fitting plots that show different release kinetics: (a) Zero-order release kinetics of H; (b) zero-order release kinetics of HG-CP; (c) first-order release kinetics of H-CP	67
Figure 4.1: SEM images of the cross-sections of the samples showing the effects of additives on the void formation in the interior of the extrudates. (The additive particles are highlighted by the red arrows in each image).....	76
Figure 4.2: Cross-sections (top) and 3D visualisation (bottom) of the X μ CT images of the extrudates with additives.	77
Figure 4.3: Moisture contents of raw materials measured by TGA.....	79
Figure 4.4: Correlation between the void diameter and the moisture contents in the raw materials.	81
Figure 4.5: SEM images of the cross-sections showing the effect of drying of the raw materials on the formations of the voids.....	81
Figure 4.6: The average torque values (%) recorded during the hot melt extrusion process of the formulations (a) without and (b) with Gelucire 50/13. The data are represented as the mean \pm SD, n = 3 (**P<0.001, ** P<0.01, *P<0.05 and (***) indicates that the torque value is statistically significantly (with a P<0.001) different from the rest of the formulations in the group).	82
Figure 4.7: SEM images of the cross-sections showing the combination effect of drug loading and addition of the additive on the formation of the voids. (a) H20; (b) H30; (c) H50; (d) H-NaSG; (e) H-NaSG30; (f) H-NaSG50; (g) H-FDN.....	83
Figure 4.8: The summaries of the extrudates diameters	84
Figure 4.9: (a) DSC and (b) PXRD results of the binary extrudates with the drug loading ranging from 20-50% w/w.	85
Figure 4.10: SEM images of the cross-sections of the extrudates showing the effect of matrix polymer type and drug loading on the void formation. All formulations were additive-free (red arrows indicate the presence of possible recrystallized drug particles).	88
Figure 4.11: DSC (a and c) and PXRD (b and d) data of Sol-30, Sol-50 and EPO-30 and EPO-50.....	89
Figure 4.12: Extrudate diameters of the H30, H50, EPO 30, EPO 50, Sol-30 and Sol-50.	89
Figure 4.13: SEM images of the cross-sections of the interior structures of H-NaSG	91
Figure 4.14: The in vitro drug release (0-2 hours in pH 1.2 simulated gastric pH followed by replacement of pH 6.8 PBS as the dissolution media)	92
Figure 4.15: Void diameter change of H-CNa and HG-CNa during the dissolution process with the bottom panel showing the representative reconstructed cross-section images of the	

X μ CT data of the H-CNa and HG-CNa extrudates taken at different time intervals during the dissolution test.....	93
Figure 4.16: SEM images of the surfaces and the cross sections of the extrudates after 2 hours of the dissolution tests in pH 6.8 PBS followed by drying (the crusty texture of the surfaces is a results of salt crystallisation of the dissolution media used during drying).....	95
Figure 5.1: (a) Representative HPLC chromatograms of tolbutamide at different concentrations and (b) Calibration curve of tolbutamide in phosphate buffer solution (pH = 6.8).....	102
Figure 5.2: SEM with elemental analysis results of (a)TBA20, (b)TBA40,(c) TBA60 and (d)TBA80. The Sulphur peak is used as the indicator of excess TBA adsorbed on the surfaces of MPS particles. The elemental analysis spectra are the average values of the selected areas highlighted in red squares.....	103
Figure 5.3: (a) PXRD and (b) MTDSC results of TBA20, TBA40, TBA60 and TBA80 formulations with the detectable Tg highlighted by the arrows.	103
Figure 5.4: The <i>in vitro</i> TBA release profiles of TBA20, TBA40, TBA60 and TBA80 formulations in pH 6.8 PBS.	104
Figure 5.5: SEM and elemental analysis of LD1, LD2, LD3 and LD4 showing the absence of sulphur signal in LD1 and LD2 and the presence of the sulphur peak in LD3 and LD4 (sulphur signals are highlighted with the white arrows. The crosses are the tested points of elemental analysis and S stands for the surfaces of MPS particles and P stands for polymer areas free from MPS particles.	106
Figure 5.6: (a) PXRD patterns and (b) DSC data of LD1-4 formulations.	107
Figure 5.7: The <i>in vitro</i> drug release of the HME extrudates of LD1, LD2, LD3 and LD4 formulations in pH 6.8 PBS.	108
Figure 5.8: SEM images of the cross-sections of the interior structures of (a) HD1, (b) HD2, (c) HD3 and (d) HD4 form extrudates.....	109
Figure 5.9: (a)PXRD patterns of freshly prepared HD1, HD2, HD3 and HD4 formulations, with crystalline TBA as reference and (b) MDSC thermograms of them.	110
Figure 5.10: PXRD data of HD2, HD3 and HD4 aged under 75% RH for (a) 1 month and (b) 3 months.	110
Figure 5.11: The <i>in vitro</i> drug release of freshly prepared HD2, HD3 and HD4 formulations in pH 6.8 PBS a) being tested as intact HME extrudates and b) being tested as hard gelatine capsules filled with milled extrudates.	112
Figure 6.1: An illustration showing the potential of using functional additives to control drug release from HME formulations.....	116
Figure 6.2: A graphic illustration showing the impact of internal microstructure on the drug release of HME solid dispersion.	118
Figure 6.3: schematic illustartion of using MPS to produce ASD with high drug loading.....	121

List of Tables

Table 1.1 : Biopharmaceutical Classification System of APIs [3].....	2
Table 1.2: Classification of binary SD based on physical state of APIs and their carriers [20] ...	5
Table 1.3: List of solid dispersed marketed products, adapted from [13, 26].....	7
Table 1.4: Examples of HME pharmaceutical products in the market. Adapted from Newman, 2015.....	12
Table 1.5: List of common FDA-approved plasticisers for pharmaceutical dosage forms [45] .	17
Table 1.6: IUPAC classification of porous materials.....	22
Table 2.1: Physicochemical properties of carbamazepine and tolbutamide.	28
Table 2.2: List of HPMCAS types that soluble at different pH.	29
Table 2.3: HME parameters used in the production SD extrudates.	37
Table 3.1: List of ingredients of the HME extrudates.....	42
Table 3.2: Mathematical models for comparison of dissolution profiles.....	48
Table 3.3: Interpretation of the Korsmeyer-Peppas release exponent for cylindrical matrices and the corresponding implied drug release mechanism. Table adopted and modified from [186-192].....	48
Table 3.4: Fitting parameters of the in vitro drug release data of Gelucire-free and Gelucire-containing extrudates to(a) Zero-order, (b) First-order, (c) Higuchi and (d) Korsmeyer-Peppas.....	59
Table 3.5: Weight and volume change (%) of Gelucire-free extrudates.....	65
Table 3.6: Weight and Volume change (%) of Gelucire-containing extrudates.	66
Table 4.1: Ingredients and hot melt extrusion screw speed of the formulations investigated in this study	72
Table 4.2: Temperature settings of the extrusion process using Eurolab 16.....	73
Table 5.1: List of ingredients of the ASD formulations prepared by HME.....	99

List of Abbreviations

APIs	Active pharmaceutical ingredients
ASD	Amorphous solid dispersion
BCS	Biopharmaceutics classification system
CBZ	Carbamazepine
C_p	Heat capacity
DE	Dextrose equivalent
DSC	Differential scanning calorimetry
EC	Ethyl cellulose
FDA	Food and Drug Administration
FTIR	Fourier transform infrared spectroscopy
HME	Hot melt extrusion
HPMC	Hydroxypropyl methyl cellulose
HPMCAS	Hydroxypropyl methyl cellulose acetyl succinate
MPS	Mesoporous silica
MTDSC	Modulated temperature differential scanning calorimetry
MW	Molecular weight
PBS	Phosphate buffer solution
PEG	Polyethylene glycol
PLGA	Poly(lactic-co-glycolic acid)
PM	Physical mixture
PVP	Polyvinyl pyrrolidone
PVP-VA	Polyvinyl pyrrolidone vinyl acetate
PXRD	Powder X-ray diffraction
RH	Relative humidity
RT	Retention time
SD	Standard deviation
SEM	Scanning electron microscopy
TBA	Tolbutamide
T_g	Glass transition
TGA	Thermogravimetric analysis
T_m	Melting temperature
UV-VIS	Ultraviolet-visible
XμCT	X-ray micro computed tomography

List of Publications

[1] F. Alqahtani, P. Belton, A. Ward, K. Asare-Addo, S. Qi, An investigation into the use of low quantities of functional additives to control drug release from hot melt extruded solid dispersions for poorly soluble drug delivery, *International Journal of Pharmaceutics*, 579 (2020) 119172.

[2] F. Alqahtani, P. Belton, B. Zhang, M. Al-Sharabi, S. Ross, M.S.H. Mithu, D. Douroumis, J.A. Zeitler, S. Qi, An investigation into the formations of the internal microstructures of solid dispersions prepared by hot melt extrusion, *European Journal of Pharmaceutics and Biopharmaceutics*, 155 (2020) 147-161.

[3] F. Alqahtani, P. Belton, S. Qi, An investigation into the use of mesoporous silica for improving physical stability of amorphous solid dispersion with high drug loading. (*submitted*).

General introduction

Chapter 1

1.1 Pharmaceutical Solid dispersion

Low water solubility of active pharmaceutical ingredients (APIs) for oral administration is a current major issue that can compromise drug absorption and efficacy in the patient, leading to low bioavailability. It is estimated that around 40% of drugs on the market, 75% of drug candidates on the development phases and nearly 90% of new chemical entities have poor water solubility [1]. Therefore, the Food and Drug Administration (FDA) introduced the Biopharmaceutical Classification System (BCS) as a guide for researchers to determine which drug class or group of physiochemical properties is appropriate to be a model drug [2]. The BCS categorises the APIs into four classes depending on their solubility and membrane permeability, which is described in the following table.

Table 1.1 : Biopharmaceutical Classification System of APIs [3]

Class I	Class II
<ul style="list-style-type: none"> • High Solubility. • High Permeability. 	<ul style="list-style-type: none"> • Low Solubility. • High Permeability.
Class III	Class IV
<ul style="list-style-type: none"> • High Solubility. • Low Permeability. 	<ul style="list-style-type: none"> • Low Solubility. • Low Permeability.

Based on the BCS, Class I APIs have a high solubility and permeability; hence, their bioavailability depends on the gastric residence time. Class II compounds have sufficient permeability but low aqueous solubility, causing the dissolution rate to be the limiting step. It is important to highlight that solubility is the total amount of drug that can dissolve. A poorly soluble drug could rapidly reach its solubility limit. It's probable that low solubility drugs tend to dissolve slowly because the thermodynamic driving force to go into solution is weak. Class III compounds have sufficient solubility but poor permeability; therefore, the absorption rate will be determined by passage through the gastrointestinal membrane. However, Class IV compounds have both low solubility and permeability, and the rate-limiting step will differ case by case [4]. Furthermore, it has been claimed that more than 40% of APIs belong to Class II and IV due to their poor aqueous solubility [5]. For example, danazol has a solubility of 1 µg/ml at gastric pH and the usual dose of danazol is 200 mg/day; hence, it requires roughly 200 L of aqueous volume to completely dissolve [6].

Consequently, several technological strategies have been reported to address the solubility issues. They are reliable, reproducible, scalable approaches and have been investigated intensively in research and development. Examples are particle size reduction [7, 8], salt formation [2, 9], prodrug formation [10], nanosuspension [11], polymorph modification [12] and solid dispersion (SD). Amorphous solid dispersion (ASD) has been considered one of the most promising techniques to enhance the solubility profile of poorly soluble APIs [5, 13, 14]. The technique selection depends on the physiochemical properties of APIs, carrier characteristics and the desired dosage form [5]. Amorphous materials possess a disordered structure with no long-range order, opposite to the organised structure of crystalline materials. The internal disordered structure of amorphous materials provides high mobility properties to the molecules, which can lead to increased solubility properties but also to low physical and chemical stability.

1.1.1 Amorphous materials

As mentioned above, amorphous materials have a disordered structure as well as increased volume and free energy that provide increased solubility and faster dissolution properties than crystalline materials. The possible pharmaceutical implications and advantages of ASDs, such as bioavailability enhancement of poorly water-soluble drugs, will be covered later in this literature review. Transformation from a crystalline to an amorphous form involves various physical changes and thermodynamic transitions (Figure 1.1) [6, 13]. First, the crystalline material is heated to melting temperature (T_m) until the material experiences a physical change from an organised to a disorganised structure, which involves heat transfer (first-order transition). The material is then rapidly cooled to achieve a super-cooled liquid state. One of the main characteristic parameters that determine the conversion of a molten material from a rubbery state to a solid, glassy state is defined as the glass transition temperature (T_g) (second-order transition), which forms with further cooling. After T_g is reached, the system is at a non-equilibrium phase known as the glassy state [15]. In the pharmaceutical field, amorphous solids have been divided into two types: pure amorphous materials and ASDs. Both can increase solubility and dissolution rate but are microscopically different. The amorphous materials are characterised by lack of long-range order and the molecular units are distributed randomly in the matrix; hence, the packing is changed in such a way that weakens the attractive forces (energy) among drug molecules and reduces the energy barrier, allowing APIs to dissolve into aqueous solution and requiring less activation energy in the process.

However, in ASD, amorphous drug particles are dispersed in molecular or non-molecular level within carrier, where the crystal order is disrupted [16, 17].

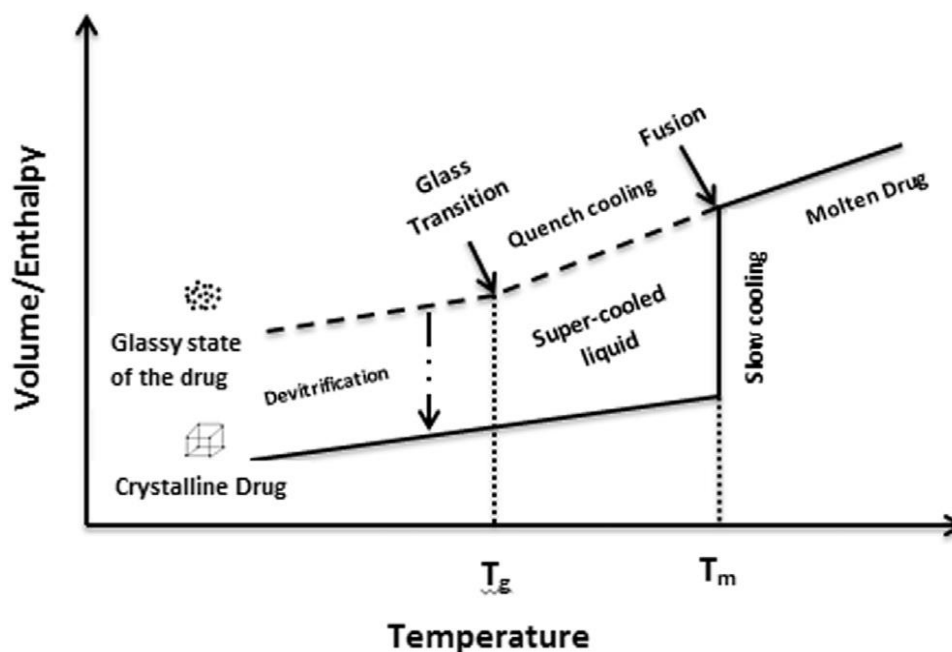


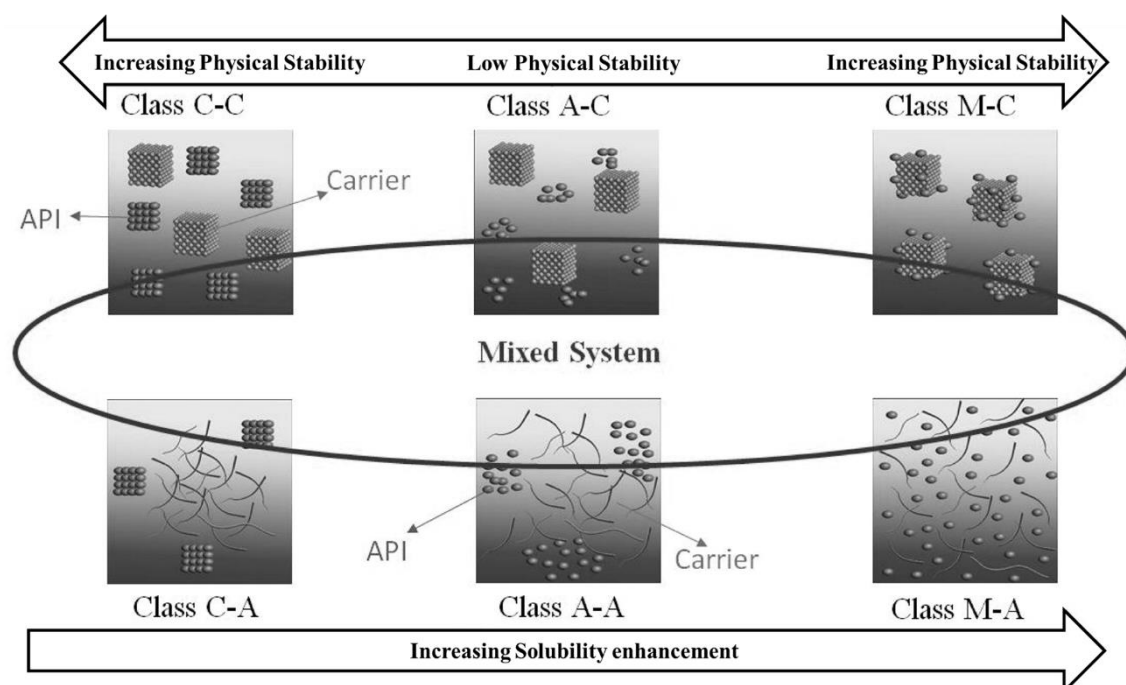
Figure 1.1: Volume and enthalpy of the amorphous state compared to a crystal, including glassy and rubbery regions [6]

1.1.2 Solid dispersion system

Sekiguchi and Obi started in 1961 the first SD using urea as a carrier mixed with sulfathiazole to make a eutectic mixture. SD was primarily defined as the process of mixing a water-soluble, inert carrier with a hydrophobic compound to generate eutectic mixtures [18]. Currently, after continuous innovations in this field, it can be described as the science of dispersing one (or more) APIs into an inert matrix or carrier at solid state and molecular level in order to obtain a highly soluble formulation and an enhanced release profile in an immediate, controlled or targeted manner. In terms of classification, Chiou and Riegelman [19] categorised the SD into six groups based on two parameters: (1) API physical structure (amorphous or crystalline) and molecular arrangement, in which APIs are molecularly dispersed in a single phase within the carrier; (2) the physical state and molecular arrangement of the carrier, which is summarised in Table 1.2 [19, 20].

Table 1.2: Classification of binary SD based on physical state of APIs and their carriers [20]

Type	API	Carrier	Stability	Solubility
Eutectics (C-C)	Crystalline	Crystalline	High	Moderate
Amorphous precipitate (A-C)	Amorphous	Crystalline	Low	High
Glass suspension (C_A) (A-A)	Crystalline	Amorphous	High	Moderate
	Amorphous	Amorphous	Low	High
Glass solution (M-A)	Molecular dispersed	Amorphous	High	High
Solid solution (M-C)	Molecular dispersed	Crystalline	High	High

**Figure 1.2: Illustration of SD classes based on physical structure, where C, A and M represent crystalline, amorphous and molecularly dispersed, respectively [20]**

Concerning the eutectic mixture (C-C), initially the crystalline API is blended and then melted with a hydrophilic crystalline carrier to generate a mixture that undergoes a rapid-cooling process. Hence, the drug and the polymer crystallise together to form the eutectic mixture. Goud et al [21] produced a eutectic mixture of curcumin and nicotinamide with a 1:2 ratio, which exhibited a dissolution rate ten-fold faster than the crystalline curcumin. The crystalline form is more stable than the amorphous one and has a larger surface area of fine crystals[13]. In addition, it has been reported that the hydrophilic feature of mannitol improved wettability of nifedipine which contribute to enhancing the dissolution rate [22]. Nevertheless, it can be problematic if one of the melted materials begins to

recrystallise before the other during the cooling process. Consequently, the mixture will be immiscible when phase separation occurs. It has been reported that the dispersion of crystalline APIs could lead to recrystallisation, limited miscibility and interaction between the polymeric carrier and APIs in solid state [20]. Despite the thermodynamic stability of the eutectic mixture, the applicability of eutectic SD was not broad in pharmaceutical industries; it is a time-consuming process and the difficulty of generating a specific eutectic composition for various APIs [23]. Class II (A-C) describes the precipitation of an amorphous drug in crystalline matrix to form two phases, which can be an issue due to the possibility for recrystallisation of the amorphous form. In the glass suspension, it exhibits improved stability and diffusivity within the suspension. In addition, the drug–polymer interaction via H-bonding and van der Waals forces can be a key factor in preventing the precipitation and physical stabilisation. However, it consists of two separate phases; therefore, the tendency to crystallise still exists even in the case of amorphous carriers, which are commonly formed when the drug has a high melting point or limited carrier solubility[5]. The molecular dispersions (M-C and M-A) are the most broadly desired methods due to their numerous advantages, including dissolution behaviour improvement and physical stability [24]. Numerous techniques have been established to produce an efficient SD by solvent evaporation, melting and precipitation, which can disperse the drug as amorphous particles, crystalline particles or even as separated molecules in an amorphous or crystalline carrier [20, 25]. The distinctive features of SD are represented in the enhancement of wettability and porosity, particle size reduction and promotion of the change from a crystalline to an amorphous state, therefore improving aqueous solubility [5]. In addition, the drug–carrier interaction can limit the agglomeration of drug particles that occurs during the dissolution process and storage [18]. Despite the large amount of research in SD and the promising results over the last three decades, the number of SD products on the market is still low (see Table 1.3). This indicates some scale-up issues and that the states of amorphisation and crystallisation may be the main reason for the instability during the manufacturing process and storage. Therefore, many researchers claim that in-depth knowledge is the key factor to tackling these drawbacks, including understanding drug and carrier properties, release mechanisms, preparation and characterisation methods [5, 15, 25].

Table 1.3: List of solid dispersed marketed products, adapted from [13, 26]

Marketed product	API	Polymer	Dispersion method
Afeditab®	Nifedipine	Poloxamer	Melt extrusion
Belsomra®	Suvorexant	PVP-VA	Melt extrusion
Certican®	Everolimus	HPMC	Melt or spray drying
Cesamet®	Nabilone	PVP	Melt extrusion
Delstrigo®	Doravirine and lamivudine, tenofovir	HPMCAS	Spray drying
Epclusa®	Sofosbuvir/velpatasvir	PVP-VA	Spray drying
Fenoglide®	Fenofibrate	PEG	Spray melt
Gris-PEG®	Griseofulvin	PEG	Melt extrusion
Harvoni®	Ledipasvir/sofosbuvir	PVP-VA	Spray drying
Incivek® and Incivo®	Telaprevir	HPMCAS	Spray drying
Intelence®	Etravirine	HPMC	Spray drying
Isoptin SRE-240®	Verapamil	HPC/ HPMC	Melt extrusion
Kalydeco®	Ivacaftor	HPMCAS	Spray drying
Kaletra®	Lopinavir and ritonavir	PVP VA	Melt extrusion
LCP-Tacro	Tacrolimus	HPMC	Melt granulation
Mavyret™	Glecaprevir/pibrentasvir	PVP VA	Melt extrusion
Nimotop®	Nimodipine	PEG	Spray drying/ fluid bed
Nivadil®	Nilvadipine	HPMC	Spray drying/ fluid bed
Norvir®	Ritonavir	PVP VA	Melt extrusion
Noxafil®	Posaconazole	HPMCAS	Melt extrusion
Onmel®	Itraconazole	PVP VA	Melt extrusion
Orkambi®	Lumacaftor/ivacaftor	HPMCAS	Spray drying
Prograf®	Tacrolimus	HPMC	Spray drying/ fluid bed
Rezulin®	Troglitazone	PVP	Melt extrusion
Sporonox®	Itraconazole	HPMC	Spray layering

Symdeko®	Tezacaftor/ivacaftor and ivacaftor	HPMC/HPMCAS and HPMCAS	Spray drying
Venclexta™	Venetoclax	PVP-VA	Melt extrusion
Viekira XR™	Dasabuvir/ombitasvir/paritaprevir/ritonavir	PVP-VA	Melt extrusion
Zelboraf®	Vemurafenib	HPMCAS	Antisolvent precipitation
Zepatier®	Elbasvir/grazoprevir	HPMC	Spray drying
Zortress®	Everolimus	HPMC	Melt or spray drying

1.1.3 Solid dispersion preparation methods

There are two main techniques that have been used intensively to prepare SD formulations are the solvent and melting based methods. The solvent evaporation method will be described briefly in the next sections. The HME will be introduced in full details as it is the main technique used in this project.

1.1.3.1 Solvent based method

1.1.3.1.1 Solvent evaporation

In the solvent evaporation method, SD is acquired via evaporation of a volatile solvent from the solution composed of drug and carrier to obtain a solid matrix. The main advantage of this technique is its capability to prevent the main issue of the melting method: the thermal decomposition of heat-unstable APIs and carriers. This is implemented through techniques that use low process temperature such as spray drying, freeze drying and electrospinning. In addition, it has been reported that the solvent evaporation method can generate a more porous final product than the melting method, hence obtaining a more favourable SD dissolution rate [18, 27]. This method can use different types of solvents that have a low boiling point such as water, methanol, ethanol, chloroform, acetone and mixtures thereof; both the API and carrier should sufficiently dissolve in the solvent [20]. Furthermore, surfactants such as Tween® 80 and sodium lauryl sulphate play an important role in increasing the solubility of the drug and carrier in solvent [5]. However, the solvent evaporation method presents numerous drawbacks. The first is that solvent residuals that remain after evaporation might cause toxicity and change in the physical properties of the SD. It has been claimed that water residual can decrease the T_g due to its plasticising feature and induce the phase separation, therefore increasing molecular motion of components and recrystallisation. Other disadvantages

include high expense due to the extra demand on facilities for solvent elimination and safety procedures to protect against explosions [28].

1.1.3.1.2 Spray drying

The spray drying technique is most used evaporation method in SD manufacturing since it provides a fast solvent removal, resulting in rapid transformation of matrix solution to solid API-carrier particles. The API-carrier solution is pressurised via a pump system and atomised into droplets with large surface areas, then sprayed into a heated gas stream to remove the solvent within a short time [5]. The critical quality attributes, such as the sprayed particle size, can be modulated by selecting the atomiser and atomisation parameters (nozzle diameter, gas pressure and solution composition) to meet the required droplet size. Occasionally, the SD produced by spray drying creates a molecular amorphous dispersion; hence, drug solubility and dissolution rate are considerably improved [13]. Furthermore, the numerous advantages of spray drying, such as the feasibility of continuous manufacturing, good uniformity, particle size and scalability, makes this technique more favourable among formulation scientists [20, 29].

1.1.3.1.3 Freeze drying

Freeze drying or lyophilisation is considered a promising method in SD. It is composed of two processes: freezing and solvent sublimation. The fundamental process can be described as immersing the drug-carrier matrix into liquid nitrogen before the solution is then frozen and lyophilised. The key advantage is that the drug is incorporated into the stabilising matrix without extreme mechanical force or thermal stress, which can efficiently reduce the risk of phase separation and degradation [30, 31]. In terms of drawbacks, over the sublimation process some organic solvents do not stay frozen due to their low freezing temperature, and this can affect the stability of the mixture. To offset this, there are two common techniques: spray freeze-drying (SFD) and ultra-rapid freezing (URF). These methods can enhance the efficiency of dispersion and avoid separation problems. In SFD the drug-carrier solution is subjected to liquid nitrogen spray or cold air, after which the frozen droplets will be lyophilised. This method controls the particle size, surface area and contact of the cooling agents. Hence, the rapid vitrification decreases the feasibility of phase separation [32]. Furthermore, SFD produces an amorphous API because the recrystallisation is inhibited by the rapid freezing rate. Van Drooge et al. [30] used SFD for generating a stable SD with up to 30% drug

loading, as well as being suitable for inhalation. However, URF is applied via spraying matrix solution on a solid cryogenic substrate that has thermal conductivity. The frozen material is then collected, and the solvent is withdrawn by lyophilisation. As the cooling rate is extremely rapid, the molecular arrangement into crystallisation is minimised or entirely prevented, resulting in an amorphous state of material [5].

1.1.3.1.4 Electrospinning

The electrostatic spinning technique is one of the main techniques that can produce an SD in a nanoscale formulation. The basic principle of electrospinning is based on applying electrostatic charge to a stream of polymer solution or melt in the presence of a high-voltage electric field. The spinneret is filled with the drug–polymer solution and connected to the microsyringe pump. High voltage is then applied to the needle tip, causing instability within the drug–polymer solution as a result of the induction of charges on the polymer droplet. Then, the reciprocal repulsion of charges generates forces that oppose the surface tension, and the droplets flow in the direction of the electric field [33]. Subsequently, due to the acceleration throughout the high-voltage electrical field, the solvent rapidly evaporates and the solid particles fall into the collector [34]. Properties of the filaments are influenced by numerous parameters: solution dielectric constant, solution surface tension, electrical field power, feeding rate and tip-to-collector distance, as well as some external parameters such as humidity, temperature and air velocity in the spinning chamber. The most attractive feature in this technique is the generation of high surface area per unit of mass, which enhances the rapid and effective solvent evaporation and the formation of ASD. Thus, nanosizing and amorphisation are the critical factors that improve the dissolution profile of poorly soluble APIs [35, 36].

1.1.3.2 Melting based methods

1.1.3.2.1 Hot melt extrusion (HME)

The term extrusion is defined as the process of feeding materials through an orifice of well-defined diameter. Hot melt extrusion (HME) is a process that rotates a screw to blend while softening materials at a high temperature through a die opening accompanied by a downstream cooling step [13]. It was invented by Joseph Brama at the end of the eighteenth century for producing lead pipes. In 1930, it was applied to plastic and food manufacturing. In the food industry, extrusion cooking is used to produce various types

of food such as cereals, pasta and snacks. Historically, El-Egakey et al. [37] launched the first melt extrusion technique in pharmaceutical manufacturing, and the first sustained release application of HME was developed by Follonier et al [38].

In recent decades, HME has emerged as a powerful processing technique in developing amorphous dispersion of APIs into polymeric carriers to generate formulations with enhanced solubility and controlled or extended-release profiles. HME possesses broad applications for oral dosage forms as an SD technique, such as tablets, capsules and transdermal routes of administration. Through the HME process, one or more APIs are mixed and melted with excipients within the extruder throughout multiple fundamental steps, i.e. mixing, melting, homogenising and shaping [39, 40]. HME provides several advantages over the traditional SD techniques including: (a) producing a molecular SD as a method to enhance the solubility and bioavailability of poorly water-soluble drugs; (b) it is solvent free, resulting in absence of solvent residuals in the final product for formulation; (c) it features time-saving techniques with decreased processing time and fewer production steps; (d) it offers continuous and efficient operation with a controlled and manageable process; (e) the formulation stability is improved at different moisture levels and pH; (f) it possesses broad capabilities to develop fast, sustained and controlled-release products [40, 41]. Nevertheless, there are a few drawbacks outlined as follows: (a) it requires a high processing temperature, which can limit HME application in thermolabile compounds, making it inappropriate for high-heat-sensitive materials such as protein; (b) there are an inadequate number of heat-stable polymers that can be used in HME; (c) polymers and excipients with high flowability are frequently required [41].

Table 1.4: Examples of HME pharmaceutical products in the market. Adapted from Newman, 2015.

API	Polymer	Dosage form	HME purpose
Dapivirine + maravirov	EVA	Implant	Shape
Etonogesterol + ethinyl estradiol	EVA	Implant	Shape
Goserelin acetate	PLGA	Implant	Shape
Etonogesterol	EVA	Implant	Shape
Dexamethasone	PLGA	Implant	Shape
Lopinavir + ritonavir	PVP-VA	Oral tablet	Amorphous dispersion
Ritonavir	PVP-VA	Oral tablet	Amorphous dispersion
Validagliptin + metformin hydrochloride	HPMC	Oral tablet	Melt granulation
Azithromycin	HPMC	Oral tablet	Taste masking
Griseofulvin	PEG	Oral tablet	Crystalline dispersion
Troglitazone	PVP	Oral tablet	Amorphous dispersion
Hydrophone	EC+ERS	Oral tablet	Controlled release
Posaconazole	HPMCAS	Oral tablet	Amorphous dispersion

HME is considered developed and versatile engineering technology. Numerous parameters, for example, temperature, residence time, process speed and torque, can be controlled during the processing time, which improves the critical quality attributes of the pharmaceutical matrix. Typically, the HME equipment encompasses a few main parts, including a control unit, hopper, steel barrel with one or more heating zones, screws for extrusion, and a die attached to the end to terminate the extrudate with shape. The extrusion process can be classified into four procedures as follows (Figure 1.3): (1) The extruder is fed through the hopper; (2) the materials are subjected to melting, mixing, grinding and homogenising by means of screws; (3) the liquefying matrix flows through the die; (4) the filament is discharged from the die [39, 42, 43]. Moreover, there are one or two screws located in the stationary cylindrical barrel that can rotate in two directions: counter-rotating or co-rotating [44]. Therefore, the barrel containing the screws is crucial to the HME technique, since they control temperature and pressure application on the materials and ensure they are sufficiently mixed and transported continuously through the barrel. Furthermore, the shearing forces of the screws and temperature provided by this heat generate a high energy for melting. Afterward, downstream processes can be applied to the final extrudates, such as milling into powder or cutting into pellets using a pelletiser [13].

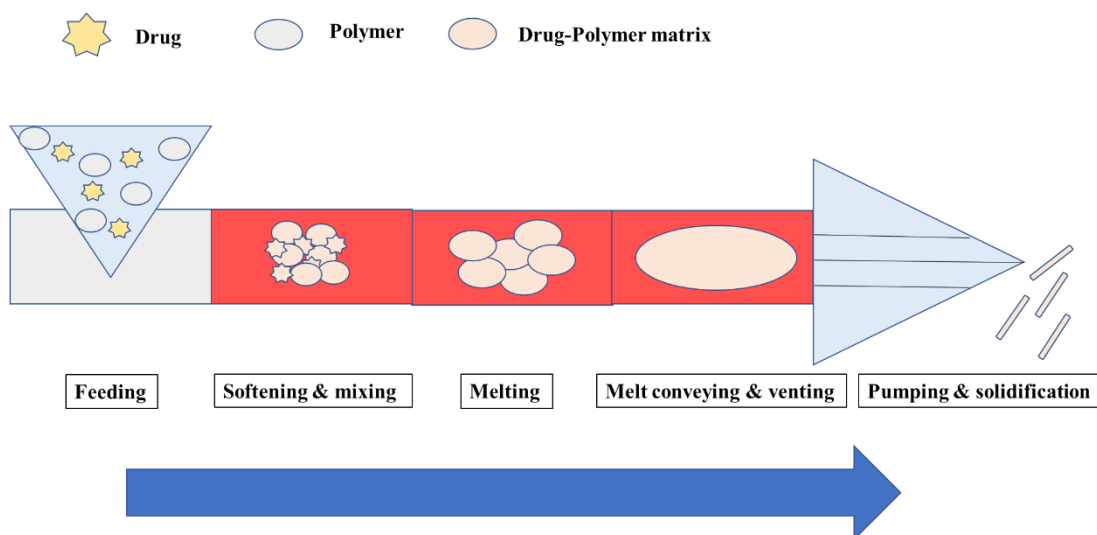


Figure 1.3: Schematic representation of the HME process and feedstock transfer.

1.1.3.2.1.1 Types of extruders

Currently, there are various designs of pharmaceutical melt extruders: single, twin and multiple-screw extruders, based on the number of screws within the barrel. The single screw extruder (SSE) is a relatively simple engineering design, consisting of one screw rotating continuously within a barrel, and providing the proper feeding, mixing and quality of melt as well as generating enough pressure for extrusion. The energy of the heaters and shear force caused by the screw causes the melt mixture to pump into the die. Due to the simplicity of its design, ease of maintenance and low price, it is a reasonable choice for extruding non-complex formulations like simple binary and ternary extrudates. However, a number of issues have been highlighted related to SSEs, such as insufficient pressure compression of dispersed particulates during melting, which leads to formation of agglomerates and inadequate mixing, making the material transport less reliable [40, 43, 45, 46].

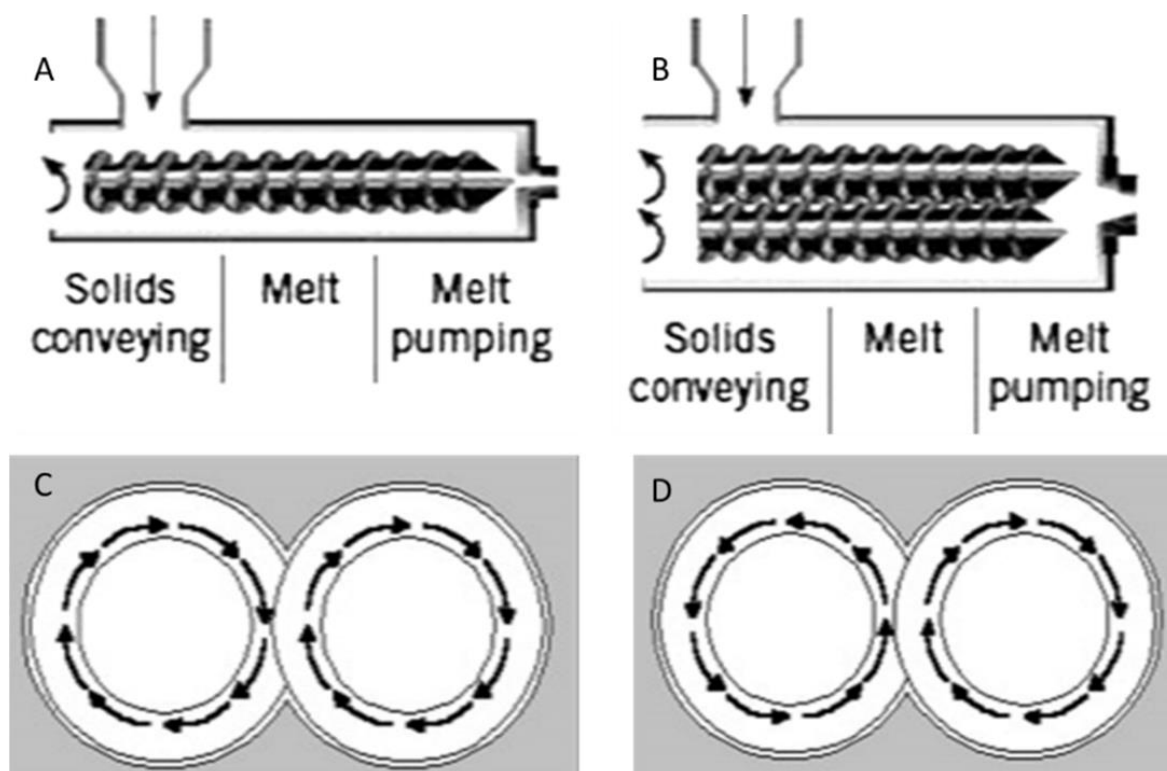


Figure 1.4: Different types of HMEs. A and B are single and twin screw extruders; C and D represent the co-rotating and counter-rotating screw movement [47]

Depending on the design of the screws within the barrel, there are two types of twin extruders, which are either counter-rotating (moving in opposite directions) or co-rotating (moving in the same direction), as seen in Figure 4. Both have noticeable advantages over the SSE. For example, the parallel alignment of two screws prevents the materials from adhering to the screw and contributes to efficient mixing. Furthermore, the processing materials have shorter extruding time and less exposure to overheating. Compared with the counter-rotating extruder, the co-rotating twin extruders can generate increased production rates as the rotational speed is high, providing proper mixing and solid transport and minimising air entrapment [44, 46].

1.1.3.2.1.2 Successful extrusion requirements

There are several requirements that should be considered to achieve successful extrudate production [16, 48]:

1. The raw materials should be pure and safe.
2. The raw materials should possess the ability to be melted and softened easily and solidify rapidly after the extrusion.
3. The mixture to be used should have excellent flowability within the hopper during the feeding process.

4. Uniform feeding rate is a critical factor to maintain the pressure at the compression and metering zones.
5. In the melting region, the temperature should be in the range of 15–60°C above the T_g of the amorphous polymer and the melting point of the semicrystalline polymer.
6. The polymers to be extruded should have high thermal conductivity and low melt viscosity.

1.1.3.2.1.3 Suitable materials for HME

For pharmaceutical materials to be processed by HME, they should have a high capacity to be mixed and deformed, as this generates a molecular interaction between the API and excipients. Deciding which API, meltable carriers and other functional excipients to use is one of the most significant steps during the HME process. Thermal stability of the individual compounds is a prerequisite for the process; however, in the case of heat-sensitive APIs, HME requires selection of suitable polymers that can be applied at low temperature extrusion in order to avoid the thermal degradation of the API [44, 49, 50].

1.1.3.2.1.3.1 Carrier (polymer)

The starting point of the HME process is the incorporation of a drug–polymer binary mixture prior to using multicomponent mixtures. Therefore, large numbers of polymeric excipients can be included in the HME process. In terms of SD for poorly soluble drugs, the polymer needs to be hydrophilic and able to form an intermolecular interaction with API as well as stabilising the amorphous state of APIs during manufacturing and storage [13, 45]. Moreover, the key physical property of polymers employed in HME is melt viscosity, thus it is essential that the flowability created by heating (thermoplastic behaviour) and shearing force (thixotropic behaviour) has the capability to offer consistent movement of the mixture throughout the extruder. Also, the drug–polymer miscibility, drug release profile and route of administration are all key factors for selecting carrier materials. Regarding the processing temperature, the melting and T_g of the drug and polymer can create a window for processing temperature as well as number of important considerations, such as adequately reducing viscosity and dissolving or solubilising the API in a polymer while avoiding the chemical degradation [51]. Hence, it is common to choose process temperatures 20–50°C above T_g . Crowley et al [45] listed a number of polymers used in HME applications; therefore, from a commercial

viewpoint, for pharmaceutical products manufactured by HME or SD it can clearly be seen that the most prominent polymers are as follows: (1) Hydroxypropyl methylcellulose acetate succinate (HPMCAS), (2) polyvinyl-pyrrolidone (PVP), (3) polyethylene oxide, (4) polyethylene glycol and (5) methacrylates (Eudragit®) [45, 50].

1.1.3.2.1.3.2 Active Pharmaceutical Ingredients (APIs)

The majority of drug products are manufactured in a crystalline state in order to increase the physical and chemical stability. However, this results in a poor water solubility and polymorphic changes. Therefore, to overcome these drawbacks, the pharmaceutical materials may be prepared in an amorphous state through SD techniques, which is still under development, and so far there are only 13 pharmaceutical products on the market (Table 1.4). There are important criteria to selecting suitable APIs for producing an HME stable amorphous formulation such as plasticisation and drug loading. The plasticisation property of APIs is a key consideration used to control the extrusion process. Drugs such as Indomethacin [52], guaifenesin [53] and ibuprofen [54] have been widely reported in literature. Indomethacin, guaifenesin and ibuprofen show a clear plasticizing effect on Eudragit RL PO, Eudragit L100-55 and Kollidon SR, respectively. In addition, the drug loading percent plays an important role in extrudate stability and processability. However, the risk of material recrystallisation still exists at higher drug loading levels; therefore, many researchers use a ternary mixture by adding one polymer or plasticiser to the formulation to improve extrudability and prevent crystallisation. For example, Alshahrani et al. (2015) added HPMCAS to Soluplus®-CBZ formulation using various drug loadings of 20–40%, and they observed that the dissolution rate was enhanced and crystallisation was inhibited.

1.1.3.2.1.3.3 Plasticisers

Since scientists and formulators started HME processing, there have been numerous obstacles encountered during result processing; for example, high processing temperature and polymer melt viscosity [42]. Therefore, plasticisers have been introduced in the pharmaceutical arena, which are a low molecular weight compound capable of providing functions such as, (a) lowering the processing temperature and torque, (b) being able to control drug release from the polymeric matrix and (c) improving the physical and mechanical properties of the used polymer [45]. In more detail, the plasticiser can decrease the T_g and enhance polymer flow below degradation temperature by increasing

the free volume between polymer chains, causing less energy to be needed for molecular mobility [55].

Table 1.5: List of common FDA-approved plasticisers for pharmaceutical dosage forms [45]

Type	Example
Citrate ester	Triethyl citrate Tributyl citrate Acetyl triethyl citrate Acetyl tributyl citrate
Fatty acid ester	Butyl stearate Glycerol monostearate Stearyl alcohol
Sebacate ester	Dibutyl sebacate
Phthalate ester	Diethyl phthalate Dibutyl phthalate Dioctyl phthalate
Glycol derivatives	Polyethylene glycol Polypropylene glycol
Other	Triacetin Mineral oil Castor oil

Furthermore, Zhu et al [56] investigated the plasticising effect of triethyl citrate (TEC) on various HME extrudates that contained diltiazem, chlorpheniramine and indomethacin as APIs, Eudragit® RSPO and Eudragit® RD 100, and diltiazem with Eudragit® RS3D for coating dispersion. Since then, it has been found that the drug release of chlorpheniramine and diltiazem increased, with a rise in TEC levels of the extrudates, whereas in the coating dispersion, the drug release declined with increasing TEC amounts due to the coalescence of polymer particles.

However, few studies have demonstrated the use of surfactant in HME as a plasticiser and solubility enhancer, and few have shown associated limitations of traditional plasticisers such as toxicity, moderate solubility in water and low boiling points. Ghebremeskel et al [57] used different types of hydrophilic surfactants such as Tween® 80 and docusate sodium. This study has shown the promising applicability of Tween® 80 and docusate sodium as effective plasticisers and solubilisers.

1.2 Drug release approaches via HME

Recently, HME has been earning an enormous amount of interest, as a number of its newer advantages are being examined and applied toward the field of pharmaceutical research and development. Currently, several studies have been performed for different applications with various dosage, form, size and shape. HME has demonstrated its capability in generating a variety of solid oral dosage forms, affording the flexibility to manipulate drug release as needed [43, 58].

1.2.1 Immediate drug release

As reported in the literature, HME can be used for producing immediate release formulations that can dissolve > 85 % of API within 30 minutes by employing its continuous manufacturing platform and its essential contribution to solubility enhancement [45, 49, 58-60]. It has also been utilised for successful manufacturing of semi-solid dosage forms [61, 62]. HME has been used for producing crystalline solid dispersions (CSDs) and ASDs; both systems induce solubility enhancement and control the drug release profile [42]. CSDs are systems in which the API is crystalline and suspended in the amorphous matrix. The important conditions for producing CSD include the API being completely immiscible with the carrier and that the processing temperature should be lower than the T_m of the API [46, 63]. Thommes et al [63] illustrates an extrusion-based approach to improve the dissolution rate of poorly soluble drugs (griseofulvin, spironolactone and phenytoin) using mannitol, which is highly water-soluble. The HAAKE MiniLab twin screw extruder has been employed to form an intimate mixture of the crystalline APIs crystalline excipients at 160°C (below the T_m of APIs). The resulting product displayed a two-fold enhancement in dissolution rate as opposed to pure API, and improved thermodynamic stability as compared to pure, amorphous APIs [63]. This approach is beneficial in cases where the API does not form proper glass or it is difficult to stabilise the amorphous drug. Excipients for this approach should be highly water soluble, able to recrystallise rapidly and should not have a T_m less than the API [46].

Another way of producing immediate release formulations via HME is the co-crystal system. Liu et al [64] describe the process of utilising HME of carbamazepine nicotinamide co-crystal using different polymeric carriers such as Kollidon® VA 64 and Soluplus®. Melt extrusion is performed with the twin screw HAAKE Minilab II at 160°C at 30 RPM. A single melting peak at 160°C is shown in the thermograph, which confirms the co-crystal formation. Compared with the CBZ-polymer ASDs, the final CBZ-NIC polymer extrudates demonstrated an improved dissolution rate and stability. This approach is useful in situations where the poorly soluble API degrades at elevated temperatures.

Orally disintegrating tablets (ODTs) have been gaining attention by many scientists and pharmaceutical companies. It has been patented ODTs by dry blending paracetamol with sugar alcohols such as mannitol, sorbitol and xylitol and then melt-extruding the mixture to a temperature above the melting points of the sugars. Subsequently, the extrudates are subjected to milling and then mixing with other excipients to be compressed as tablets [65]. In addition, a semi-solid capsule containing APIs prepared by HME is another application used to produce immediate release formulations. Sun et al. [66] prepared what was initially an SD incorporating nimodipine, Eudragit® E100 and Plasdone® S630 using a twin screw extruder. Later, the resultant extrudate was successfully dispersed into a semi-solid system containing PEG 400, then encapsulated into HPMC capsules. The study showed the advantageous combination of an SD technique and semi-solid filling, providing an immediate release profile and preventing recrystallisation.

1.2.2 Modified drug release

Modified release is a term that refers to formulations wherein the release and the release site are manipulated using polymers. There are many types of modified release, such as sustained-release [67-70], delayed-release and targeted-release formulations [71, 72].

Developing extended (sustained or controlled) release formulations using HME has been extensively performed in the past decade. Sustained release can be achieved by developing a matrix-based system (APIs uniformly dispersed in a rate-controlling polymeric matrix) or core-based controlled release (APIs trapped in the core with a rate-controlling polymeric coat). Sustained-release formulations can minimise frequent daily dosing and reduce the side effects resulting from drug fluctuation in the plasma. In addition, HME can be beneficially applied to manipulate the release rate of highly water-

soluble APIs by extruding the API-polymer at a temperature lower than API T_m . Dierickx's group developed a multilayer dosage form (core/coat) using co-extrusion technology. The model drugs were metoprolol tartrate as the sustained-release core and hydrochlorothiazide as the immediate-release coat. This study shows that a combination of polyethylene oxid (coat) and polycaprolactone (core) was successfully co-extruded with better control over the extrusion process. DSC and PXRD displayed that hydrochlorothiazide was dissolved in the polyethylene oxid, whereas metoprolol tartrate remained crystalline. Also, hydrochlorothiazide was completely released in less than 30 minutes, whereas metoprolol tartrate displayed sustained release over 24 hours[73].

Delayed-release systems usually have a lag time, after which they may follow sustained or immediate-release kinetics. Enteric-coated and taste-masked formulation products are a classic example of delayed-release systems. In terms of delayed release, polymers that possess time dependant and pH dependant dissolution are the required choice for delaying the release of an acid-labile API. HPMCAS has been used extensively to develop an enteric-release formulation. It is available in three grades: L, M and H. These dissolved at different pH levels of ≥ 5.5 , 6.0 and 6.8, respectively [74]. Alqahtani et al [75] has reported a successful enteric CBZ-HPMCAS extrudate with a controlled-release profile over a 24-hour time period. In situations where the API has an undesired taste, there is a high demand to employ a sweetening agent or hydrophilic polymer as a taste-masking agent for paediatric and geriatric formulations [76].

1.3 Mesoporous silica applications in drug delivery

Historically, the first use of MPS in pharmaceutical applications was reported in 1972 by Monkhouse and Lach, who used non-ordered mesoporous silica gel. This was further elaborated on by Yang [77, 78]. The mechanism of solubility enhancement comes from the stabilisation of the amorphous state in the pores and the higher surface area. It has been agreed that APIs dissolve more rapidly in their amorphous state as compared to their crystalline state. However, as the amorphous form tends to convert to the most stable form (crystalline) because of its lower energy, the physical and chemical stability of the amorphous form has remained a major concern in developing delivery systems based on drugs in the amorphous state [13, 58]. According to [79], the drug loaded silica tablets show a better dissolution compared to a normal physical mix.

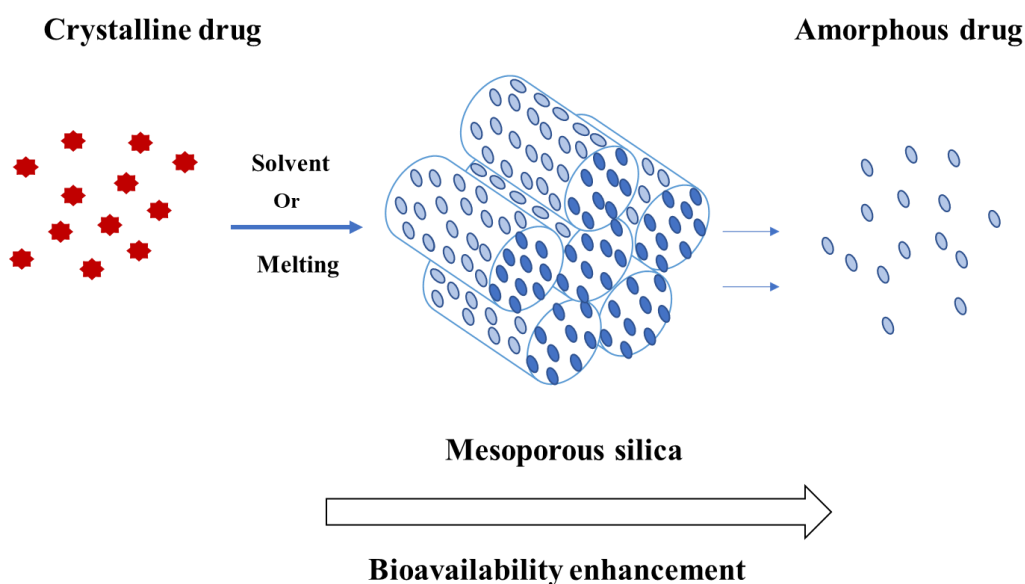


Figure 1.5: Schematic representation showing the bioavailability enhancement of API using mesoporous silica.

In 1992, the Mobil Corporation Laboratories invented a new family of MPS and named it MCM-X (Mobil Crystalline Material). Initially, these ordered mesoporous silicas (OMSs) were established for catalyst applications. Since then, they have been used for pharmaceutical applications. They have distinctive features, such as large pore volumes (up to 1.5 cm³/g), high surface area (up to 1500m²/g), manipulated pore diameter, and a silanol-rich surface that can be functionalised [42].

Depending on the pore shapes, several grades are synthesised, such as MCM-41, MCM-48 and MCM-50, having hexagonal, cubic and lamellar pore structures [16]. In 1998,

Zhao et al. synthesised the Santa Barbara Amorphous mesoporous silica, including SBA-15 and SBA-16, which possess hexagonally ordered cylindrical pores. Enormous efforts are continuing to prove the use of OMS application in drug delivery. According to the International Union of Pure and Applied Chemistry (IUPAC), porous materials are classified according to their pore diameter as presented in Table 1.6.

Table 1.6: IUPAC classification of porous materials

Type of pore	Mean pore diameter (nm)
Micropore	< 2
Mesopore	2–50
Macropore	> 50

1.3.1 Dissolution rate enhancement

Mesoporous silica demonstrated a great potential to be proper substrates for improving dissolution rate and bioavailability of poorly soluble APIs. In the confined pore, the chance of recrystallisation is prevented and the drug is trapped in its amorphous form. Due to the high surface area and the hydrophilic nature of MPS, the wettability is enhanced and achieves a faster dissolution rate. A wide body of research conducted by various investigators on several active drug substances using different types of MPS [80–84]. Mellaerts et al. explored the effect of the loading method on dissolution profiles. Ibuprofen and itraconazole were loaded into SBA-15 using three different methods: solvent evaporation, incipient wetness impregnation and the melting method. It was shown that the samples prepared by the solvent evaporation method and incipient wetness provided a faster dissolution rate than samples obtained by the melt method. Hence, it can be summarised that the effect of the loading method depends on the physical and chemical properties of the API[85].

The poor stability of amorphous APIs is considered the main challenge and should be addressed to enhance the solubility and the dissolution rate [16]. With the advantageous features of MPS, such as high surface area and pore volume, the high surface energy of MPS decreases the free energy of the loaded API, and the chance of crystal growth is reduced from the constrained pore [84]. A number of researchers have investigated stability enhancement of drugs by incorporation into MPS. It was found that there is

significant improvement in the stability of indomethacin after storage under stressed conditions, as well as improvement in the dissolution rate of indomethacin [81]. Furthermore, Kinnari et al. (2011) observed that the amorphous state of itraconazole was maintained for three months at 40°C, with 75% relative humidity (RH) in MPSs such as Syloid® 244 FP silica [86]. Another study conducted by Genina et al. (2018) employed HME as a solvent-free method to prepare a stable ASD using MPS. This showed that ibuprofen mainly adsorbed to MPS, whereas carvedilol was in the polymer. In addition, it confirmed that all the HME formulations are stable and have a higher intrinsic dissolution rate [80].

1.3.2 Controlled drug release via MPS

Several factors could control the drug release from MPS such as pore volume, pore diameter, surface area and surface silanol group. These parameters can be manipulated during synthesis of MPS and the drug release can be controlled by tailoring the physiochemical features of MPS. If the pore diameter is narrow, the time for the drug to be dissolved is longer, prolonging the drug release. In addition, surface treatment of MPS controls the drug release based on the interaction between MPS and the loaded API [16, 87]. Zheng et al [88] developed MPS with functional group modifications to provide pH-sensitive drug release. Doxorubicin hydrochloride loaded on poly (glutamic acid) grafted MPS shows higher drug release at pH 5.5 compared to 7.4. Furthermore, the study used surface-coated polyelectrolytes to perform pH-dependent drug release for cancer chemotherapy [89]. Another approach to prolong drug release from MPS was conducted by Mortiz and Laniecki [90]. They utilised excipient-like stearic acid and hydroxypropyl cellulose, which suggests they have the ability to prolong the drug release by blocking the pores by the hydrophobic nature of stearic acid. In addition, Park and Pendleton [91] modulated the pore width and pore volume to achieve the controlled-release profile of allyl isothiocyanate. Another study reported that ibuprofen drug release from dimethylsilyl-modified MCM-41 was delayed due to the presence of hydrophobic groups on the pore surfaces [92].

1.3.3 Drug loading method into MPS

1.3.3.1 Solvent immersion

The process of drug loading onto MPS can be achieved by adsorption from a drug solution. A pre-determined quantity of MPS is added and suspended in a solution of the drug dissolved in a volatile solvent. After continuous stirring, the suspension should be filtered and then the wet mass dried in an oven to achieve the powder of drug-loaded silica. A mixture of two or more solvents can also be used to ensure maximum drug loading. Once the solvent is evaporated, the same process can be repeated to increase percentage drug loading. Kovačič et al [93] prepared a porous silica-based SD of carvedilol using a solution of the drug in the solvent tetrahydrofuran. Using different levels of drug content caused a noticeable effect on amorphisation, crystallinity and dissolution.

1.3.3.2 Melt mixing

This method includes a pre-defined ratio of a crystalline API and MPS as a physical mixture, followed by applying heat until the drug reaches T_m . By capillary forces, the amorphous APIs are trapped (melted) in the confined pores of MPS. Watanabe et al. (2001) concluded that the melted mixture of MPS and indomethacin shows a high amount of amorphisation. In addition, it was observed that if the drug is melted without MPS, it starts converting to its original crystalline state on storage. The rate of recrystallisation is dependent on the mixing time and varies inversely with it. This method is advantageous due to being a solvent-free technology; however, the heating step involved in this method makes it inappropriate for thermolabile drugs.

1.4 Objectives

Hot melt extrusion has been broadly used for producing pharmaceutical solid dispersions. There is an extensive body of literature has been accumulated in terms of their pharmaceutical applications for improving the dissolution rates of poorly soluble drugs as a binary mixture with limited functionalities. However, designing a stable ternary system (drug, polymer and additives) with different purposes such as controlling drug release rate and improving drug loading capacity still has not been investigated in full details. In this study, complex solid dispersions systems were prepared using several blends of carbamazepine and tolbutamide with various functional additives having different applications. This work investigated widely the potential and principles of using functional additives in HME as a formulation approach to produce a complex polymer based solid dispersions with multiple purposes. The project conducted herein demonstrate the practicality of producing slow release and fast release products in a single-step hot melt extrusion (HME) process and use a range of model systems to systemically explore the factors that could induce the formation of such cavitated internal microstructure and their influence on the drug release rate of the HME extrudates. Furthermore, the formulation principle of forming stable ASD with high drug loading by the aid of MPS were systemically investigated.

The specific aims of the study include:

1. To investigate the use of various additives in HME solid dispersion and their impact on the final extrudate.
2. To develop tuneable drug release capability of ASD formulations produced by HME.
3. To understand the governing factors that could induce the formation of such cavitated internal microstructure.
4. To investigate the use of MPS to design a hybrid (polymeric-MPS) matrix containing two sources of capabilities for stabilising the amorphous drugs and drug solubility in the polymer in order to form a stable and high drug loaded ASD via HME.

Materials and methods

Chapter 2

2.1 Materials and methods

2.1.1 Materials

2.1.1.1 Model drugs

2.1.1.1.1 Carbamazepine

Carbamazepine is classified as one of tricyclic antidepressants (TCA) drugs and has multiple pharmacological effects such as anticonvulsant, mood stabiliser and analgesic. Carbamazepine is widely used in the treatment of epilepsy and bipolar disorder. Also, it is commonly prescribed to treat trigeminal neuralgia [94]. The chemical structure of CBZ is shown in table 2.1. It is a white powdered crystal and has at least four different polymorphs (Table 2.1). As CBZ is one of the poorly soluble drugs (class II), improving the bioavailability of CBZ has been studied by many researchers[95-98]. In this work, anhydrous CBZ (polymorph III) has been used as it is the most stable polymorph at room temperature. In figure 2.1, the polymorphic form of CBZ is identical to what has been reported previously in the literature[99-101].

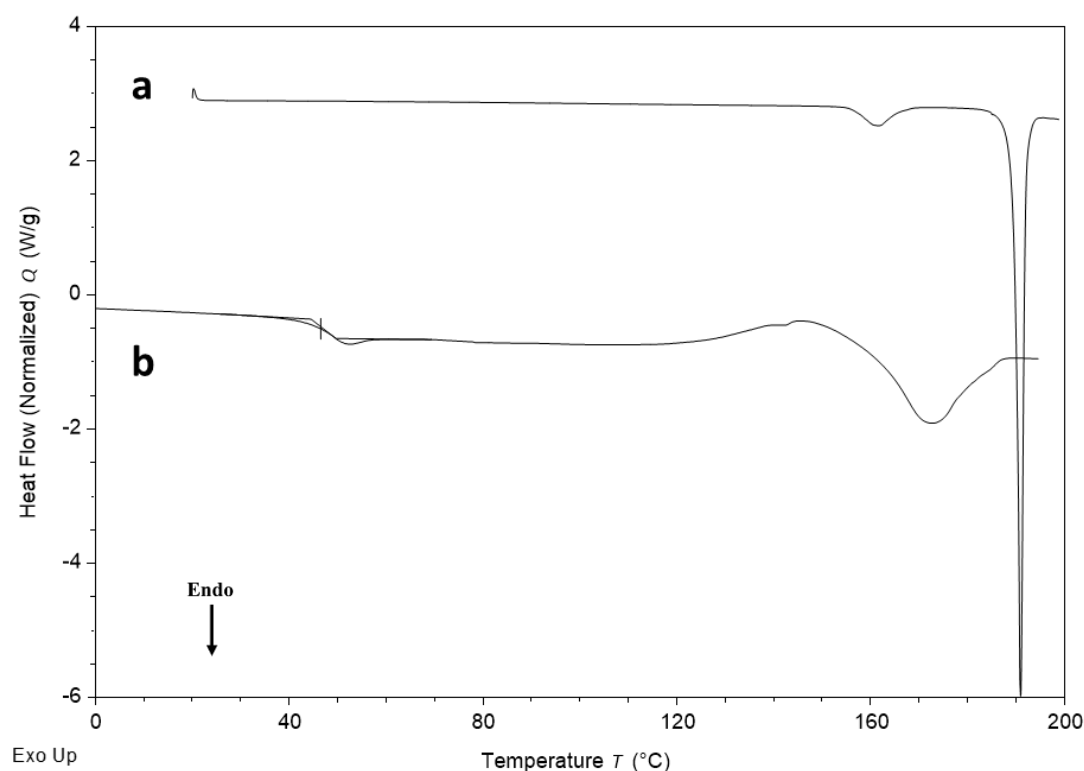


Figure 2.1: DSC thermogram of (a) crystalline and (b) amorphous carbamazepine.

2.1.1.1.2 Tolbutamide

Tolbutamide is one of the sulfonylurea drugs, oral antihyperglycemic agent commonly prescribed to treat non-insulin-dependent diabetes mellitus. It is a white crystalline

powder with 5 different polymorphs and has a melting point of 127-129°C (table 2.1). It is classified as class II drug (BCS), with the properties of low solubility and high permeability. Various research efforts have been demonstrated to enhance the bioavailability of TBA [102, 103]. In this study, polymorphic form I was used [104-106].

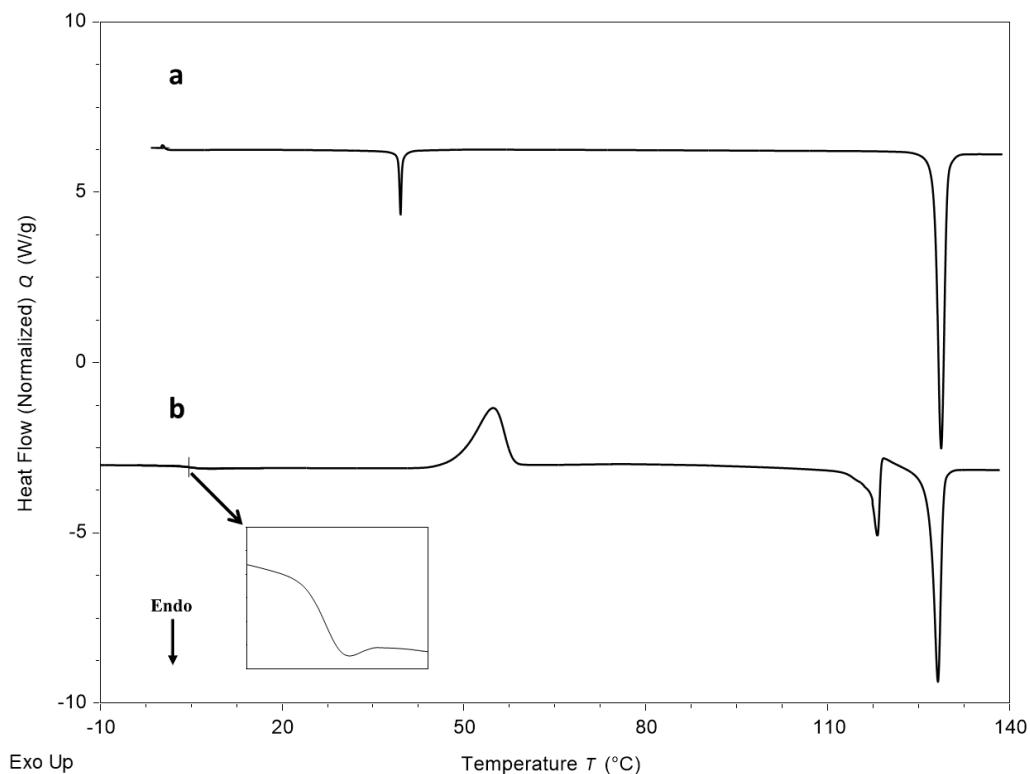
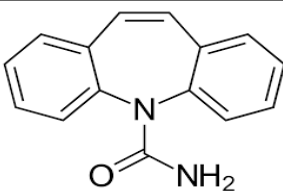
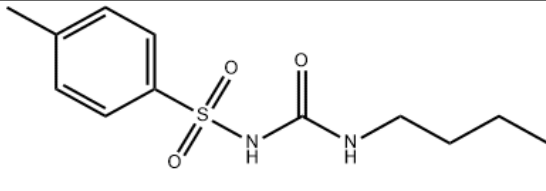


Figure 2.2: DSC thermogram of (a) crystalline and (b) amorphous tolbutamide.

Table 2.1: Physicochemical properties of carbamazepine and tolbutamide.

Reference	CBZ [99-101, 107-110]	TBD [104-106, 111]
Structure		
Melting point	192 °C	127 °C
Glass transition	46-52 °C	(0) – 3 °C
Molecular weight	236.27	270.35
Aqueous solubility (mg/L)	125	109

Log P	2.45	2.34
Polymorphs	4 (I,II,III and IV)	5 (I,II,II, IV and V)

2.1.2 Polymeric carriers

2.1.2.1 HMPCAS

HPMCAS is the partially esterified derivative of HPMC. It is part of a group of widely used pharmaceutical enteric polymers, which can be used in the development of controlled release formulations targeting the intestines for both regular enteric coating and sustained release formulations. More recently, HPMCAS has been studied as a potential carrier in solid dispersion formulations prepared via spray drying or hot melt extrusion, which leads to dissolution enhancement and crystallisation inhibition in poorly water-soluble drugs [112-117]. Moreover, the crystallisation inhibition effect on amorphous drugs achieved using HPMCAS has been reported to be a good solid dispersion formulation carrier. According to the substitution ratio of acetyl and succinyl groups in the polymer, HPMCAS is classified in different grades that dissolve at different pH values (Table 2.2). Due to the succinate moiety, HPMCAS is un-ionised at low pHs. Thus, it dissolves in the intestines, where the release is targeted to. In this study, HPMCAS LF grade was used. This HPMCAS grade can be easily dissolved at $\text{pH} \geq 5$ [74].

Table 2.2: List of HPMCAS types that soluble at different pH.

	LF	MF	HF
Acetyl (wt%)	5-9	7-11	10-14
Succinyl (wt%)	14-18	10-14	4-8
pH	>5.5	>6	>6.5

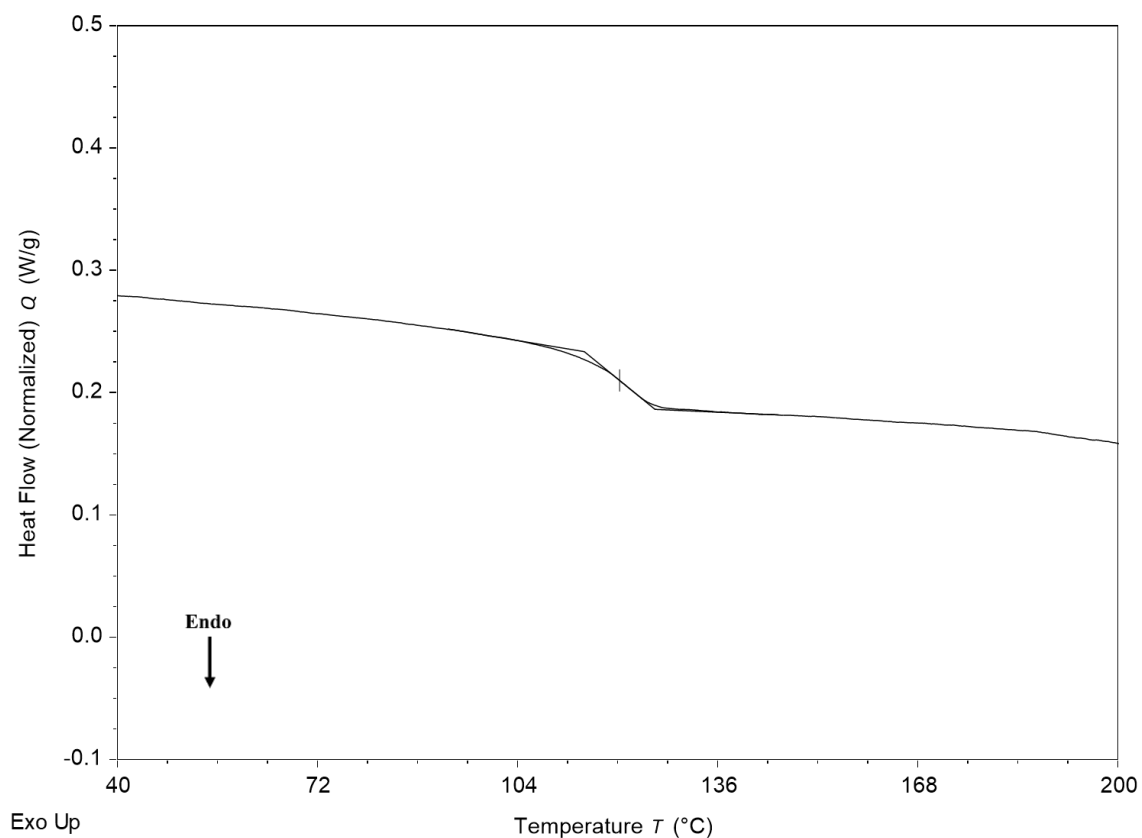


Figure 2.3: DSC thermogram showing the glass transition of HPMCAS

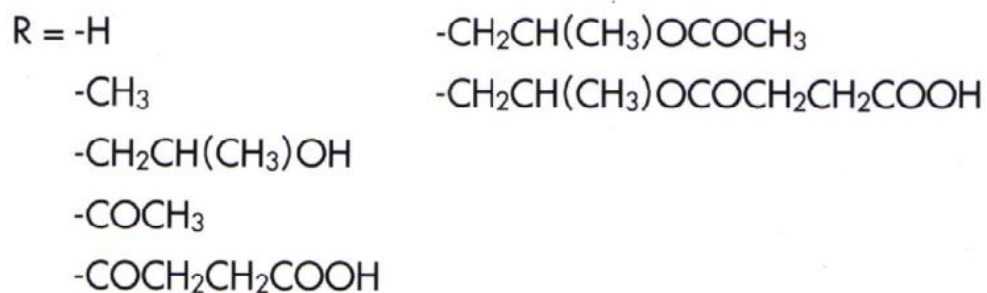
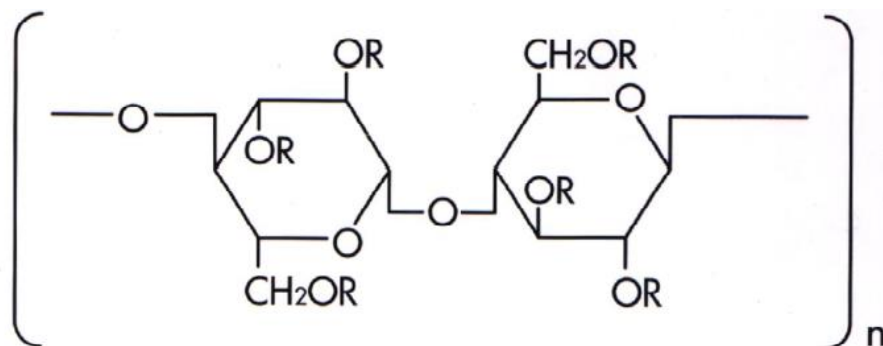


Figure 2.4: Chemical structure of HPMCAS [74]

2.1.2.2 Soluplus

Polyvinyl caprolactam–polyvinyl acetate–polyethylene glycol graft copolymer (Soluplus) is a novel polymer with amphiphilic features developed particularly to improve the bioavailability of poorly soluble drugs (BCS class II). An advantageous characteristic of Soluplus is its bifunctional ability; it can disperse the drugs molecularly in the polymeric matrix and acts as an active solubiliser via micelles formation. It is hydrophilic and non-ionic (pH independent) [118]. Due to its low T_g (70 °C) and excellent thermoplastic properties, this make it a suitable for HME processes, and it has been investigated for this purpose by several researchers [119-123]. In this project, soluplus was used as the model polymer with mesoporous silica for producing a high drug loading amorphous solid dispersion.

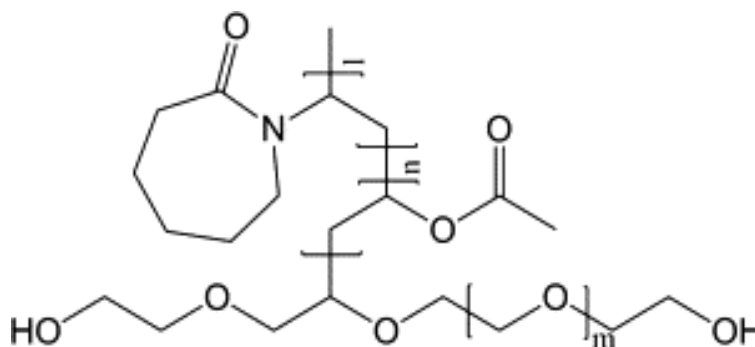


Figure 2.5: Chemical structure of Soluplus [124].

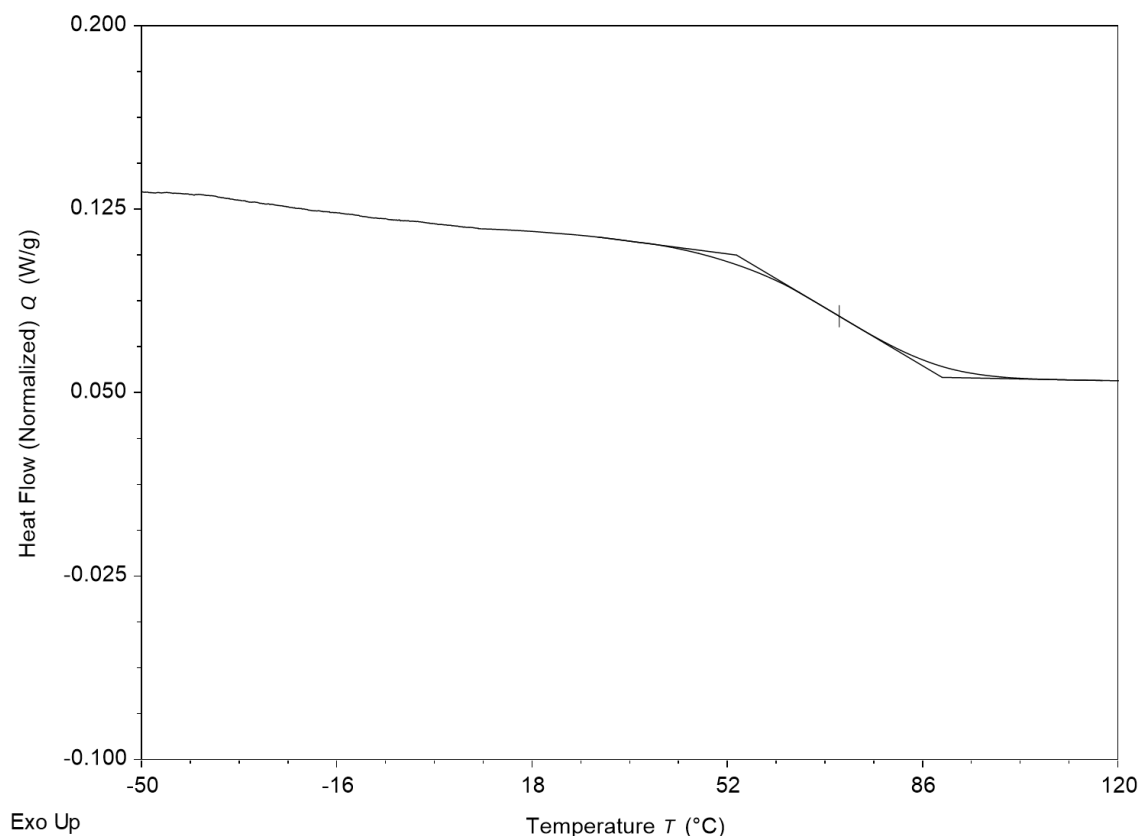


Figure 2.6: DSC thermogram showing the glass transition of soluplus.

2.1.3 Additives

2.1.3.1 Croscarmellose sodium

Croscarmellose sodium is a cross-linked polymer of carboxymethylcellulose sodium. It is insoluble in water and rapidly swells upon contact with water due to its high swelling capacity. This results in rapid disintegration. Furthermore, it also has a water wicking capability that establishes a capillary network for water to penetrate the tablet. Both mechanisms are performed via cross-linking, which creates insoluble hydrophilic and highly absorbent fibres. Regarding oral pharmaceutical formulations, croscarmellose sodium was used as a superdisintegrant at concentrations of 10–25% and 0.5–5% in capsule and tablet formulations (either by direct compression or wet granulation), respectively [125].

2.1.3.2 Sodium starch glycolate

Sodium starch glycolate is the sodium salt of a cross-linked partly O-carboxymethylated potato starch. These modified starches are also called superdisintegrants based on their degree of cross-linking and substitution. Their main mechanism is swelling, which starts with the rapid absorption of water and leads to a vast increase in volume that generates

pressure that overcomes tablet cohesiveness [126]. During the tableting process, SSG is commonly used as a superdisintegrant at concentrations of 2–4% and 4–6% in direct compression and granulated tablet formulations, respectively [125].

2.1.3.3 Crospovidone

Crospovidone is a water-insoluble synthetic crosslinked homopolymer of N-vinyl-2 pyrrolidinone. One of its main uses is as a tablet superdisintegrant at 2–5% concentration for tableting prepared by direct compression and wet/dry granulation. Due to its porous nature, it has high capillary activity and sufficient hydration capacity, as well as volume expansion and rapid tablet disintegration with no signs of gel formation [127]. With regard to disintegration, a research group confirmed that strain recovery is its main mechanism, where crospovidon is deformed during compression. Once it interacts with the water, crospovidone may revert to its original shape and volume because of the recovery of energy of viscoelastic deformation followed by capillary action and the disruption of particle–particle bonds. In contrast to sodium starch glycolate and croscarmellose sodium, crospovidone exhibit no swelling and no tendency towards gel formation [126, 128].

2.1.3.4 Gelucire

Gelucire is the family of polyethylene glycol (PEG) ester, derived from mixtures of mono-, di- and triglycerides with PEG esters (MW 1500) of fatty acids (mono- and di-esters of palmitic (C16), stearic (C18) acids and polyoxylglycerides). It is an amphiphilic, non-ionic (pH independent), water-dispersible surfactant for lipid-based formulations to solubilise. It also increases the oral bioavailability of poorly water-soluble active pharmaceutical ingredients (APIs). Its main uses are as a solubiliser for poorly-soluble APIs and as a bioavailability enhancer. Some applications of oral formulations include solubility and bioavailability enhancement [129-134], sustain drug release [135-137], taste masking [138-140] and active pharmaceutical ingredient (API) protection from pH oxygen, light and humidity [141-143]. Regrading immediate drug release application, Gelucire comprising only PEG esters are the ideal for this purpose. However, Gelucire containing glycerides, or a mixture of glycerides and PEG esters are used in the preparation of sustained release formulations. Due to their hydrophobicity and low density, they are considered as suitable carriers for developing sustained release drug delivery systems [70, 75, 144-146].

2.1.3.5 Maltodextrin

Maltodextrin is an amorphous saccharide prepared via the controlled hydrolysis of corn starch with acid and/or enzymes. As MD is characterised by its dextrose equivalent (DE), there are two types of MD: high DE and low DE. Their physicochemical properties vary. MD with high DE is commonly used in pharmaceuticals due to its capacity to improve the stability and solubility of a formulation [147]. DE 39 was used as one of the excipients of ODT, prepared via freeze drying for dissolution rate enhancement [148]. Maltodextrin can be used to make binder solution for fluidised bed granulation [149], dry binder for direct compression [150]. It can also increase the viscosity of a solution and prevent the recrystallisation of syrups [151].

2.1.3.6 α -Lactose monohydrate

Lactose monohydrate is a natural disaccharide consisting of one galactose and one glucose moiety. Lactose has been broadly used in the pharmaceutical industry as a filler or diluent in tablets and capsules [125] due to its low hygroscopicity, bland taste, cost effectiveness and physical and chemical stability [152]. Furthermore, lactose can be utilised as a diluent in dry-powder inhalation (i.e. metered dosage inhalators) with different particle size distribution and flow characteristics [153]. Another application of lactose is use in lyophilised products and infant products [154, 155], where lactose is added to freeze-dried solutions to increase plug size and aid cohesion [156]. Lactose monohydrate is also employed to prepare sugar-coating solutions [157].

2.1.3.7 Mesoporous Silica

Mesoporous silica is a novel, inert and inorganic silicon dioxide (SO₂) with a uniform and tailorable pore diameter (2–50 nm), high surface area and pore volume. In addition to its broad range of pharmaceutical uses (wetting, anti-caking, anti-static agents and stability improver), scientists and researchers are massively interested in it as an efficient carrier for poorly soluble APIs, either in micro or nanoscale [58]. This vehicle aims to improve the solubility and bioavailability of poorly water-soluble drugs by stabilising the amorphous form of API in the sub-critical dimension or by absorptive interaction, hence inhibiting the recrystallisation of APIs during storage and transportation [158-160]. There are many examples of drugs that greatly improve bioavailability using Mesoporous

silica, such as phenylbutazone [161], fenofibrate [162], griseofulvin [163] and ibuprofen [164, 165].

The material characterisation for all the ingredients described in this section are detailed in their respective section in the relevant chapters.

2.2 Methods

2.2.1 Hot melt extrusion

In this study, hot melt extrusion is the main manufacturing technique for preparing SD formulations. The HAAKE Minilab intermeshing twin screw extruder was used with different extrusion conditions to produce HME extrudates (Figure 2.7).



Figure 2.7: Hot Melt Extruder of Thermo Scientific HAAKE MiniLab II

In terms of extrusion conditions, the extrusion temperatures used were selected depend on the T_m and T_g of the APIs and polymers (HPMCAS & Soluplus). Furthermore, the overall extrusion temperatures were used below 150 °C to avoid the concern of degradation. the residence time of 5 minutes were kept constant in all the formulations. A conveyer belt was employed to receive the final extrudate with a pre-determined speed for adjusting the extrudate diameter and giving at time for solidifying the extrudate help the final extrudates during flushing time. The operational parameters are shown in table 2.3.

2.2.2 Drug loading into MPS:

Recently, several methods have been investigated for drug loading into mesoporous silica such as melt loading, dry loading, and solvent loading. In this study, melt loading method has been used to load tolbutamide into mesoporous silica (Syloid® XDP 3050). The drug and the host were mixed together in a glass vial for 5 min using a spatula. Then, the powder mixtures were transferred into aluminum hot plate at 135 °C (above T_m of TBA) and mixed continuously with a spatula for 5 min in order to ensure that TBA was successfully adsorbed within the pores. Subsequently, the samples were either cooled to room temperature or added directly into polymer mix to be extruded using HME.

The ingredients contents for all the formulations will be discussed in full details in their respective section in the relevant chapters.

Table 2.3: HME parameters used in the production SD extrudates.

Formulation code	Extrusion temperature (°C)	Screw speed (rpm)	Retention time (min)
H	150	100	5
H-CNa	150	100	5
H-NaSG	150	100	5
H-CP	150	100	5
H-MD	150	100	5
H-LM	150	100	5
HG	150	100	5
HG-CNa	150	100	5
HG-NaSG	150	100	5
HG-CP	150	100	5
HG-MD	150	100	5
HG-LM	150	100	5
HG (placebo)	150	100	5
H20	150	100	5
HG20	150	100	5
H-NaSG	150	100	5
H-NaSG (EL)*	150	100	5
HG-NaSG	150	100	5
H30	150	100	5
H-NaSG30	150	100	5
H50	150	100	5
H-NaSG50	150	100	5
H-2NaSG	150	100	5
H-7NaSG	150	100	5
Sol-30	150	100	5
Sol-50	150	100	5
EPO-30	150	100	5
EPO-50	150	100	5
H-FDN	150	100	5
4Si	130	30	5
8Si	130	30	5
12Si	130	30	5
16Si	130	30	5
0Si	130	30	5
30Si	130	30	5
35Si	130	30	5
40Si	130	30	5

**An investigation into the use of low quantities of
functional additives to control drug release from
hot melt extruded solid dispersions for poorly
soluble drug delivery**

Chapter 3

3.1 Introduction

Hot melt extruded (HME) solid dispersions have been widely used as a formulation strategy to improve the dissolution rate of poorly soluble drugs but less commonly reported for producing sustained/controlled release formulations [45, 52]. The HME extrudates traditionally have to be downstream processed into powder form to allow further tableting or capsules filling. Controlled release products can improve patient compliance by reducing the dose frequency and therapeutic outcome due to more stable plasma drug concentration in comparison to non-controlled released products [166]. This study reports the use of the single-step HME process to directly manufacture cylindrical shaped monolithic solid dispersion based extrudates as the finished product, which can be directly filled in capsules for oral controlled release of drugs. Such a shape can also allow easy control of the drug release rate when either diffusion or surface erosion are the dominate the release mechanism [167]. Therefore, from a manufacturing point of view, HME carries clear advantages as a readily scalable and a single-step method for producing amorphous solid dispersion based controlled release products.

In addition to releasing the API in a controlled manner, the challenge of developing monolithic controlled release formulations based on amorphous solid dispersions containing poorly soluble drug is that the prolonged exposure to the GI fluid could increase the risk of the recrystallization of the drug in the dispersion matrices [168]. If the drug is recrystallized instead of molecularly dispersed in the polymeric matrix, the release rate is limited by the dissolution rate of the crystalline drug particles, but not purely governed by other mechanisms such as matrix erosion and diffusion of the drug molecule through the matrix materials. In order to minimise the drug recrystallization in a solid dispersion based controlled release matrices, the polymer excipient used in the matrices should be able to not only control the release rate of the drug, but also prevent the drug crystallisation in the matrix during the course of dissolution. In this study, the polymer, HPMCAS, which has crystallisation inhibition properties, was used to form the matrix of the extrudates [112, 114, 115]. HPMCAS is a one of a group of widely used pharmaceutical enteric polymers, which can be used in the formulation development of controlled release formulations targeting the intestines. HPMCAS can be obtained with a predetermined ratio of hydrophilic succinate groups and hydrophobic groups such as the acetyl and methoxy substituents [113]. The succinate moiety ionisation at high pH results in an increased solubility and dissolution rate compared to the un-ionised state at low pH. Furthermore, the hydrophobic groups of HPMCAS play an important role in suppressing

the amorphous drug mobility in a HPMCAS based solid dispersion of and inhibiting the drug recrystallisation due to the hydrophobic interaction between drug and HPMCAS [169, 170]. With such intrinsic properties, it is reasonable to predict that if HPMCAS was used to form the HME monolithic solid dispersions, it should be able to hold its structural integrity during drug dissolution and inhibiting the crystallisation of amorphous poorly soluble drugs, both in solid dispersions and in solutions [116, 117, 171, 172]. From the processing prospective, HPMCAS-LF, the low-fine grade of HPMCAS, has been reported to be the most stable grade for HME with the lowest level of free acid released during HME even at high HME temperature and speed [74]. Therefore, LF grade was used in this study.

Carbamazepine (CBZ) was selected as the model drug. It is a well-documented, poorly water-soluble drug, used as an anticonvulsant and specific analgesic for trigeminal neuralgia in the treatment of epilepsy and neuropathic pain, [173, 174]. Clinically, controlled release CBZ products (Tegreto[®] prolonged release and Carbagen[®] SR) have demonstrated fewer side effects than immediate release CBZ products [175, 176]. However, they are manufactured by multi-step tableting process. The motivation of this study is to demonstrate the practicality of producing slow release and fast release products in a single-step process. To modulate the CBZ release rate of HPMCAS based extrudates, disintegrants, pore formers and lipid excipients were added to the HME extrudates. These were crosscarmellose sodium, Na starch glycolate, crosspovidone, maltodextrin, α -lactose monohydrate and Gelucire 50/13. The intention of using disintegrants and pore-formers in the extrudates was to increase the drug release rate by speeding up the water penetration and disintegration of the HPMCAS matrices; whereas adding the swellable lipid excipient, Gelucire 50/13, was intended to slow down the release rate by increasing the swelling and reducing the breakdown of the HPMCAS matrices. In order to attempt to visualise the swelling and erosion process in real time, this work also evaluates for the first time the feasibility of using a UV imaging technique that is primarily used in the determination of intrinsic dissolution rates (IDR) [177-183].

3.2 Materials and Methods

3.2.1 Materials

Carbamazepine (CBZ, form III) was purchased from (Molecula, UK). Hydroxypropyl Methylcellulose Acetate Succinate (HPMCAS-LF) with the substituent ratios of $-\text{CH}_3$, $-\text{CH}_2\text{CH}(\text{CH}_3)\text{OH}$, $-\text{COCH}_3$, and $-\text{COCH}_2\text{CH}_2\text{COOH}$ being 1.87, 0.25, 0.48, and 0.37 average number/glucose ring unit was kindly donated by Shin-Etsu Chemical Co. Ltd. (Tokyo, Japan). Gelucire 50/13, crosscarmellose sodium (Can) and sodium starch glycolate (NaSG) were kindly donated by Gattefosse (Saint-Priest, France), IMCD UK Ltd (Sutton, UK) and Roquette (Lestrem, France), respectively. Crosspovidone (Polyplasdone-XL) (CP) was kindly donated by Ashland (Limavady, UK), maltodextrin (MD) and α -lactose monohydrate were purchased from (Sigma Aldrich, UK).

3.2.2 Preparation of hot melt extruded (HME) filaments

HME filaments were prepared using a co-rotating twin screw Haake Minilab extruder (Thermo Fisher, Karlsruhe, Germany) with a 2 mm orifice die. The materials were weighed (10 g) and pre-mixed via mortar and pestle for 5 minutes. For each experiment, 7 g of the mixture was fed manually into extruder. All the formulations were extruded at 150°C for CBZ-loaded (20% w/w loading) formulations, 100 rpm screw speed and the retention time was 5 minutes. During the flushing (the exiting period of the filament from the die) period, the screw speed was decreased to 30 rpm. It is worth noting that the extrusion temperature used is above the reported dehydration temperature of lactose monohydrate [184]. The melted strands were guided onto a conveyer belt using a circular die of 1.75 mm diameter and collected continuously. CBZ containing extrudates were further used to investigate the effects of additives on the dissolution behaviour of the formulations. The HME formulations containing CBZ are summarised in Table 3.1. In all formulations the weight of CBZ was kept constant at 20% of the total weight. Excipients were added at the rate of 5% of the total weight of the formulation and Gelucire was added at the rate of 15% of the total weight of the formulation.

Table 3.1: List of ingredients of the HME extrudates

Formulation Code	HPMCAS (% w/w)	Drug loading (% w/w)	Excipient/loading (% w/w)	Gelucire 50/13 (% w/w)
H	80	20		
H-CNa	75	20	Crosscarmellose Na/5	-
H-NaSG	75	20	Na starch glycolate/5	-
H-CP	75	20	Crosspovidone/5	-
H-MD	75	20	Maltodextrin/5	-
H-LM	75	20	α -lactose monohydrate/5	-
HG	60	20	-----	20
HG-CNa	60	20	Crosscarmellose Na/5	15
HG-NaSG	60	20	Na starch glycolate/5	15
HG-CP	60	20	Crosspovidone/5	15
HG-MD	60	20	Maltodextrin/5	15
HG-LM	60	20	α -lactose monohydrate/5	15

3.2.3 Materials characterisation

3.2.3.1 Attenuated total reflection-Fourier transform Infrared (ATR-FTIR) Spectroscopy

The IR spectra of the raw materials, physical mixture and extrudates were collected using an FTIR spectrometer (Vertex 70 model from Bruker Optics Limited, United Kingdom) connected with single-reflection diamond ATR accessory (MIRacl™, Pike Technologies, United States). Thirty-two scans were acquired for each sample with a resolution of 2 cm^{-1} scanning from 600-4000 cm^{-1} . All the measurements were carried out on three separate extrudates and analysed via Opus software.

3.2.3.2 Powder X-ray diffraction (PXRD)

A Thermo ARL Xtra X-ray diffractometer (Thermo Scientific, Switzerland) with a Cu $\text{K}\alpha 1$ X-ray Tube was used for to study the physical form of raw materials, physical mixture and extrudates in the different formulations and the possible changes in the nature of the components due to processing. The voltage and current of the X-beam used were 45 kV and 40 mA respectively. The angular scanning range was from 5 to 60° with a (2 θ) scan type, a step size of 0.01° and the scan rate was 4 s/step.

3.2.3.3 Differential scanning calorimetry (DSC)

The DSC experiments were carried out to analyse the raw materials and HME extrudates using Q-20 (TA Instrument, Newcastle, USA) at a heating rate of 10 °C/min from 25 to 210 °C. A nitrogen purge at a flow rate of 50 ml/min was used and sample weights were in range of 2-3 mg. TA standard crimped pans and lids were used for all measurements as well as universal analysis software for analysing the obtained results.

3.2.4 Swelling/erosion measurement of the HME extrudates during dissolution testing

The extrudates were selected within range of 17 ± 2 mm in length and 1.85 ± 0.3 mm in width. All the experiments were performed under 100 rpm stirring rate. The extrudates were placed in the basket of dissolution apparatus containing 900 ml of either pH 1.2 (for maximal 2 hours) or pH 6.8 phosphate buffer (PBS). The measurements were taken at time points of 0, 0.5, 1, 2 (up to 2 hours for pH 1.2 samples), 3, 4, 5, 6, 8, 12 and 24 hours (for pH 6.8 samples). The diameter and length of the (cylindrical-shaped) extrudates were

measured at each time point in order to calculate the changes in volume caused by swelling or erosion (Eq. 1). The volume (%) and weight (%) changes of Gelucire-free and Gelucire-containing extrudates were calculated using Equations. 2 and 3. The data are shown in Table 3.3 and 3.4. The swelling behaviour (presented in weight and volume changes %) of the placebo extrudates is shown in Figure 3.7.

$$V = \pi r^2 h \quad \text{Eq. 3.1}$$

Where, r is the radius of the cylinder cross section and h is the height of the cylinder.

$$\text{Volume \%} = \left(\frac{V_t - V_0}{V_0} \times 100 \right) \quad \text{Eq. 3.2}$$

Where V_t is the volume of extrudate at time t and V_0 is the volume of dry extrudates.

$$\text{Weight \%} = \left(\frac{W_t - W_0}{W_0} \times 100 \right) \quad \text{Eq. 3.3}$$

The W_t is the weight of extrudate at time t and W_0 is the weight of dry extrudate.

3.2.5 UV and visible imaging of HME extrudates

The surface imaging instrument (SDI2) is a UV dissolution imaging technique. In this study, it was used in the simultaneous determination of the swelling and drug release from a select few of the HME extrudates (placebo extrudate, H, HG, H-NaSG and HG-NaSG). These selected HME extrudates allowed the investigation of the effect of Gelucire on the HPMCAS as well as the NaSG effects on the produced extrudates. A schematic of the drug release measurements is depicted in Figure 3.1a & b, also displays how the dosage form is placed inside the whole dose cell, the direction of media flow and the measurement zone adapted for swelling evaluation. Each extrudate (placebo extrudate, H, HG, H-NaSG or HG-NaSG) was mounted using a custom designed stainless steel wire holder featuring two loops to secure the extrudate in place (Figure 3.1c). To perform each test the whole dosage cell with glass beads loaded (to help reduce turbulence) was inserted and connected to the fluid lines. To determine the swelling effects on the extrudates (placebo extrudate, H and HG), a 2 h flow-through assessment was conducted to determine the characteristic behaviour of each extrudate. Each experiment was conducted using both pH 1.2 and pH 6.8 at 37 °C using a flow rate of 8.2 mL/min. A 520 nm wavelength was selected for swelling measurements. Swelling is referred to as “growth” in the Figures. These measurements were taken using the data analysis software supplied with the SDI2 system and processed using Microsoft Excel™.

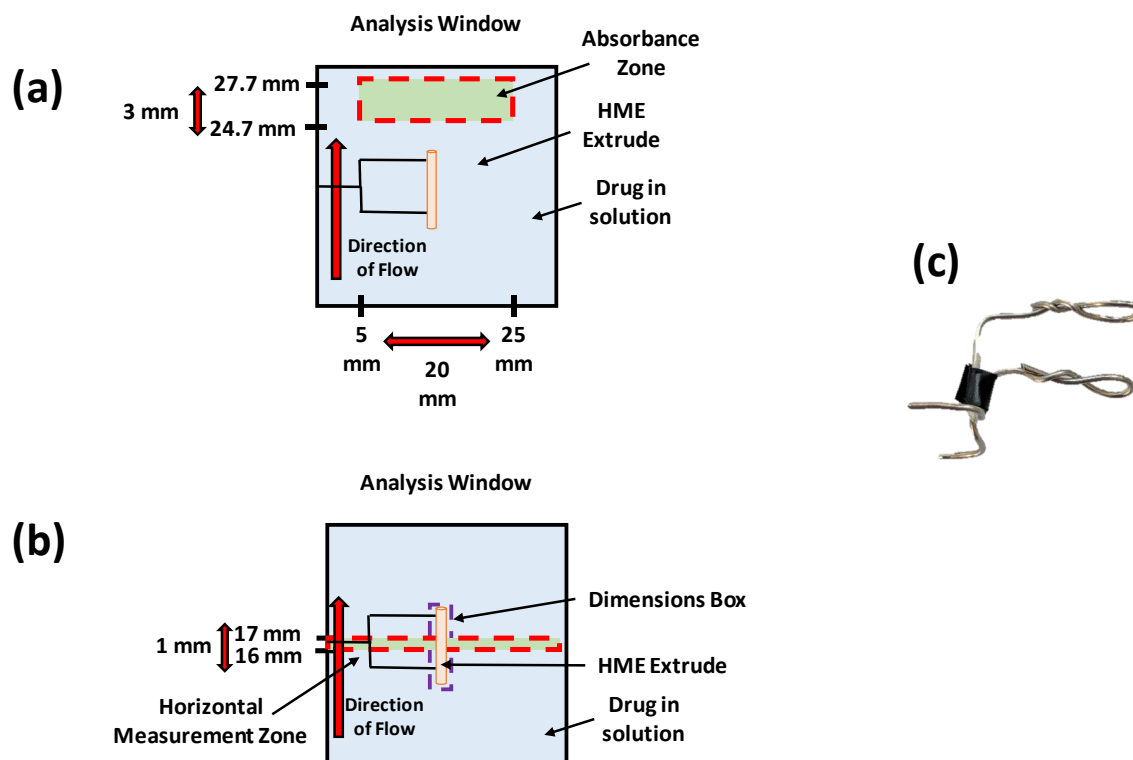


Figure 3.1: Set-up of the SDI2 for the assessment of HME filaments for the measurement of CBZ release (a), width growth (swelling) (b), custom stainless steel holder to mount HME filaments in the whole dosage cell (c).

The first use of a dual closed loop assessment of drug loaded HME extrudate (H, HG, H-NaSG and HG-NaSG) was explored and implemented (Figure 3.2). Two beakers containing 900 mL of each medium (pH 1.2 and pH 6.8) were placed on stirrer plates and allowed to warm to 37 °C before use. To form the first loop, the primary fluid line was connected to the pH 1.2 beaker along with the ‘open loop’ waste fluid line. To form the secondary closed loop, the secondary fluid line was connected to the pH 6.8 beaker along with the ‘closed loop’ waste fluid line. As the SDI2 has the ability to transfuse between different media in situ the software was set to clear 70 mL of media during change over to ensure that the pH 1.2 did not contaminate the pH 6.8 media. Each closed loop experiment was conducted for 6 h (2 h in pH 1.2 before 4 h in pH 6.8 media). Each experiment was conducted at 37 °C at a flow rate of 4.2 mL/min. A 280 nm (for CBZ release from the HME extrudate) and a 520 nm (for the HME extrudate swelling (growth) measurements) LED were selected as the light sources. Drug release and growth measurements were collected using the supplied data analysis software and processed using Microsoft Excel™. Normalisation of growth measurements was achieved by subtracting the size of the extrudate at the start of the experiment from the subsequent growth data points (Equation 3.2).

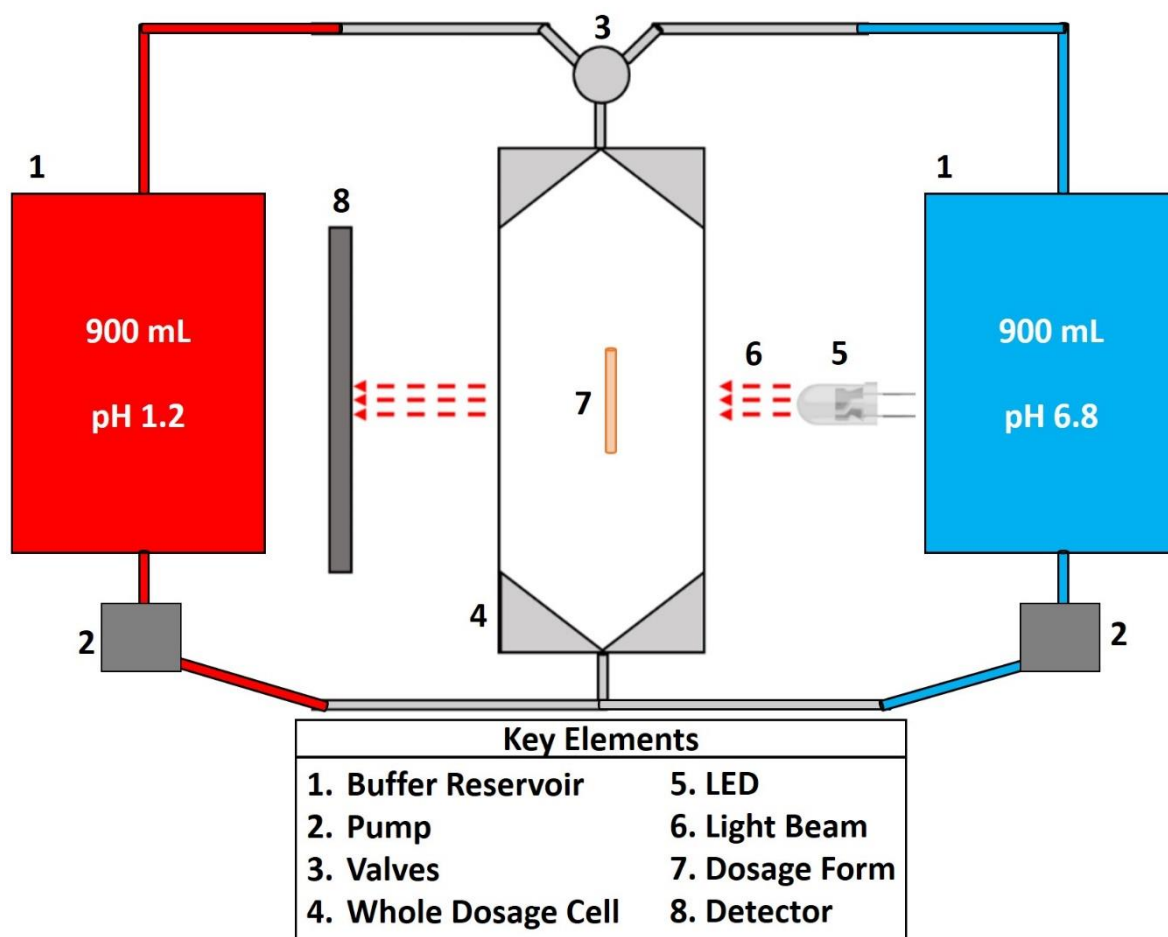


Figure 3.2: A schematic representation of the dual closed loop method for the assessment of the HME filaments in both pH 1.2 and pH 6.8 media.

3.2.6 *In vitro* drug release studies

All *in vitro* drug release experiments were performed using the British Pharmacopieal (BP) rotating basket method (Copley CIS 8000, Copley Scientific) under sink condition for 24 hours. A 100 rpm paddle rotation speed and 900 mL of either HCl dissolution medium (pH 1.2) or pH 6.8 PBS were used for each test. The temperature of the vessel was controlled at 37 ± 0.5 °C. All dissolution tests were performed as 2-stage experiments to mimic the physiological process of gastric emptying and the transport of gastric content into the intestinal environment. Therefore after 2 hours of dissolution being performed in pH 1.2 HCl, the extrudates were removed and the dissolution media was changed to pH 6.8 PBS for the following 22 hours. Strands of extrudate weighing ≈ 50 mg and containing 10 mg of CBZ were used in 900 ml medium to ensure the satisfaction of the sink conditions (CBZ water solubility 125 mg/L) [110, 185]. 3 ml of the media from each vessel were filtered through 0.45 μ m filters (Minisart Sartorius, Goettingen, Germany) and sampled at predetermined time intervals (0.5, 1, 2, 4, 6, 8, 12 and 24 hours) for the swellable strands and (0.5, 1, 2, 2.5, 3, 3.5, 4, 4.5, 5, 5.5, 6 and 6.5 hours) for the rapidly

erodible strands to determine the release mechanisms. The amount of CBZ in each sample was measured by an UV spectrometer (PerkinElmer Lamda XLS, USA) at 285 nm. All measurements were performed in triplicate. For the dissolution samples, the measured absorbance values at different time intervals were converted to concentration values using the calibration curves shown in Figure 3.3.

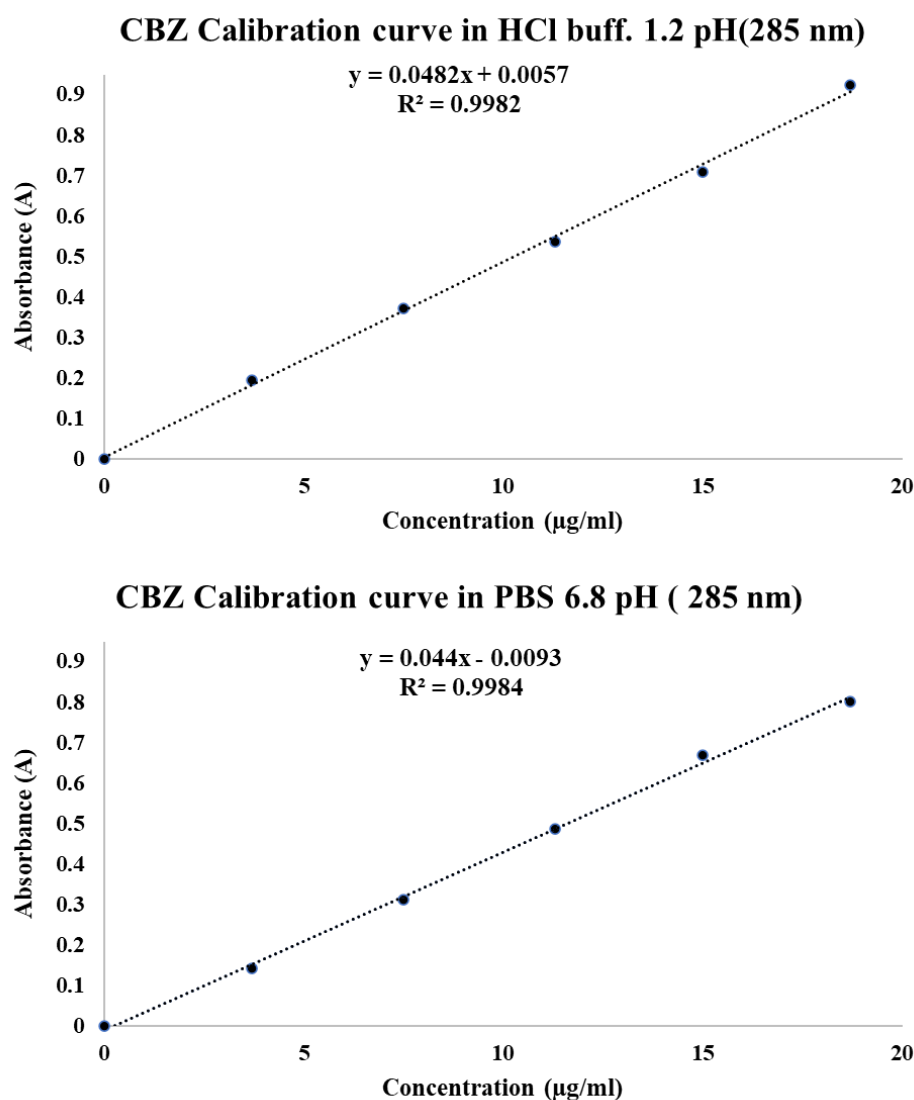


Figure 3.3: Calibration curves of CBZ in HCl buffer (pH=1.2) and phosphate buffer solution (pH = 6.8), respectively.

3.2.7 Dissolution kinetics model fitting

In order to understand the release kinetics and transport mechanisms (diffusion, swelling or erosion) involved in the CBZ release from the HME matrix, four different models such as Zero-order, First-order, Higuchi and Korsmeyer-Peppas were applied to fit the experimental data using DDSolver (Add-ins) with Microsoft Excel software. In Korsmeyer-Peppas model, only the first 60% of the drug release data were fitted in this

model. The equations for different models are represented in Table 3.2. Based on Korsmeier-Peppas equation, the release exponent n value is used to describe different release mechanisms as shown in Table 3.3.

Table 3.2: Mathematical models for comparison of dissolution profiles.

Model	Equation	
Zero-order	$M_t = K_0 * t$	eq. 3.4
First-order	$M_t = M_\infty * (1 - e^{-k_1 t})$	eq. 3.5
Higuchi	$M_t = K_H * \sqrt{t}$	eq. 3.6
Korsmeier-Peppas	$M_t / M_\infty = k_k * t^n$	eq. 3.7

Where M_t : amount of drug released in time t , M_∞ : amount of drug released as t approaches infinity, K_0 , K_1 , K_H , K_k : release rate constants.

Table 3.3: Interpretation of the Korsmeier-Peppas release exponent for cylindrical matrices and the corresponding implied drug release mechanism. Table adopted and modified from [186-192].

n -value (Release exponent)	Drug Release Mechanism	Explanations
0.45	Fickian Diffusion	<ul style="list-style-type: none"> • Entirely diffusion mechanism. • Diffusion is considerably larger than the process of chain relaxation. • Representative of first-order release kinetic. • Time dependant.
0.45 < n < 0.89	Anomalous transport	<ul style="list-style-type: none"> • Predominantly coupled diffusion/polymer relaxation. • The rate of diffusion and relaxation are comparable. • Time dependant.
0.89	Case II transport	<ul style="list-style-type: none"> • Corresponds to Zero-order release kinetics and the driving mechanism of the drug release is governed by one or multiple phenomena such as polymeric chains relaxation, swelling and polymer degradation. • Independent of time.
n > 0.89	Super case II	<ul style="list-style-type: none"> • Mainly erosion controlled mechanism, where extreme form of transport occurs through the sorption process including tension and breaking of the polymer. • Also, Surface erodible matrices exhibit zero-order release kinetics. • Independent of time.

3.3 Results and Discussion

3.3.1 Characterisation of binary CBZ-HPMCAS extrudates

The DSC results of the main components of the extrudates indicate the T_g of the amorphous CBZ and HPMCAS at 48.54 ± 1.3 and 123.8 ± 0.2 °C, respectively (Figure 3.4a). After HME, CBZ at 20% drug loading formed clear extrudates with HPMCAS. The DSC result of the drug-loaded extrudates displays a single T_g at 77.5 ± 1.5 °C, confirming the formation of a molecular dispersion (Figure 3.5a). The fully amorphous nature of the binary extrudates was further confirmed by the full halo pattern of the PXRD results. (Figure 3.5b). The experimental T_g is higher than the Gordon-Taylor equation predicted T_g (69.7 °C) [193, 194]. Such positive deviation has been attributed to the strong specific intermolecular interactions in the literature including hydrogen bonding, electron donor-acceptor complexes and ionic interactions [195]. ATR-FTIR confirmed the amorphous state of the binary matrix and consistency with a molecularly dispersed system but not showing strong signs of hydrogen bonding interactions. Therefore, any intermolecular interaction between HPMCAS and CBZ could be dominated by van der Waals interactions which are consistent with the hydrophobic interactions proposed by Ueda et al. [116, 117].

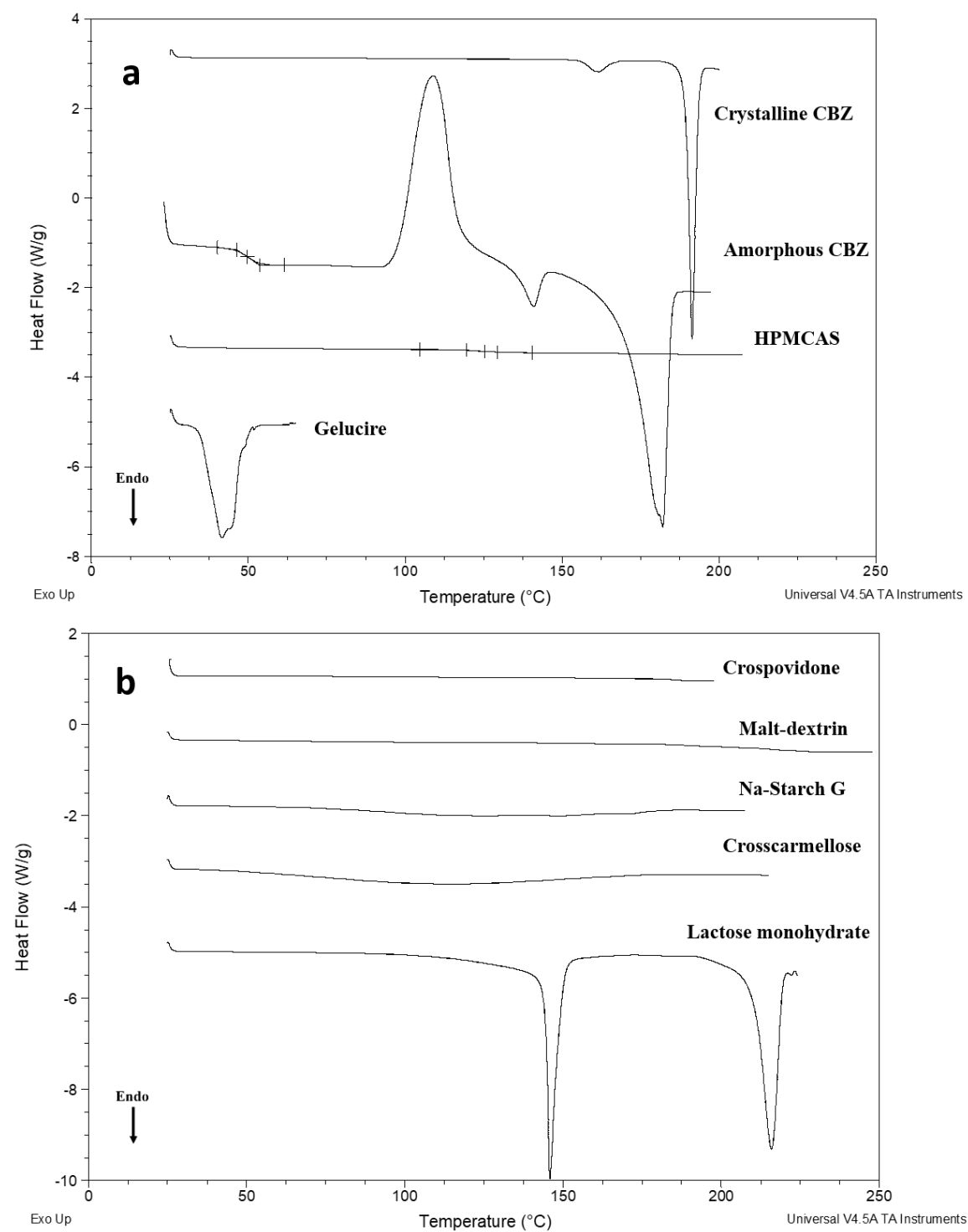


Figure 3.4: DSC results of (a) the main ingredients and (b) the additives.

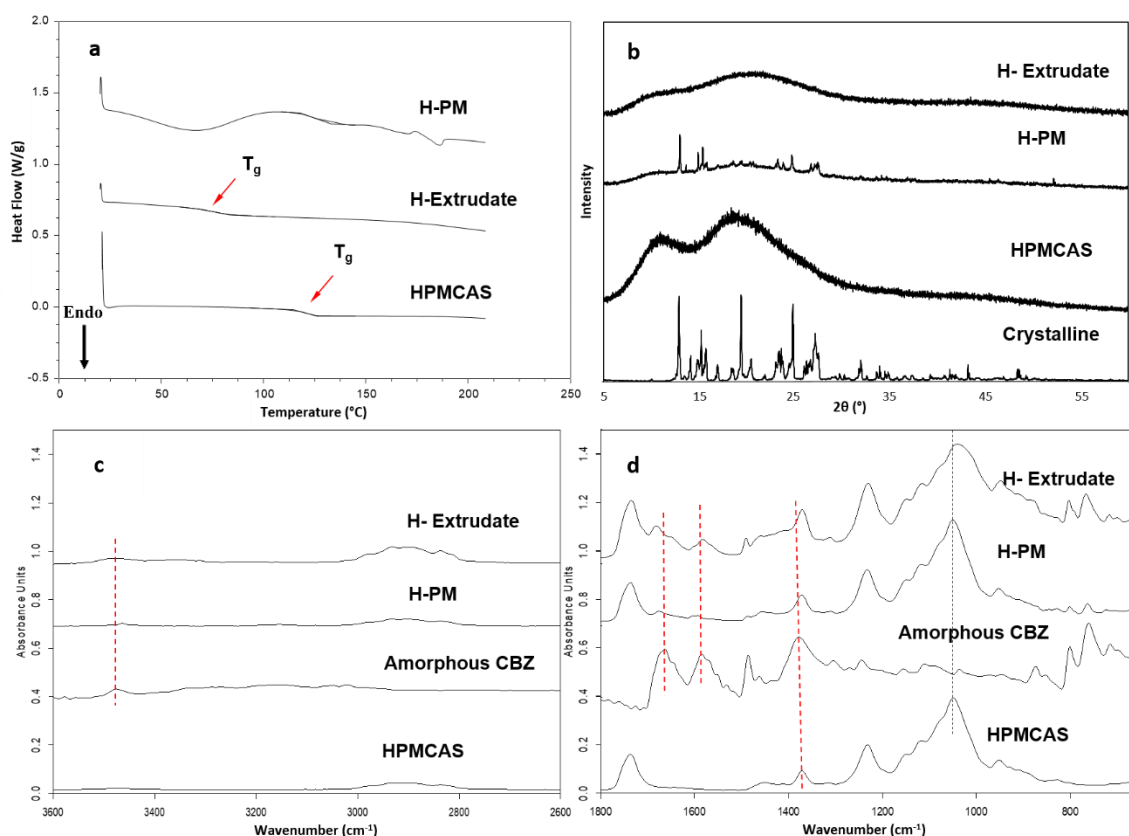


Figure 3.5: (a) DSC; (b) PXRD; partial ATR-FTIR data within the wavenumbers of (c) 3600-2600 cm⁻¹ and (d) 1800-600 cm⁻¹ of the crystalline, amorphous CBZ and extrudates of CBZ-HPMCAS binary formulation.

As seen in Figure 3.6a, the HPMCAS-CBZ binary extrudates examined by the rotating basket method show limited release in the first hours at pH 1.2 media and a continuous zero order drug release within the 24 hours in pH 6.8. The fitting of the release data to can be found in Table 3.4. It clearly seen that the binary extrudate followed zero order kinetics with case II transport mechanism with a R^2 value of 0.99 and an n value of ≈ 0.89 . Case-II transport is governed mainly by chain relaxation or combined with other phenomena such as swelling and erosion. Such sustained release can be explained by the over 281% swelling in weight and volume of the binary CBZ-HPMCAS extrudates Table 3.5 after 12 hours in pH 6.8. This is in clear contrast to the HPMCAS placebo extrudates which only showed approximately 30% and 101% increases in weight and in volume, respectively, after 12 hours in pH 6.8 Figure 3.7. A clear swelling layer of the CBZ-HPMCAS extrudates can be seen (Figure 3.6a insert).

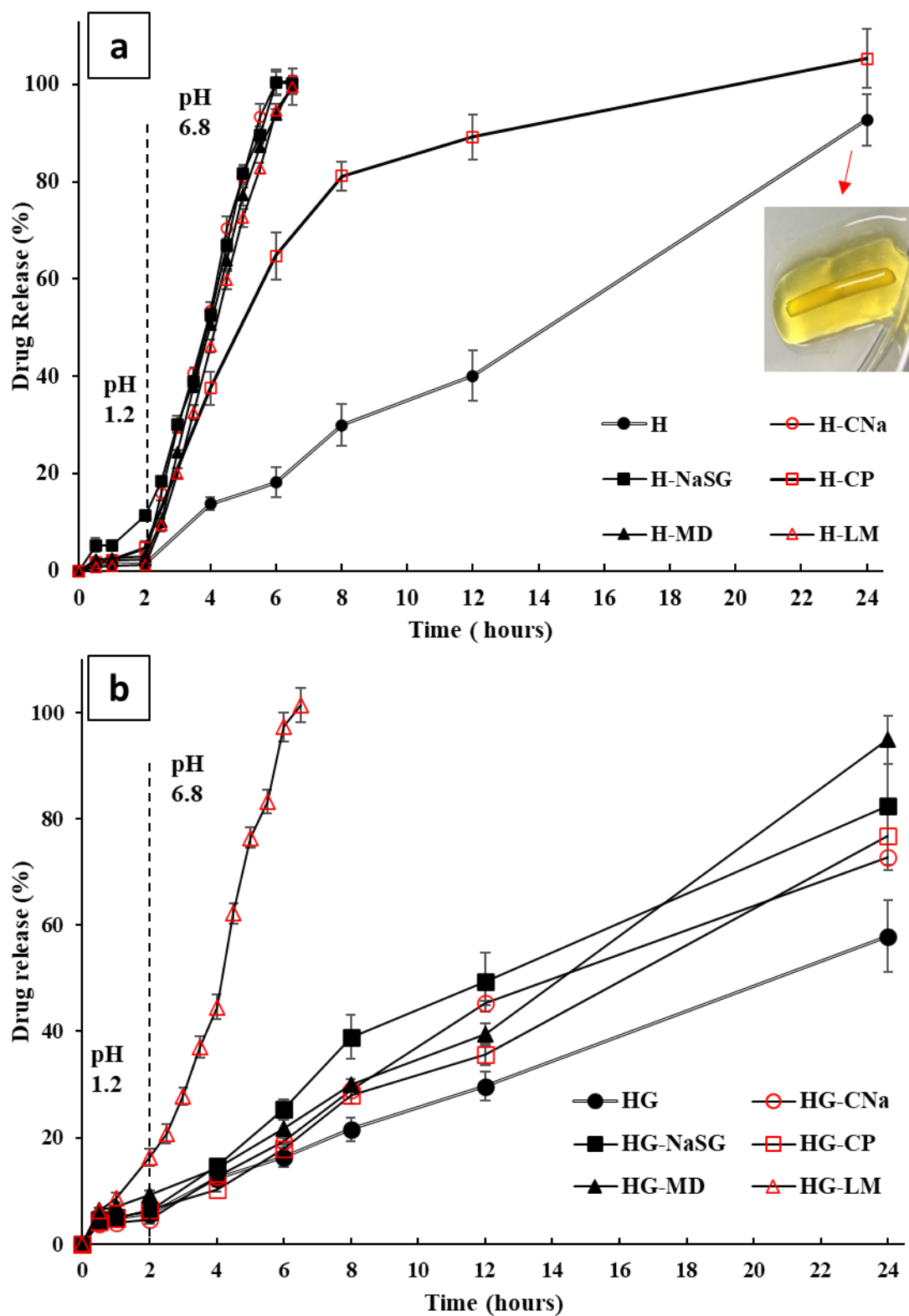


Figure 3.6: The 24-hour in vitro drug release of (a) CBZ-HPMCAS-additive ternary extrudates and (b) Gelucire-containing extrudates.

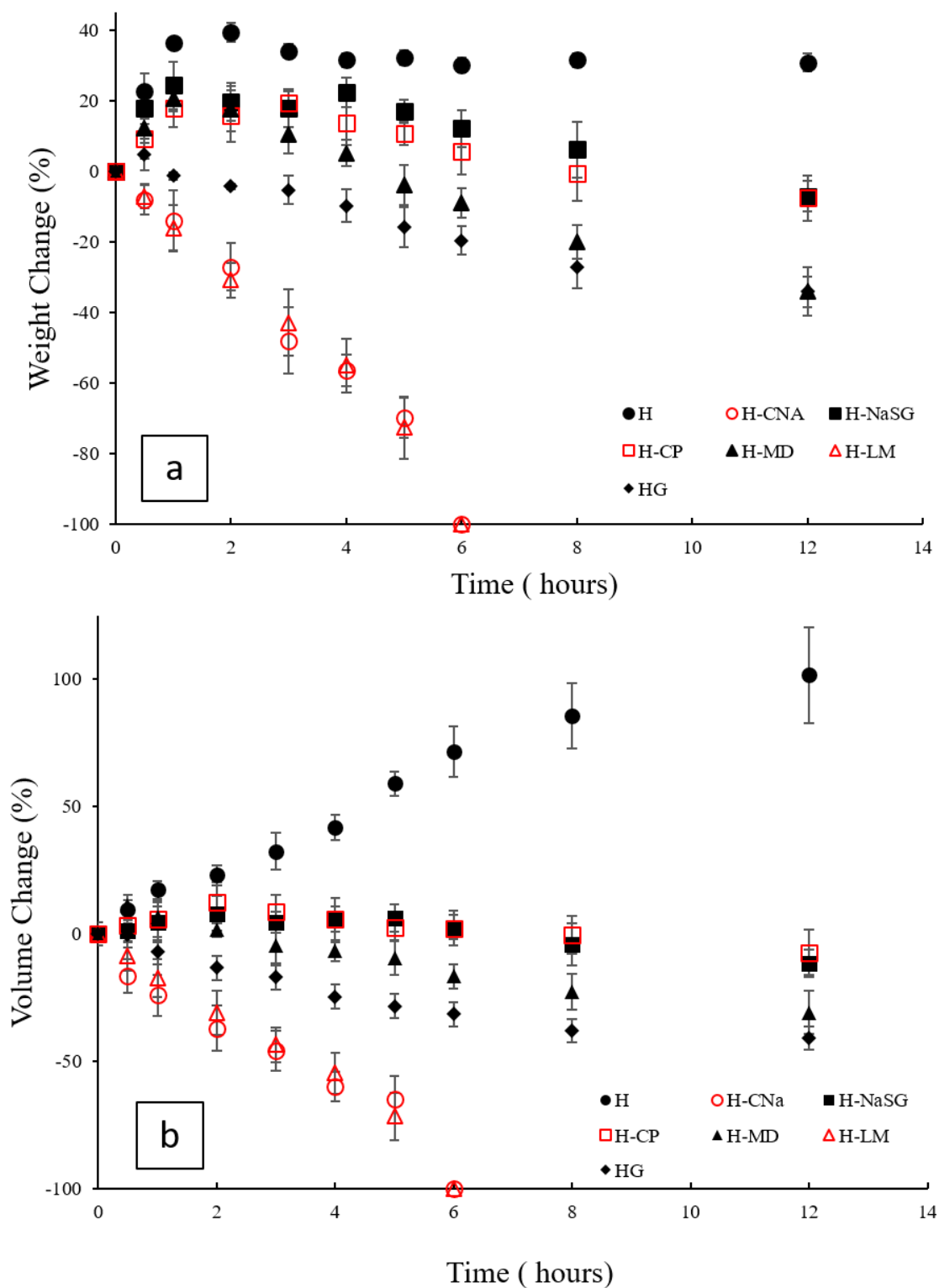


Figure 3.7: Swelling behaviour of the extrudates in pH 6.8 buffer measured in (a) weight and (b) volume.

Similar swelling behaviour of HPMCAS matrices was reported in the literature [196]. The slow erosion/dissolution of the swelled HPMCAS layer was thought to be caused by the drop in the local pH due to ionisation of the acid groups on the polymer. This resulted in the pH dropping below the threshold necessary for the dissolution of this polymer. [196]. However we would argue that when the succinate groups ionise at pH 6.8, they release hydrogen ions and become negatively charged. This should increase electrostatic repulsion which tends to lead to polymer-polymer repulsion and disentanglement and dissolution. To counterbalance this effect, the ionisation also can lead to a local increase in ionic strength and therefore an increase in shielding of the charges. Therefore, the effects generated from the local ionisation of the HPMCAS acid groups may not be as large as might be expected on a simple charge model. Therefore, whilst an argument about the effect of local pH may not fully explain the slow polymer relaxation, swelling and dissolution of the polymer, the concentration of ions locally due to ionisation may reduce charge-charge repulsion and result in a reduction of the rate of swelling and dissolution. When CBZ is added to the polymer, the amount of swelling increases compared to the placebo. The most likely cause of this is the increased free volume created by the inclusion of the drug enabling polymer disentanglement to occur more easily. Evidence for this is given by the decrease in T_g of the mixed system compared to the pure polymer.

3.3.2 Accelerating the drug release using low quantity additives

In order to explore the formulation strategies for accelerating the complete drug release from the extrudates from 24 hours to 12 hours, a range of additives with 5% (w/w) loading were blended in the formulation during HME. These additives are traditionally used as either disintegrants (CNa, NaSG, and CP) or diluent/pore formers (MD and LM) in oral dosage forms. It was hypothesised that the addition of these excipients could speed up the physical disintegration process of the extrudates, subsequently the drug release rate.

Single T_g s were detected for all ternary extrudates indicating the fully amorphous nature of the drug and polymer in the extrudates (Figure 3.8a and b) which is further confirmed by the PXRD (Figure 3.9a). The phase separation of the additives were not detected by the DSC, but suggested by the SEM (Figure 3.10) The ATR-FTIR data shown in Figure 3.9c show no significant changes of CBZ peaks in comparison to the HPMCAS-CBZ binary extrudates indicating that the addition of the additives had no effect on the intermolecular interactions between CBZ and HPMCAS. The DSC results indicate slight shifts in T_g to lower temperatures in comparison to the binary HPMCAS-CBZ extrudates. This may be ascribed to the increased the relative ratio of CBZ to HPMCAS (20:75 w/w)

in the ternary formulation than the binary system (20:80 w/w). From the SEM images shown in Figure 3.10, it can be confirmed that except H-CP, all other additives are phase separated from the HPMCAS-CBZ dispersion. Significant levels of porosity were observed in the cross-section of these ternary extrudates with the exception of H-CP. The underpinning mechanisms for the formation of the internal pores will be discussed in the next chapter.

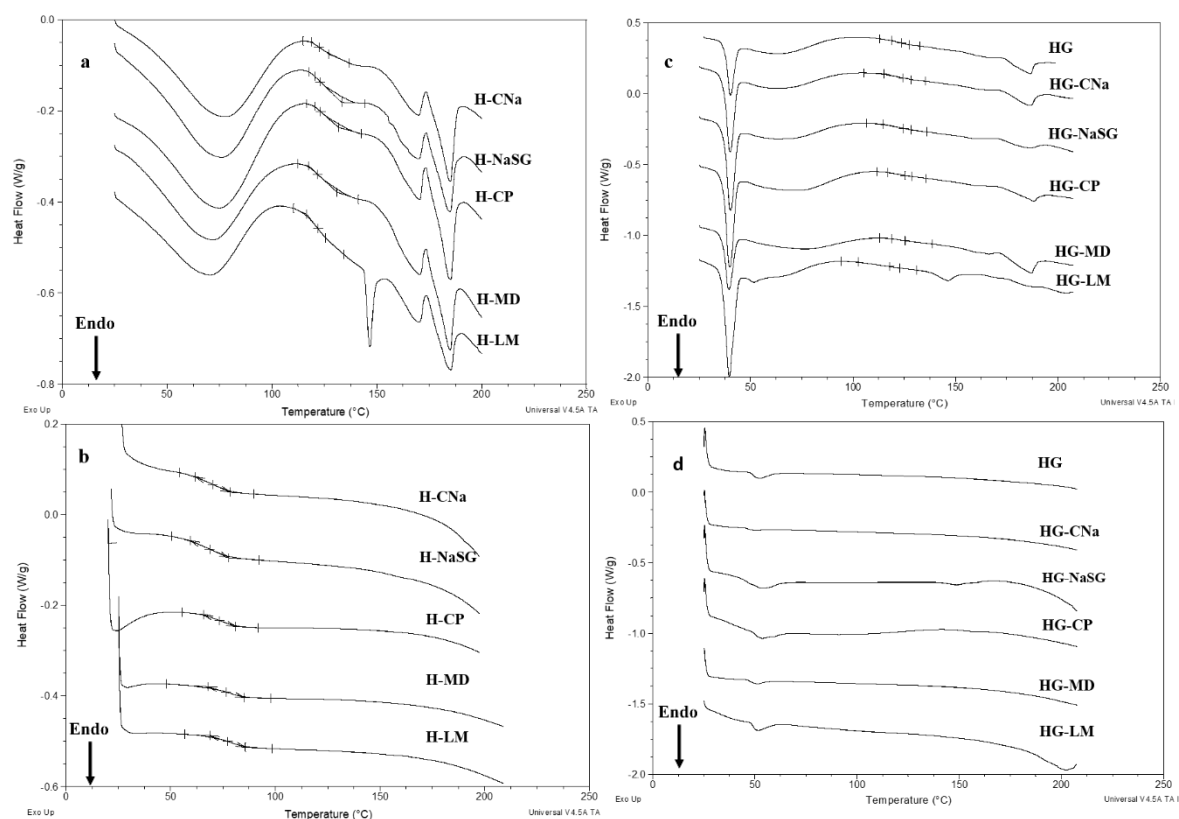


Figure 3.8: DSC thermograms of the (a) physical mixes and (b) HME extrudates of the CBZ-HPMCAS-additive ternary formulations; (c) physical mixtures and (d) HME extrudates of Gelucire-containing formulations.

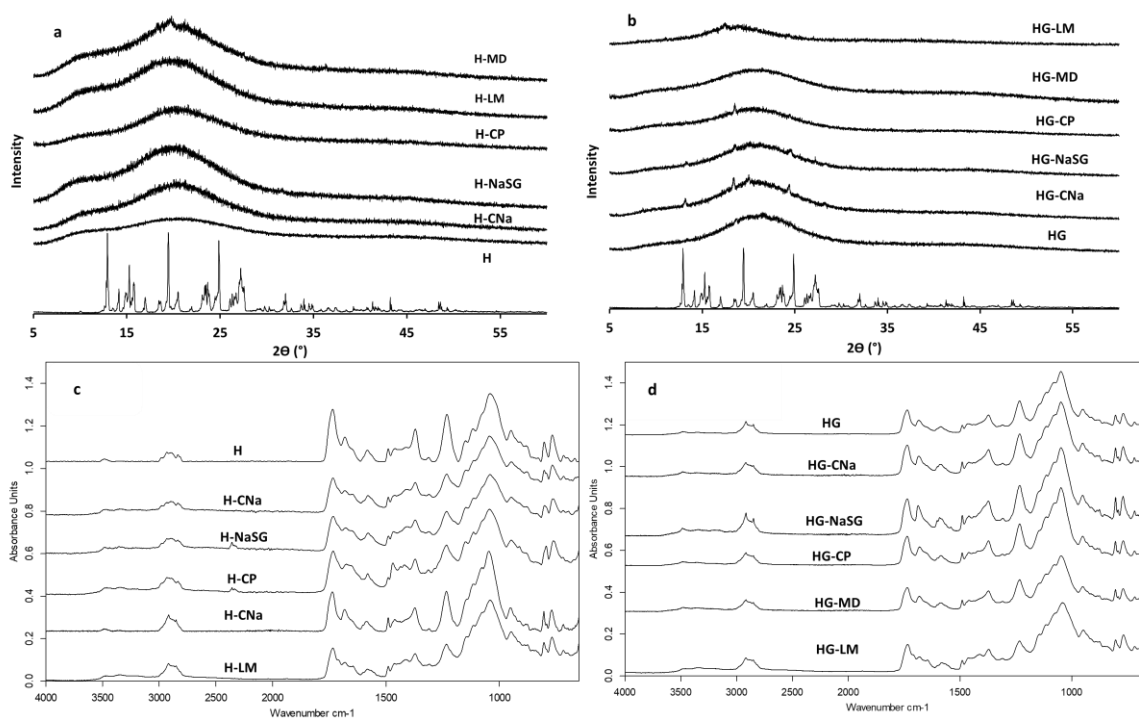


Figure 3.9: PXRD patterns of (a) the CBZ-HPMCAS-additive ternary extrudates and (b) the Gelucire-containing extrudates; the partial ATR-FTIR spectra of (c) the CBZ-HPMCAS-additive ternary extrudates and (d) the Gelucire-containing extrudates

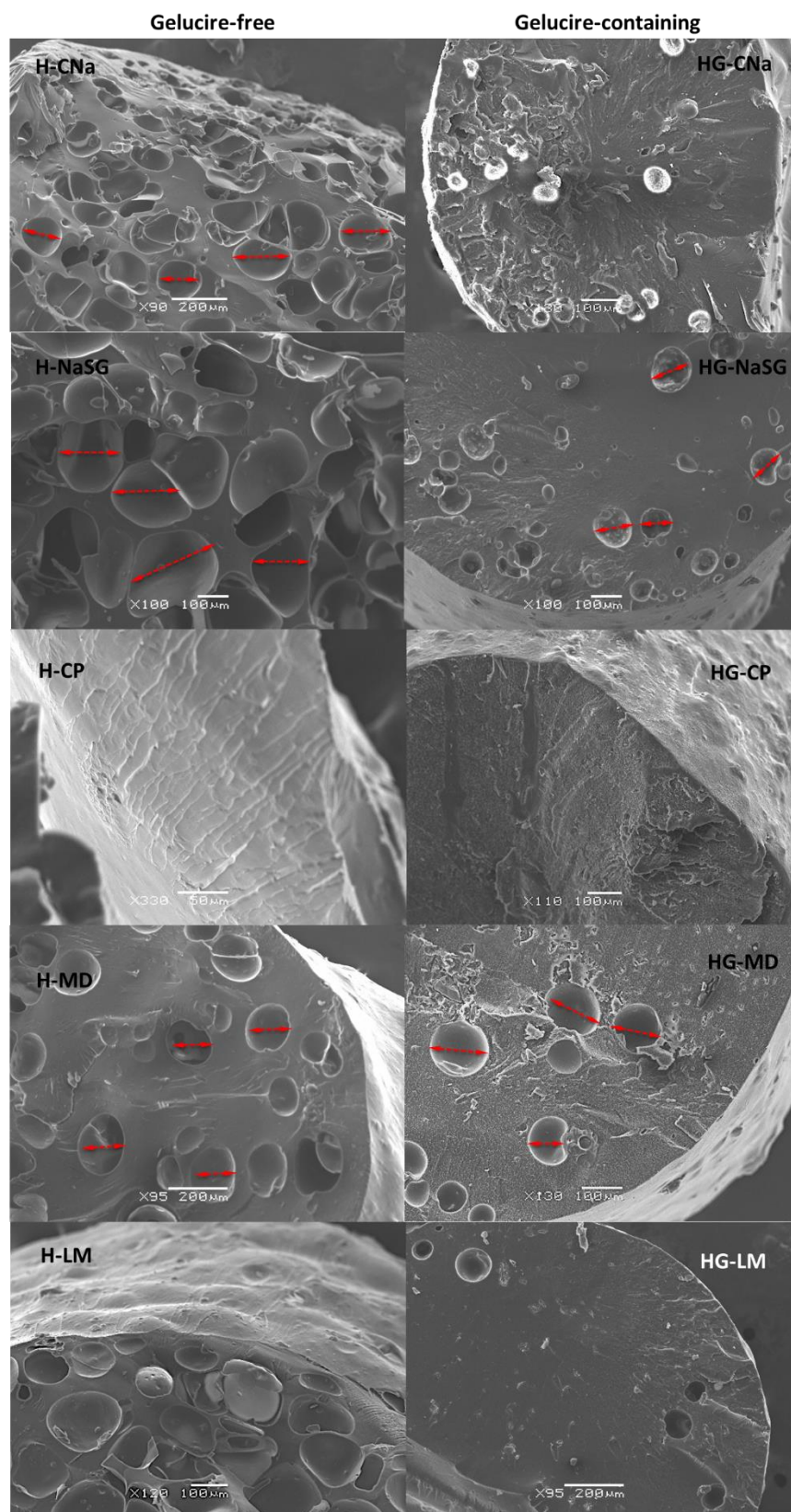


Figure 3.10: SEM images of the comparison of the cross-sections of the CBZ-HPMCAS-additive ternary extrudates and Gelucire-containing extrudates (freshly prepared by HME).

In comparison to the binary HPMCAS-CBZ extrudates (zero order release kinetics), shown in figure 3.7 and table 3.4, much faster drug release was achieved for all ternary extrudates that shifted the complete drug release from the extrudates from 24 hours to 6-12 hours. As seen in samples H-LM, H-CNa, H-NaSG and H-MD, good fits were achieved with both the zero-order release model and the Korsmeyer – Peppas power law, which was indicated by higher R^2 values of both models. The values of n higher than 0.89 revealed that the drug release mechanism shifted from pH-dependent swelling and relaxation to surface erosion (Table 3.4)[189, 190, 192]. H-CP was exceptional in that its release profile best fitted to a first order model and Korsmeyer – Peppas model with an R^2 value of 0.99 and an n value of 0.33, suggesting that the drug is released predominantly by Fickian diffusion. In this mechanism, the rate of solvent transport much higher than polymer relaxation, leading to rapid equilibrium of absorption at matrix surface, which results in time dependent process and follows first order kinetic [189, 191]. With 5% (w/w) addition of CP in the binary system, the change in T_g may be too subtle to be detected by DSC (Figure 3.8b). Therefore, it is difficult to use DSC to determine whether CP formed homogeneous molecular dispersion with HPMCAS and the drug. However, it is clear in the SEM images (Figure 3.10) that at least there is no micron scale phase separation in the H-CP extrudates. This continuous morphology of H-CP (in contrast to the highly porous interior of other formulations) may contribute to the difference in rate process. A homogeneously distributed soluble additive such as CP will enhance water absorption into the matrix and in dissolving will uniformly erode the matrix. However, if the material is not homogeneously distributed its swelling or dissolution will fracture the matrix or create pores filled with water.

Table 3.4: Fitting parameters of the in vitro drug release data of Gelucire-free and Gelucire-containing extrudates to (a) Zero-order, (b) First-order, (c) Higuchi and (d) Korsmeyer-Peppas.

	Zero Order R ²	First Order R ²	Higuchi R ²	Korsmeyer-Peppas R ²	<i>n-value</i>	Drug release mechanism
H	0.99	0.86	0.70	0.99	0.88	Case II transport (Zero order)
H-CNA	0.99	0.94	0.88	0.99	0.94	Super case II (Erosion)
H-NASG	0.99	0.91	0.86	0.97	0.90	Super Case II (Erosion)
H-CP	0.82	0.99	0.88	0.97	0.33	Fickian Diffusion
H-MD	0.99	0.93	0.85	0.99	1.02	Super case II (Erosion)
H-LM	0.99	0.93	0.83	0.98	1.10	Super case II (Erosion)
HG	0.98	0.94	0.92	0.99	0.74	Anomalous transport
HG-CNA	0.99	0.94	0.92	0.99	0.73	Anomalous transport
HG-NASG	0.99	0.90	0.94	0.99	0.68	Anomalous transport
HG-CP	0.98	0.97	0.88	0.99	0.84	Anomalous transport
HG-MD	0.99	0.92	0.86	0.98	0.89	Case II transport (Zero order)
HG-LM	0.95	0.81	0.68	0.98	1.24	Super case II (Erosion)

H-LM showed fastest release rate among all ternary extrudates. This could be caused by the local dissolution of the lactose particles which create high sugar solution in the pockets (which were previously occupied by lactose particles). This localised high sugar solution would generate high osmotic pressure which would tend to result in the faster ingress of water and consequent swelling of the lactose solution filled pockets thus contributing to the faster drug release from H-LM extrudates.

The results from the rotating basket method are confirmed by the UV imaging results. Using H-NaSG as an example, Figure 3.11 depicts the UV images obtained from the SDI2 instrumentation in both the UV and visible wavelength. The UV images in the UV region show no significant CBZ release in the pH 1.2 media for the binary extrudates. As seen in Figure 3.11, there is an increase in the CBZ release in the pH 1.2 media with the addition of NaSG to the extrudates. This agrees well with the approximately 5% release observed in the conventional dissolution test for H-NaSG within 1 hour of dissolution in pH 1.2 (Figure 3.6a). The red dashed lines in Figure 3.11 after the 2 h images are where the media change to pH 6.8 occurs. A change in the pH shows significant amounts of drug being released as a result of this pH shift. The results correlate well with Figure 3.6a where the incorporation of the NaSG brought about significant increases in the CBZ release in pH 6.8.

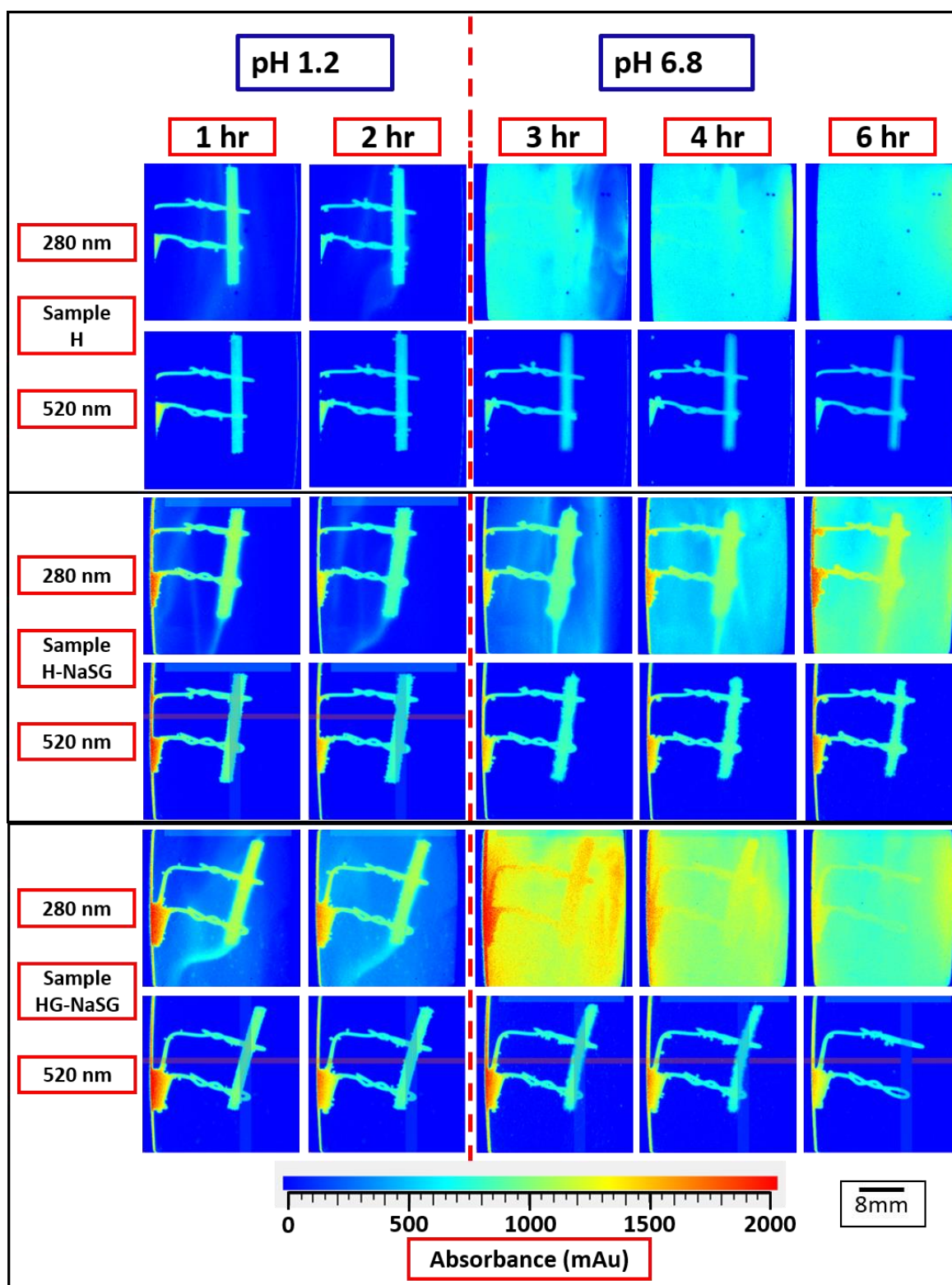


Figure 3.11: False coloured SDI2 images for the HME extrudates (H, H-NaSG, and HG-NaSG) obtained from the SDI2 instrument when the dissolution tests were performed in pH 1.2 for the first 2 hours and in pH 6.8 from 2-6 hours. Images depict CBZ release and swelling using UV and Vis wavelengths at 280 nm and at 520 nm, respectively.

Little erosion was observed in the binary extrudate of HPMCAS-CBZ in both media. Figure 3.12a showed there was hardly any swelling to occur for the binary extrudate in

pH 1.2. The introduction of the pH 6.8 brought about the swelling of the filament (Figure 3.12a). This was also evident in Figure 3.12b which is a zoomed in image of the self-same extrudate in pH 6.8 (after 60 min in the pH 6.8 media). This showed an increase in swelling to occur due to the media ingress into the extrudate and it was also possible to visualise the gel layer. The incorporation of NaSG into the formulation brought about changes in the swelling at pH 1.2 when compared with the binary filament (Figure 3.12a). This may be attributed to the porosity of the H-NaSG which encourage rapid water uptake into the extrudates. The extrudate continued to swell to a greater extent in pH 6.8 till after ~180 min when extrudate degradation can be observed. This continues to occur as can be visualised from Figure 3.12c (zoomed in image after 180 min in pH 6.8 showing the gradual extrudate degradation). The filament continues to degrade past its normalised size (orange circle in Figure 3.12a).

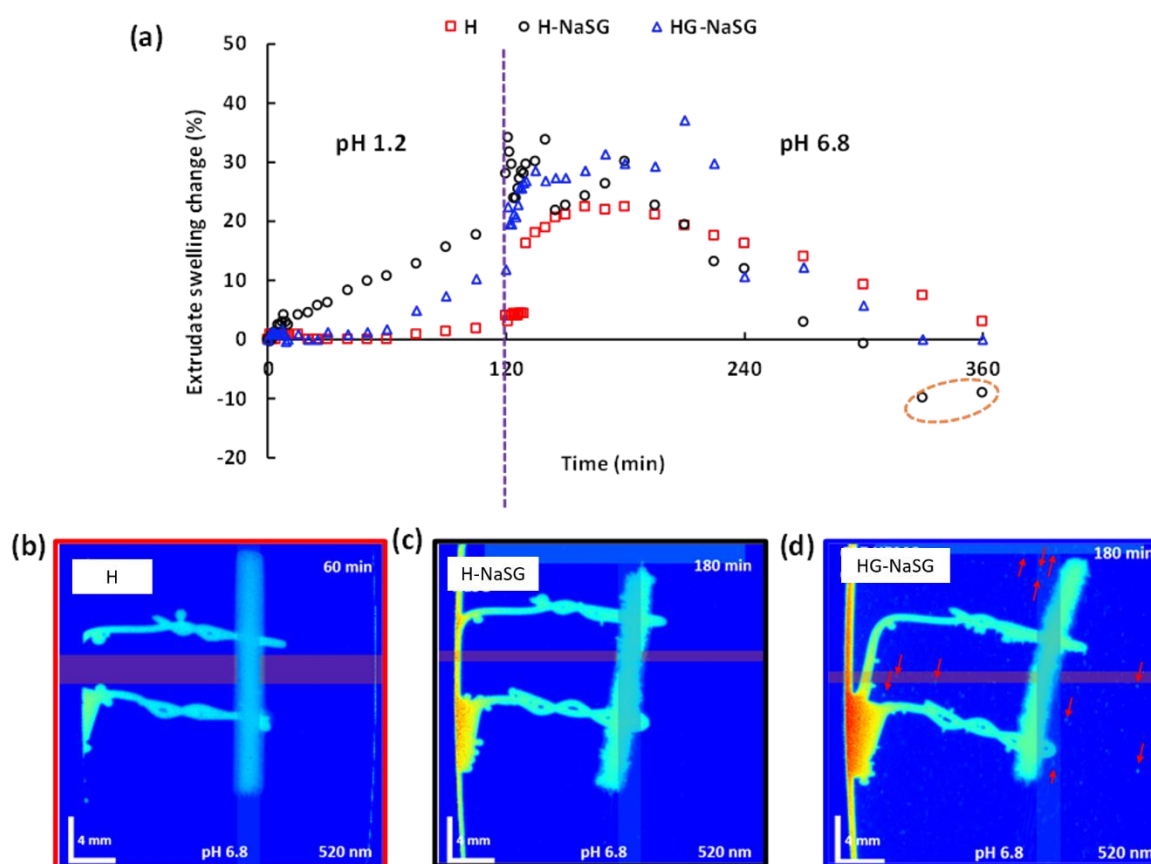


Figure 3.12: Normalised swelling measurements for the HME extrudates (H, H-NaSG and HG-NaSG) in (a) pH 1.2 with a pH shift to pH 6.8 obtained from the SDI instrument at 520 nm. False-coloured SDI2 swelling images for (b) the H extrudate after 60 min in pH 6.8 showing the gel layer due to media ingress; (c) the H-NaSG extrudate after 180 min in pH 6.8 showing the degradation as a result of the incorporation of NaSG; (d) the HG-NaSG extrudate after 180 min in pH 6.8. The disintegrated extrudate particulates can be visualised in the media (as highlighted by the red arrows) and may have contributed to the extended release of CBZ seen in Figure 5 (b).

3.3.3 Sustaining the drug release using lipid additives

Gelucire 50/13 is one of the Gelucire group of self-emulsifying excipients often used in oral preparations. Gelucire 50/13 has been reported to exhibit significant water uptake and gel forming ability. [197]. It has been co-extruded with polymers for forming solid dispersions for taste masking and modified release applications [70, 143, 198]. It was selected to blend with HPMCAS in this study to modify the swelling behaviour of the HPMCAS matrices and allow further prolonged release of CBZ. As seen in Figure 3.8, with a small amount of Gelucire remains phase separated as shown by the small residual melting peak in the DSC. Small amounts of crystalline Gelucire are also evident in the PXRD results shown in Figure 3.9b. As with the ternary extrudates, the ATR-FTIR spectra of Gelucire-containing extrudates show no shifts of the signature IR peaks of amorphous CBZ and HPMCAS indicating that the addition of Gelucire had no effect on the state of the drug and the interaction between CBZ and HPMCAS in the extrudates and that no specific interaction with Gelucire is evident.

As seen in Figure 3.6b, with the exception of the HG-LM, all the samples containing Gelucire show a much slower release profile than the samples without Gelucire. All drug release data were best fitted by Zero order and Korsmeyer - Peppas models with higher R^2 values. n -values of HG, HG-CNa, HG-NaSG and HG-CP are in the range of $0.45 < n < 0.89$, which is usually associated with the anomalous transport as a drug release mechanism, governing by both diffusion and swelling (Table 3.4). Comparing to fickian diffusion, the rate of swelling and diffusion are comparable in anomalous transport [189, 192]. HG-MD and HG-LM showed an n value of 0.89 and 1.24 fitted ($R^2 = 0.98$), indicating case II transport and super case II that corresponded to zero order release and surface erosion, respectively.

HG-LM was exceptional in that its rate was very similar to that of the corresponding sample without Gelucire indicating that for this excipient the nature of the excipient itself determined the rates of release. Whereas for the remainder the presence of Gelucire was the determinant of the release rate. With the exception of the HG-LM sample, the volumes increased in linear fashion but the weight, although increasing, tended to level off at longer times indicating that some erosion may be taking place.

The slow hydration of the placebo is consistent with the results seen for the samples without Gelucire and is likely to be due to the same action of CBZ in increasing the free volume of HPMCAS thus enabling easier disentanglement.

In contrast to the ternary extrudates without Gelucire, which dissolved through surface erosion, the Gelucire-containing extrudates (except HG-LM) all show similar rates of the continuous swelling (Table 3.6). These were up to 450-650% by 24 hours, implying that the addition of the low quantity additives had a minimal effect on the matrices. The SEM images shown in Figure 3.10 reveal the much less porosity at the surfaces of the Gelucire containing extrudates in comparison to the Gelucire-free extrudates.

HG-NaSG was used as an example to further study the impact of Gelucire 50/13 on the drug release behaviour. The UV (280 nm LED) and visible (520 nm LED) were used to simultaneously measure the CBZ release and swelling from the binary extrudates formulated with Gelucire and NaSG (HG-NaSG). The images in Figure 3.11 suggest the incorporation of Gelucire further increases CBZ release in the pH 1.2 media in comparison to H-NaSG (approximately 7% within 1 hour in pH 1.2). The order for drug release from the extrudates therefore in pH 1.2 prior to the pH shift to 6.8 was $H < H\text{-NaSG} < HG\text{-NaSG}$. This agrees well with the dissolution data for the first 2 hours in pH 1.2 (Figure 3.6). In terms of the trend of the swelling behaviour of the extrudates, the trend is $H < HG\text{-NaSG} < H\text{-NaSG}$. The addition of Gelucire increased the swelling of the extrudates in pH 1.2 in comparison to binary extrudates but reduced the swelling when it is compared to H-NaSG (Figure 3.12a). This agrees well with the swelling data of the extrudates tested under conventional rotational basket dissolution condition Table 3.5 and 3.4.

Table 3.5: Weight and volume change (%) of Gelucire-free extrudates.

WEIGHT CHANGE %						
TIME (HOURS)	H	H-CNa	H-NaSG	H-CP	H-MD	H-LM
1 (1.2 PH)	0.57	-0.66	-2.33	-0.47	-1.66	-2
2 (1.2 PH)	0.86	-1.33	-4.1	-1.19	-3.33	-3.66
0.5 (6.8 PH)	18.97	-11.19	-2.61	-1.22	-5.63	-18.60
1	49.10	-26.68	-15.795	-7.71	-13.15	-49.63
2	86.07	-38.92	-35.07	-16.11	-34.23	-60.68
3	118.39	-53.74	-55.94	-28.68	-55.35	-75.98
4	145	-68.35	-73.50	-37.77	-76.04	-85.53
5	156.60	-100	-100	-46.37	-100	-100
6	167.85			-58.04		
8	199.28			-72.72		
12	281.14			-100		
24	601.98					
VOLUME CHANGE %						
1 (1.2 PH)	0.020	-0.95	-1.51	-0.73	-1.85	-1.10
2 (1.2 PH)	0.020	-1.86	-3.55	-1.49	-3.64	-3.26
0.5 (6.8 PH)	21.74	-6.65	-8.19	-2.08	-9.23	-6.52
1	36.25	-20.35	-16.97	-6.89	-33.93	-13.67
2	56.62	-32.25	-46.42	-13.19	-58.85	-47.43
3	99.20	-43.05	-61.07	-20.77	-74.16	-72.53
4	116.15	-60.26	-76.66	-28.44	-84.68	-86.63
5	142.57	-100	-100	-40.20	-100	-100
6	173.73			-50.77		
8	213.96			-65.82		
12	297.34			-100		
24	768.24					

Table 3.6: Weight and Volume change (%) of Gelucire-containing extrudates.

WEIGHT CHANGE %						
TIME (HOURS)	HG	HG-CNa	HG-NaSG	HG-CP	HG-MD	HG-LM
1 (1.2 PH)	3.05	2.78	4.17	5.69	4.45	- 2.33
2 (1.2 PH)	4.45	5.83	9.90	10.8	10.41	- 6.4
0.5 (6.8 PH)	36.53	17.02	15.78	42.10	38.77	-1.52
1	62.32	38.37	51.68	85.96	85.71	-4.71
2	106.73	114.59	113.15	116.49	132.65	-29.22
3	149.03	185.40	178.94	145.61	168.16	-54.26
4	184.84	237.29	226.31	185.96	221.83	-67.72
5	249.23	258.67	263.10	219.29	267.77	-77.93
6	292.30	302.70	307.34	256.14	344.89	-100
8	369.23	375.67	342.10	301.75	404.08	
12	401.92	437.02	436.84	340.35	453.06	
24	557.69	616.21	507.89	645.61	638.77	
VOLUME CHANGE %						
1 (1.2 PH)	2.13	3.95	4.99	4.84	5.60	-1.37
2 (1.2 PH)	6.06	10.09	10.42	12.42	11.58	-5.88
0.5 (6.8 PH)	5.06	4.46	2.31	6.15	5.47	-6.38
1	19.64	21.41	8.82	13.78	15.85	-15.55
2	43.70	34.50	17.56	26.01	27.09	-36.24
3	76.19	57.10	29.84	38.07	39.59	-54.03
4	99.80	71.79	57.65	69.46	67.28	-63.83
5	137.85	91.05	75.20	84.62	90.7	-78.94
6	177.24	111.70	108.15	102.33	138.02	-100
8	273.55	192.10	157.05	171.70	197.41	
12	382.83	291.92	228.18	261.88	353.50	
24	715.84	534.06	502.85	693.17	902.03	

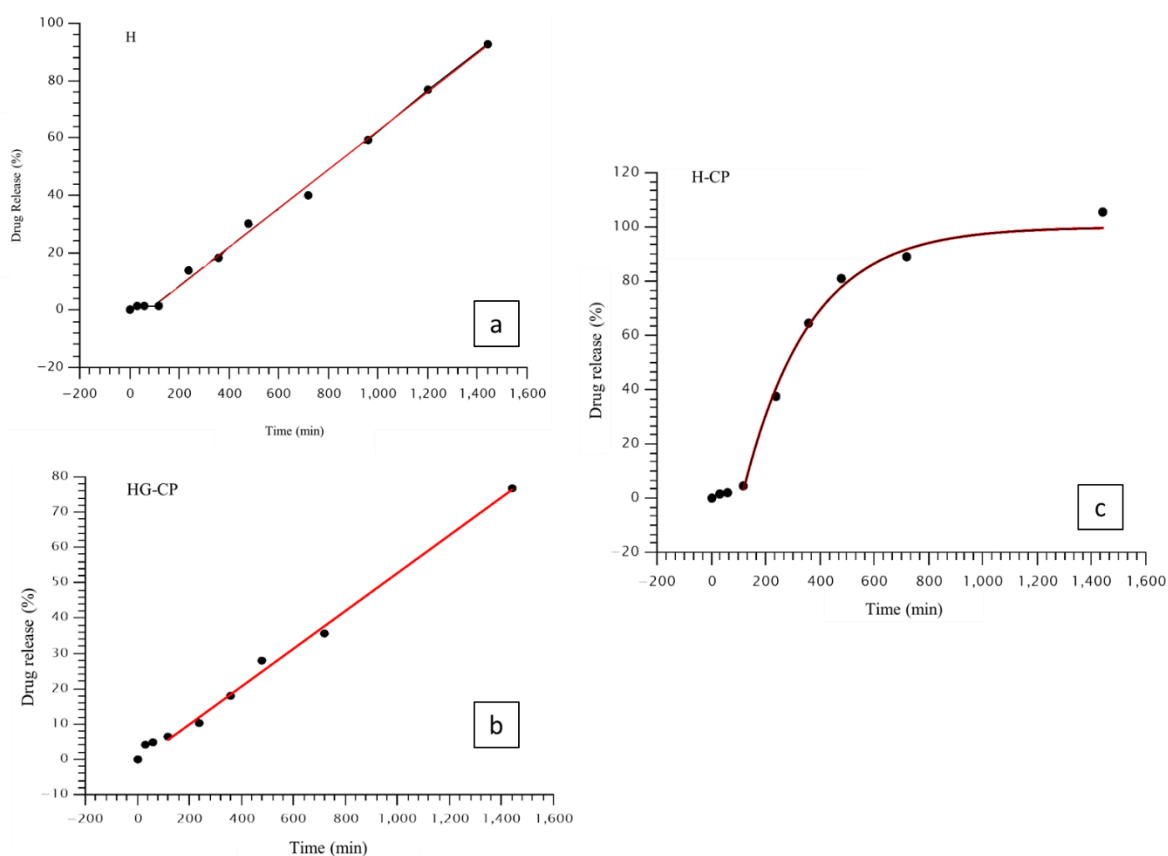


Figure 3.13: Examples of the fitting plots that show different release kinetics: (a) Zero-order release kinetics of H; (b) zero-order release kinetics of HG-CP; (c) first-order release kinetics of H-CP

The change to pH 6.8 as evidenced in the UV images at 280 nm suggests much faster drug release and disintegration of the HG-NaSG extrudates when tested using SDI2 apparatus than the results obtained using the conventional dissolution test. It was interesting to note the changes to the extrudates in the visible wavelength of 520 nm: clear rapid initial swelling was seen in HG-NaSG up to 2 hours after the pH change to 6.8. After 2 hours in pH 6.8, the rapid disintegration of the extrudates into fragments starts to occur. Figure 3.12d shows particulates of the filaments in the media using the 520 nm LED depicting further degradation of the extrudates. This may have contributed to the significantly faster CBZ release observed in the SDI2 experiments. It is however important to note that the hydrodynamics of this miniaturised flow cell dissolution system (~70 ml volume with constant lamellar flow at 8.2 ml/min) is different to that of the standard dissolution system (900 ml with rotational basket) which may lead to differences observed with drug release behaviour. As the sample swells the polymer chains will disentangle and the mechanical strength of the sample will decrease. If the hydrodynamic regime is such that the pressure differences across the sample or the drag forces acting on it are sufficient to cause mechanical disruption, then fragmentation and erosion will

follow. In the flow cell this appears to be the case but not in the rotating basket. In addition, the custom-made sample holder may also apply additional mechanical strain to the swelled extrudates and contribute to the disintegration of the integrity of the structure. These results also highlight the importance of hydrodynamic effects on the in vitro drug release results and more in depth investigation is undergoing.

3.4 Conclusion

This study proposed the use of HME to directly manufacture controlled release oral formulations. HPMCAS-LF showed good potential for being used as the matrix excipient for monolithic controlled release formulations. As binary formulations, CBZ-HPMCAS extrudates showed zero-order controlled release of CBZ over 24 hours. The intermolecular interactions (most likely to be either van der Waals or hydrophobic interactions which were not detected by IR) between CBZ and HPMCAS and the microenvironments are responsible for the sustained release of CBZ. The release rate of the HME extrudates could be accelerated by the incorporation of low quantities (5% w/w) of additives and sustained further by adding lipid excipient, Gelucire 50/13. The highly water-soluble additive, lactose, led to rapid water penetration and erosion of the extrudates resulting in a faster drug release rate than the CBZ-HPMCAS binary extrudates. Clear phase separation of the disintegrants including NaSG, CNa, MD and LM in the extrudates led to higher interior porosity and quicker erosion in these matrices in comparison to the binary extrudates. The gel-forming ability of Gelucire, which is also phase separated in the extrudates, provided the substantial swelling capability of the extrudates and further prolongation of the drug release. UV imaging was also able to provide direct visualisation and further insights into the simultaneous drug release and swelling/erosion phenomena occurring. This study thus provides clear formulation strategies for modulating the drug release rate from controlled release formulation prepared directly by HME.

**An investigation into the formations of
the internal microstructures of solid
dispersions prepared by hot melt
extrusion**

Chapter 4

4.1 Introduction

Hot melt extrusion (HME) has been increasingly used in the large-scale manufacturing and lab research of producing amorphous solid dispersions. In addition to the active pharmaceutical ingredient and the matrix polymer, additives such as plasticizers are often used in HME formulations. Most plasticizers are miscible with the polymer, thus can form a single-phase amorphous dispersion [26, 199-201]. However, recently a number of studies reported the use of additives, such as disintegrants and other particulate excipients that form a separate phase to the drug dispersion [75, 202-207]. Occasionally, voids were observed in extrudates [75, 202, 207-210]. We specifically term such structural features as voids rather than pores because they typically are isolated pockets in the interior of the extrudates and they are not, in most cases, apparent on the surface of the extrudates. The formation of such voids in the extrudates can potentially have significant impact on the physical stability and drug release performance due to their high internal surface area. As an example, in our previous study, a range of additives was used to modulate the drug release rate of HME extrudates containing carbamazepine (CBZ). With 5% w/w loading of these additives, the extrudates exhibited cavitated internal void microstructure [75]. It was observed that the extrudates with cavitated interiors exhibited accelerated release rates in comparison to the binary polymer-drug solid dispersion [75]. Therefore, a fuller understanding of why such voids form and how to control them is important to the field of pharmaceutical HME. To the best of our knowledge, there is no study in the literature that has systemically investigated the origin of formation of such internal void structures. The aim of this study was to use a range of model systems to systemically address this question with a clear focus on examining the factors that could induce the formation of such cavitated internal microstructure.

It is hypothesised that voids in the extrudate are formed by bubbles that are held in place when the extrudate solidifies. The bubbles may be formed either by nucleation by residual particles (as the nuclei) in the extruding material or by evaporation of water from water containing particulates. The stability of the bubbles and their survival as cavities will depend on the conditions of extrusion. This study report the detailed investigation into the factors that affect the formation of the voids which leads to our hypothesis of the origin of these voids. The factors studied include the effect of the types of the materials (i.e. drug, polymer and additive) used in the formulation, the quantity of the drug and the additives used, the key extrusion processing parameters, the type of extruder, and the

drying of the raw materials prior to extrusion. The results bring new insights into the control strategies of void formation in the pharmaceutical HME extrudates.

4.2 Materials and methods

4.2.1 Materials

Carbamazepine (CBZ) and felodipine (FDN) were purchased from Molecula (Darlington, UK). According to the melting point (193 °C) and the PXRD diffraction pattern, the crystalline CBZ used for the extrusion experiments is the polymorphic form III [100, 108]. Hydroxypropyl methylcellulose acetate succinate (HPMCAS-LF) with the substituent ratios of $-\text{CH}_3$, $-\text{CH}_2\text{CH}(\text{CH}_3)\text{OH}$, $-\text{COCH}_3$, and $-\text{COCH}_2\text{CH}_2\text{COOH}$ being 1.87, 0.25, 0.48, and 0.37 average number/glucose ring unit was donated by Shin-Etsu Chemical Co. Ltd. (Tokyo, Japan). Poly(vinyl)caprolactam–poly(vinyl)acetate–poly(ethylene)glycol graft co-polymer (Soluplus®), dimethylaminoethyl methacrylate–co-polymer (Eudragit® E PO) and sodium starch glycolate (NaSG) were received as generous gifts from BASF (Ludwigshafen, Germany), Evonik (Darmstadt, Germany) and Roquette (Lestrem, France), respectively. Gelucire 50/13, crosscarmellose sodium (CNa) and Crosspovidone (Polyplasdone-XL) (CP) were supplied by Gattefossé (Saint-Priest, France), IMCD UK Ltd (Sutton, UK) and Ashland (Limavady, UK), respectively. Maltodextrin (MD) and α -lactose monohydrate were purchased from (Sigma Aldrich, UK).

4.2.2 Preparation of HME filaments

All formulations listed in Table 4.1 (except H-NaSG (EL)) were prepared using a co-rotating twin screw Haake Minilab extruder (Thermo Fisher, Karlsruhe, Germany). The composition of the formulations used for each formulation were summarised in Table 1. All HME formulations were extruded at 150 °C with 5 min retention time and at a screw speed at 100 rpm. Clear effects of the process and the addition of NaSG on the void formation were observed for H-NaSG formulation. Therefore H-NaSG is the base formulation of this study and was used to compare the impact of the screw speed and the different scales of extruders on the void formation. When the effects of screw speed on the void formation were studied, 50 and 150 rpm screw speed were also used to extrude H-NaSG formulation. The average extrusion torque value during the retention period was recorded for each experiment. 10 grams of the materials were accurately weighed then

premixed using mortar and pestle for 5 minutes. For each extrusion experiment, 7 g of the powder mixture was fed manually into the extruder.

In order to investigate the impact of the extruder on the void formation, a larger scale extruder (EuroLab 16, Thermo Fisher, Darmstadt, Germany) was used to extrude the H-NaSG (EL) formulation at a screw speed of 100 rpm and the detailed processing parameters are shown in Table 4.2. A circular die of 1.75 mm diameter was used and the extruded strands were guided onto a conveyer belt and collected continuously.

Table 4.1: Ingredients and hot melt extrusion screw speed of the formulations investigated in this study

FORMULATION CODE	HPMCAS (% W/W)	CBZ LOADING (% W/W)	ADDITIVES (% W/W)	GELUCIRE 50/13 (% W/W)	TOTAL WEIGHT (mg)
H	100	-	-	-	50
HG	80	-	-	20	50
H20	80	20	-	-	50
HG20	60	20	-	20	50
H-NASG	75	20	5 (NaSG)	-	50
H-NASG (EL)*	75	20	5(Na SG)	-	50
HG-NASG	60	20	5 (NaSG)	15	50
H30	70	30	-	-	33.3
H-NASG30	65	30	5 (NaSG)	-	33.3
H50	50	50	-	-	20
H-NASG50	45	50	5 (NaSG)	-	20
H-CP	75	20	5(CP)	-	50
HG-CP	60	20	5 (CP)	15	50
H-CNA	75	20	5 (CNa)	-	50
HG-CNA	60	20	5 (CNa)	15	50
H-LM	75	20	5 (LM)	-	50
HG-LM	60	20	5 (LM)	15	50
H-MD	75	20	5 (MD)	-	50
HG-MD	60	20	5 (MD)	15	50
H-2NASG	78	20	2 (NaSG)	-	50
H-7NASG	73	20	7 (NaSG)	-	50

SOL-30	70 (Soluplus)	30	-	-	33.3
SOL-50	50 (Soluplus)	50	-	-	20
EPO-30	70 (EPO)	30	-	-	33.3
EPO-50	50 (EPO)	50	-	-	20
H-FDN	75	20 (FDN)	5	-	50

*This sample prepared on the Eurolab 16 extruder

Table 4.2: Temperature settings of the extrusion process using Eurolab 16

HME ZONES	1	2	3	4	5	6	7	8	9	10
°C	25	50	80	130	150	150	150	150	150	150

4.2.3 Materials characterisation

4.2.3.1 Thermogravimetric analysis (TGA)

TGA 5500 discovery series (TA Instruments, Newcastle, USA) was used to test the moisture content of the raw materials prior to the extrusion experiments. 5–7 mg of each ingredient were loaded into the instrument and a temperature program of 10 °C/min was used. Trios (TA Instruments, Newcastle, USA) software was used to analyse the acquired results.

4.2.3.2 Powder X-ray diffraction (PXRD)

XRPD was performed to determine the crystallinity of raw materials, physical mixtures, and extruded formulations using a Thermo ARL Xtra X-ray diffractometer (Thermo Scientific, Switzerland) operated with CuK α radiation, generator voltage at 45 kV and the current was 40 mA. The angular scan range of 5 – 60° was operated with a (2 θ) scan type, 4 s/step scanning rate and the step size was 0.01°.

4.2.3.3 Differential scanning calorimetry (DSC)

The DSC experiments were carried out using a TA Universal Q2500 Discovery series DSC (TA Instruments, Newcastle, DE, United States) to characterise the raw materials and HME extrudates. A heating rate of 10 °C/min was used from 25 to 210 °C with 50 ml/min nitrogen purge flow. The sample weights in the range of 2-3 mg were used for all

samples. TA standard crimped pans and lids were used for all measurements as well as Trios software for analysing the obtained results.

4.2.3.4 Scanning electron microscopy (SEM)

Zeiss EVO HD15 Scanning Electron Microscope built with Lanthanum Hexaboride LaB₆ emitter (Zeiss Microscopy GmbH) and JSM 5900LV Field Emission Scanning Electron Microscope (Jeol Ltd., Japan) equipped with a tungsten hairpin electron gun were used to study the surface microstructure of the formulation extrudates. The samples were coated with gold using a Polaran SC7640 sputter gold coater (Quorum Technologies, city, country) prior to imaging.

4.2.3.5 X-ray microcomputed tomography (X μ CT)

X-ray microcomputed tomography (X μ CT) measurements were performed on the different extrudate samples using a Skyscan 1172 instrument (Bruker, Antwerp, Belgium) to investigate their microstructure characteristics and to visualise the distribution of the different ingredients, such as the additive particles, in the extrudates. The X μ CT measurements were conducted using a cone-beam configuration without applying any filter. The 3D imaging of the sample was performed by rotating the sample over 180° with an angular rotation step of 0.4° and collecting the shadow projected images of the sample at an isotropic voxel resolution of 4.46 μ m and an exposure time of 350 ms. 7 frames were averaged per position. Reconstruction of the projected images was then conducted using NRecon software (Bruker, Version: 1.7.4.2) to acquire cross-sectional images of the different extrudate samples. DataViewer software (Bruker, Version: 1.5.3.4) was used to visualise and align the reconstructed images of the samples. The reconstructed images were further analysed using Avizo software (FEI Company, Hillsboro, Oregon, USA, Version: 9.4.0) to create 3D models of the extrudate samples. ImagJ software version 1.52e was also used to measure the pore/void diameter using the reconstructed images of the extrudate samples. For each formulation, two separate samples were tested and the X μ CT data were collected and analysed.

4.2.3.6 *In vitro* drug release studies

All *in vitro* drug release studies were carried out using the USP rotating basket method (Copley CIS 8000, Copley Scientific) under sink conditions operating at 100 rpm rotation speed with 900 mL of either HCl dissolution medium (pH 1.2) or pH 6.8 phosphate buffer

saline (PBS) maintained at 37 ± 0.5 for each test. Two-stage experiments were performed for all dissolution tests to mimic the physiological environment of gastro-intestinal tract. After 2 hours of dissolution in HCl at pH 1.2, the extrudates were removed and the dissolution medium was changed to PBS at pH 6.8. Accurately weighted extrudates containing approximately of 10 mg of CBZ were used in 900 ml medium to ensure sink conditions. 3 ml of the dissolution media were withdrawn from each vessel and filtered through 0.45 μm filters (Minisart Sartorius, Goettingen, Germany) and sampled at predetermined time intervals. After each sampling, 3 ml of fresh pre-warmed media were replenished to the dissolution vessel. The samples were analysed using a UV–VIS spectrophotometer (PerkinElmer Lamda XLS, USA) at 285 nm. All measurements were performed in triplicate. The measured absorbance values at different time intervals were converted to concentration values using the calibration curves described in Chapter 3.

4.2.3.7 Statistical analysis

Statistical analysis was conducted using Graphpad Prism 7 statistical analysis software by the independent Student's T test for comparison of two groups, and one-way ANOVA for multiple groups. All the data are presented as the mean \pm SD. P values of < 0.05 were considered statistically significant. In all the figures *** is used to indicate $P < 0.001$, ** is used to indicate $P < 0.01$, and * is used to indicate $P < 0.05$.

4.3 Results and Discussion

4.3.1 The formation of the interior void structure in HME extrudates

As seen in Figure 4.1, except the H-CP and its placebo extrudates, the rest of the formulations all exhibit an interior with voids. From the previous study, it was confirmed by the DSC results that CP is miscible with HPMCAS and CBZ (with 20% drug loading) and forms a single-phase solid dispersion after HME [75]. As seen in Figure 4.1, the phase separated additive particles can be identified in both placebo and drug loaded extrudates containing CNa, NaSG, LM and MD. However, it is obvious that without the addition of CBZ, the placebo extrudates are either void-free or have much lower density and smaller sized voids than the CBZ loaded extrudates.

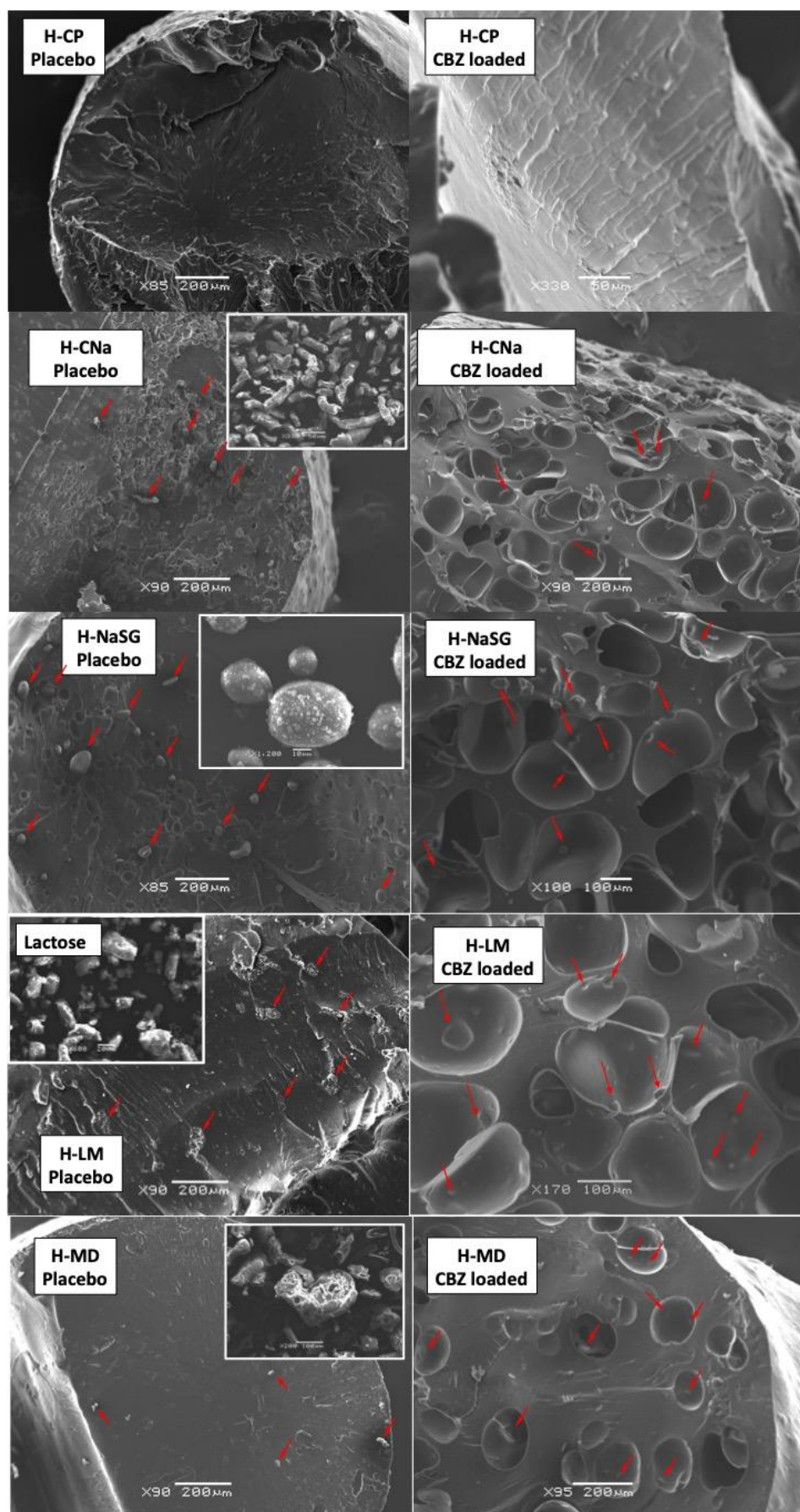


Figure 4.1: SEM images of the cross-sections of the samples showing the effects of additives on the void formation in the interior of the extrudates. (The additive particles are highlighted by the red arrows in each image)

X μ CT allows the detection of the additive particles when they contain either Na or Ca, which have higher atomic mass than the atoms of HPMCAS and the drug. The colour coding is used to visualise the additive particles in the extrudates. As seen in Figure 4.2, the atomically denser additive particles can be seen as the red dots showing in the X μ CT images. This is particularly evident in the case of H-NaSG and H-CNa. The X μ CT analysis of the extrudates confirms that the additive particles are mostly located at the surface of the voids. The voids often have a distorted spherical shape. Both SEM and X μ CT results confirm that the voids are not interconnected, but that the individual voids are present in isolation. These results indicate that the co-existence of the drug and the additives are essential for the formation of the voids inside the extrudates. The fact that the single-phase dispersion H-CP extrudates are void-free indicates that the additive particles play an important role in the formation of the voids. It is hypothesised that the possible factors involved in void creation are moisture, particulate additives, drug, viscosity, extruder conditions. In the following sections we investigate these factors systematically.

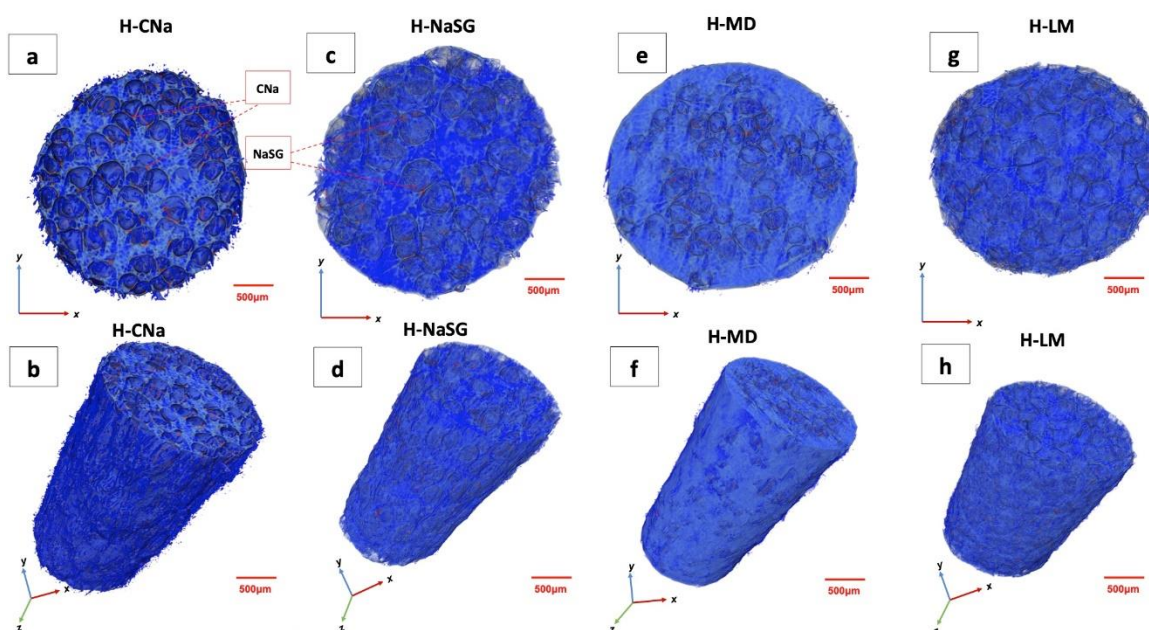


Figure 4.2: Cross-sections (top) and 3D visualisation (bottom) of the X μ CT images of the extrudates with additives. The matrix of the polymer-based extrudates are in blue and the red dots embedded in the blue matrices of H-CNa and H-NaSG are the CNa and NaSG particles. The higher atomic density of sodium in CNa and NaSG than the polymer matrices increased the contrast and allowed the identification of these particles in (a)-(d).

4.3.2 Effect of moisture contents of the raw materials

Both HPMCAS and CBZ contained less than 1% (w/w) moisture. The moisture contents of the additives were measured using TGA (Figure 4.3) and the results are summarised in Figure 4.4a. The additives all carried 3-7.5% (w/w) moisture prior to extrusion, thus it is reasonable to hypothesise that the moisture contents of the raw material may have an effect on the void formation. As the extruder is well ventilated, any volatile solvent from the feed powder mix should be easily eliminated during the heating and mixing process of the extrusion, unless the molten mass in the extruder was too viscous to allow the escape of the entrapped gas. This is supported that the data shown in Figure 4.4b and 4.4c indicating no clear correlation between the amount of moisture content with the void diameter. This indicates that the moisture content of the particles of the additives is not the sole cause of the formation of the voids. Nevertheless, it is clear that in order to reduce the number and density of voids, reducing the initial moisture in the raw materials may be desirable. When the raw materials of the additives were dried for 6 hours at 105 °C, both void size and void density in the extrudates were dramatically reduced, as seen in Figure 4.5.

Therefore, it is hypothesised that during the extrusion process, the particles of the additives are the source of water that forms vapour which in turn results in the voids that can be detected in the finished extrudates. Since dry particles produce some voids it is also likely that they act as nuclei for dissolved air. These gas bubbles are entrapped, i.e. they cannot escape, due to the high viscosity of the mix and thus remain as voids that can be observed in the extrudates after cooling. Therefore, the effects of viscosity of the formulations were investigated in the following sections.

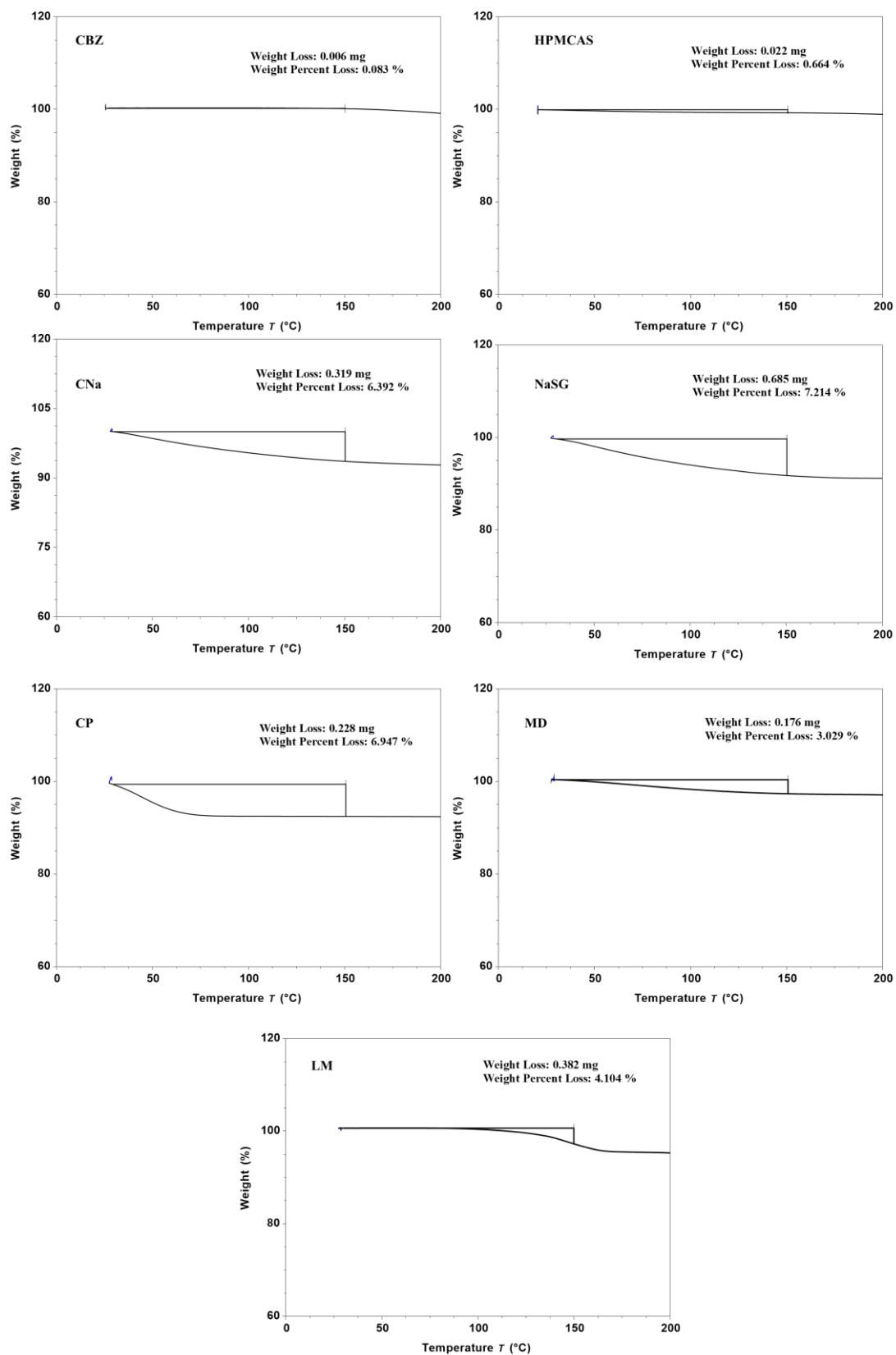


Figure 4.3: Moisture contents of raw materials measured by TGA.

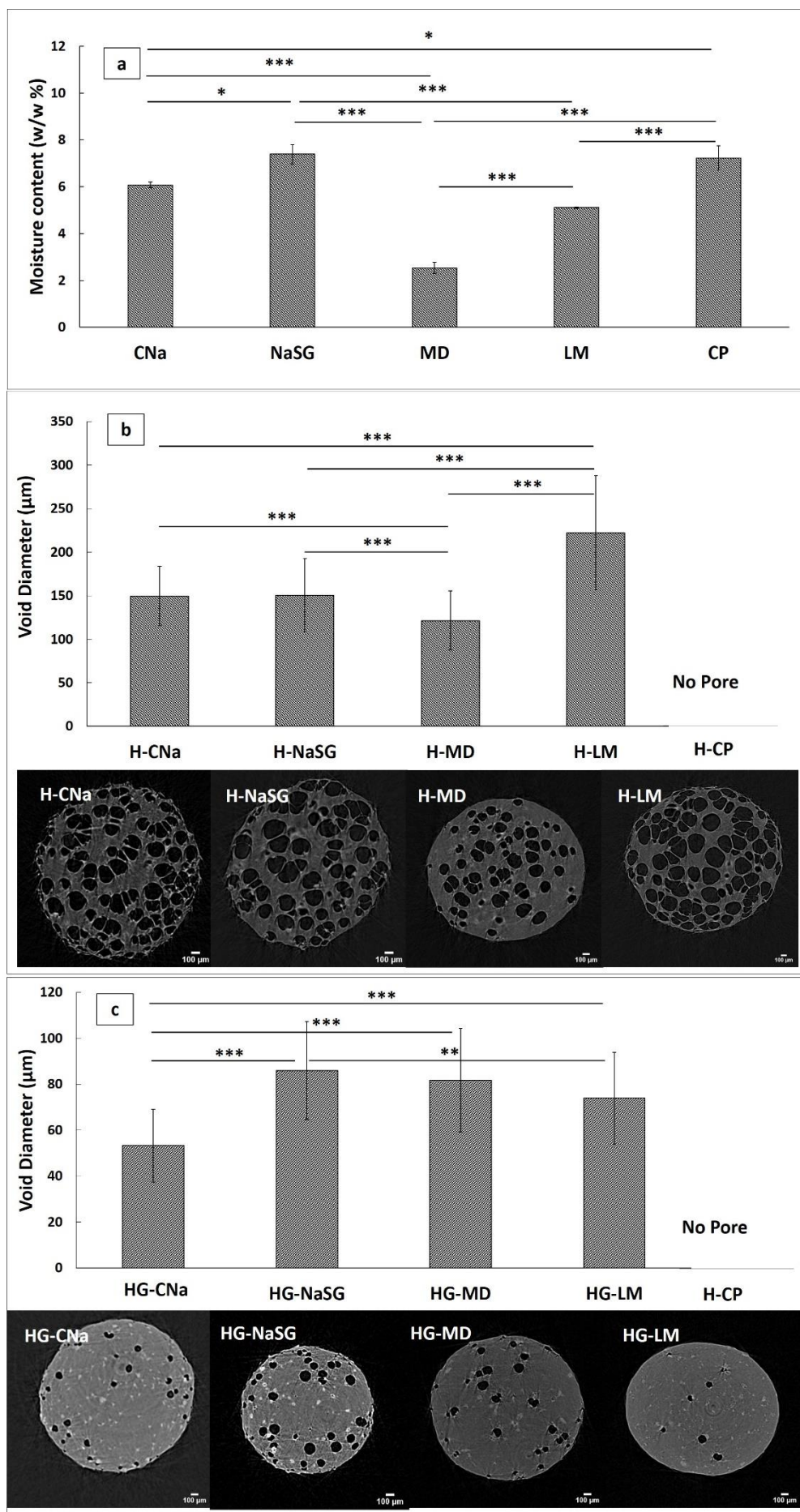


Figure 4.4: Correlation between the void diameter and the moisture contents in the raw materials. (a) Moisture contents of raw materials measured by TGA; (b) pore diameters of the HME extrudates with additives; (c) pore diameters of HME extrudates with Gelucire 50/13 and the additives. The pore diameters in (b) and (c) were measured using the X μ CT data. Representative X μ CT images of the cross-section of each formulation are shown at the bottom panels of (b) and (c). As the extrudates of H-CP and HG-CP are completely void-free, no X μ CT images are shown here. The data are represented as the mean \pm SD, n = 2 (P<0.001, *P<0.01, and *P<0.05).**

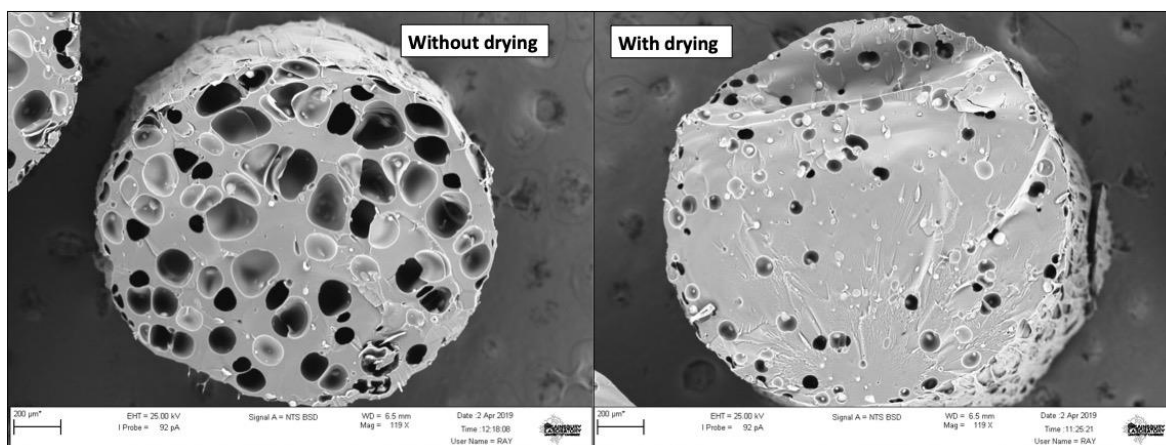


Figure 4.5: SEM images of the cross-sections showing the effect of drying of the raw materials on the formations of the voids.

4.3.3 Effect of Viscosity

During the HME process, the recorded torque value is a direct reflection of the viscoelastic properties of the material being processed in the extruder. Figure 4.6 shows the recorded torque values of all the formulations with and without drug (Figure 4.6a) and with and without Gelucire 50/13 (Figure 4.6b) in the formulations. The binary mixture of HPMCAS and 20% CBZ (H20), the drug is completely solubilised in the polymer and forms an amorphous solid dispersion [75]. With a lower glass transition temperature (T_g) of 56 °C compared to HPMCAS (with a T_g of approximately 120 °C), CBZ exhibited a clear plasticisation effect on the polymer and reduce the viscosity of the mixture in the extruder which led to the significant reduction in torque required for extrusion in comparison to HPMCAS alone. As seen in Figure 4.7a-c, the binary extrudates without the particulate additives, with increasing the drug load from 20% to 50% w/w, the density of the voids increases. This indicates that reduced viscosity to a certain level could potentially favour the formation of the voids. In general terms, if the air bubbles were entrapped in a viscous liquid, increased viscosity of the liquid would make the escape of the air bubbles (using velocity of the bubble as the measure) more difficult (slower velocity of movement in the liquid) according to the Stokes formula [211, 212]. However

in the case of this study, the results indicate that a balance is required: if the viscosity is too high bubbles won't grow and if it is too low bubbles will grow to burst or escape to the surface. Since both polymer type and drug loading may affect viscosity of the molten mixture in the extruder, both may affect cavity formation by changing viscosity. This result agrees well with the similar void-forming phenomena reported in the literature [202, 208, 209].

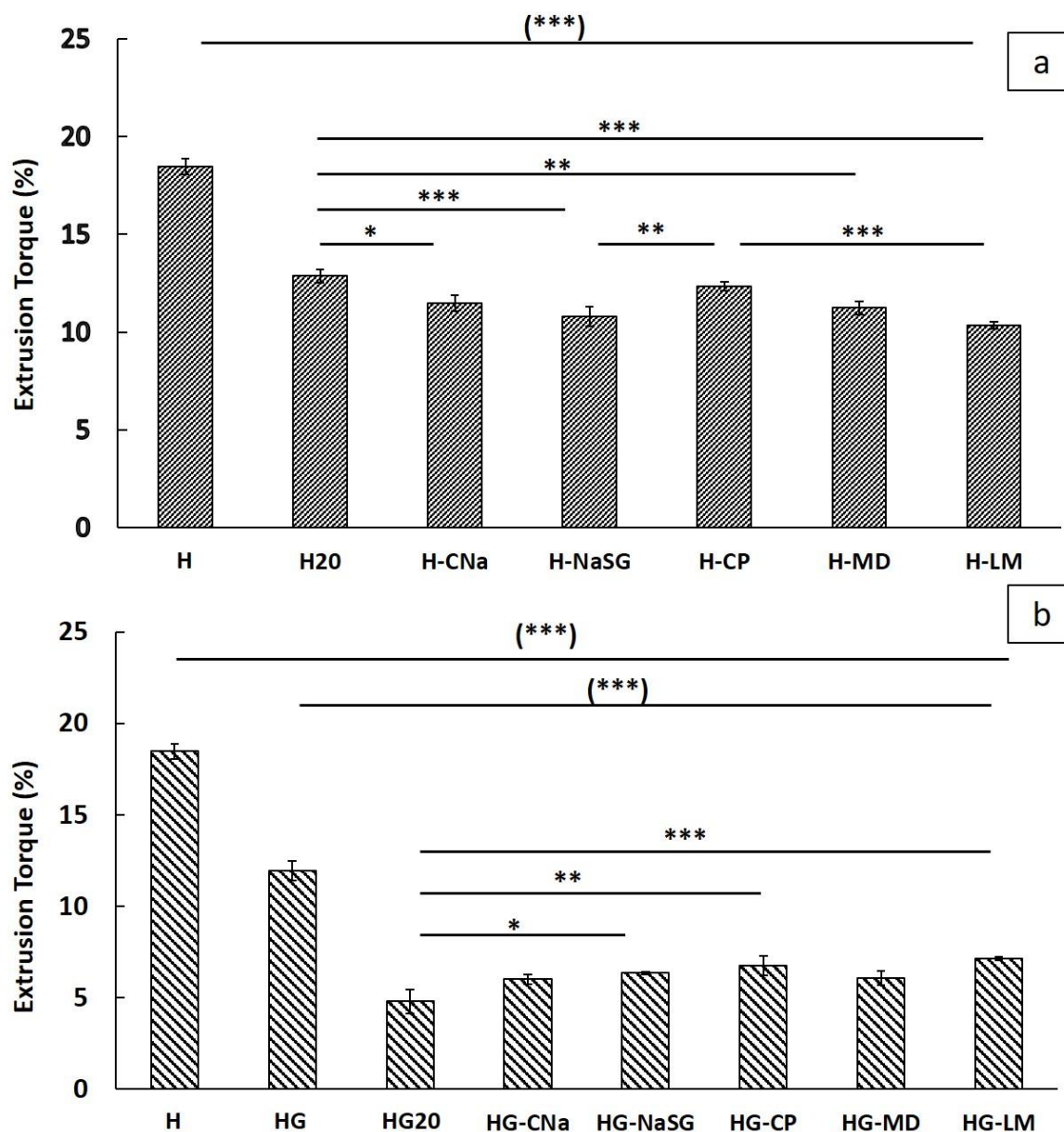


Figure 4.6: The average torque values (%) recorded during the hot melt extrusion process of the formulations (a) without and (b) with Gelucire 50/13. The data are represented as the mean \pm SD, $n = 3$ (*) $P < 0.001$, ** $P < 0.01$, * $P < 0.05$ and (***) indicates that the torque value is statistically significantly (with a $P < 0.001$) different from the rest of the formulations in the group.**

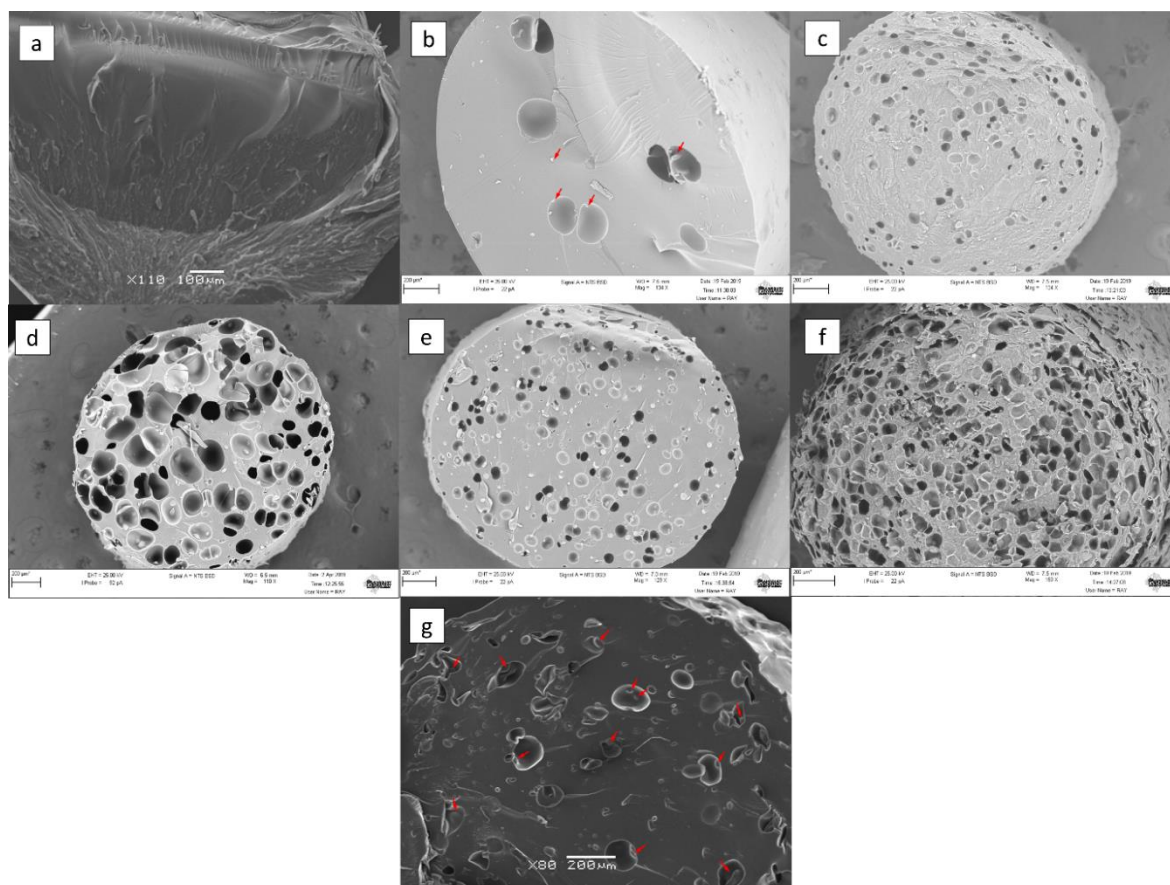


Figure 4.7: SEM images of the cross-sections showing the combination effect of drug loading and addition of the additive on the formation of the voids. (a) H20; (b) H30; (c) H50; (d) H-NaSG; (e) H-NaSG30; (f) H-NaSG50; (g) H-FDN.

In addition to the differences observed in the numbers of voids in the extrudates with different drug loadings, the diameters of the extrudates also increases with increasing the drug content and the screw speed, as shown in Figure 4.8. The larger diameter of the extrudates with higher drug contents (both with and without the particulate additives) may be a result of the higher numbers of voids than the ones with lower drug loading systems (Figure 4.8a). At the extruder die orifice, the sudden pressure drop allows the gas in the voids to expand in volume. This leads to the expansion of the diameter (often referred as “die swell”). Higher screw speed provides higher shear stress and internal pressure in the extruder which leads to more die swell. However, this did not lead to significant difference in the diameter of the extrudates produced by different screw speeds, as observed in Figure 4.8b.

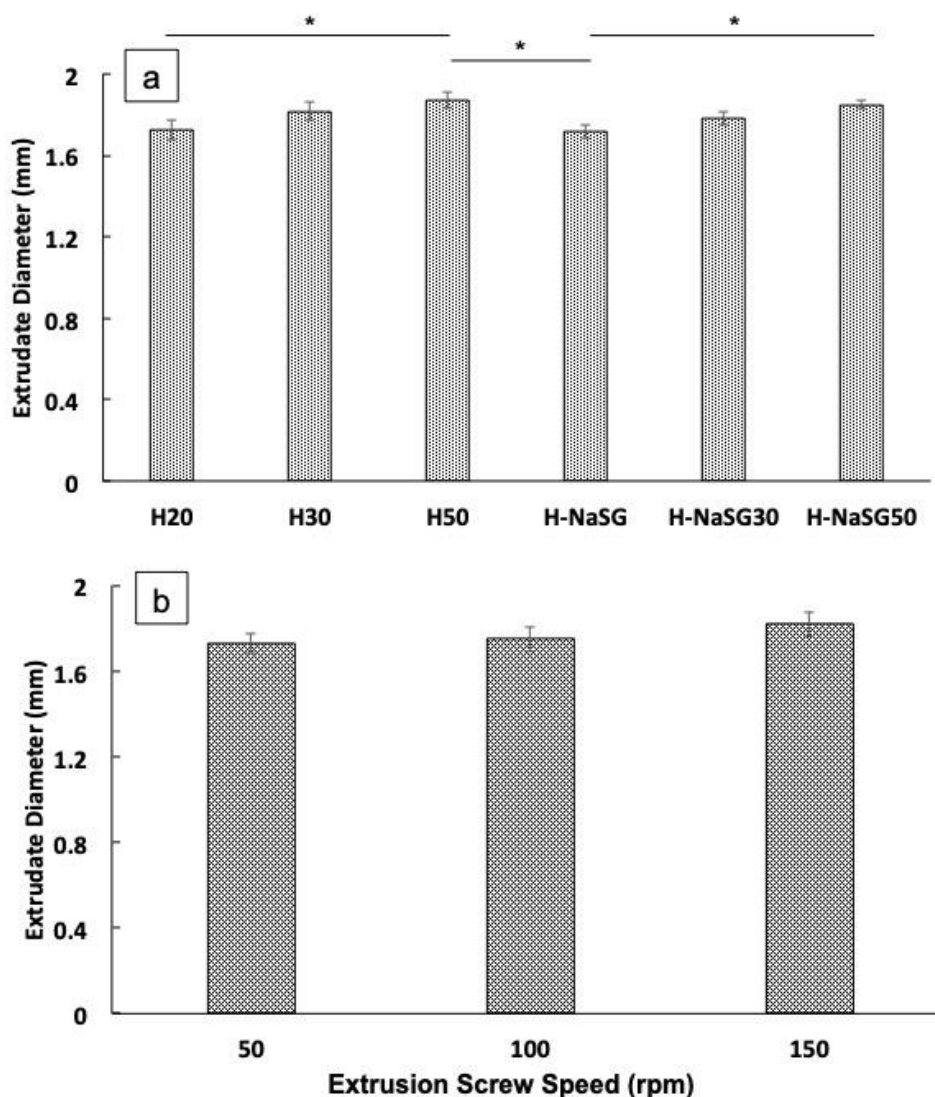


Figure 4.8: The summaries of the extrudates diameters (a) The extrudates containing 20, 30, 50 % w/w CBZ loaded in HPMCAS (H20, H30, H50) and 20, 30, 50 %w/w CBZ loaded in HPMCAS with 5 %w/w NaSG (H-NaSG, H-NaSG30, H-NaSG50); (b) HPMCAS-CBZ binary extrudates diameters produced using screw speeds of 50, 100 and 150 rpm. The data are represented as the mean \pm SD, $n = 3$ (* $P < 0.05$).

It is noted that very few small particles can be seen in the interior of the extrudates with 30% drug loading. As seen in Figure 4.9, the DSC results of the 30% drug loaded extrudates show a T_g at approximately at 65 °C which is lower than the theoretical calculated T_g of the binary mixture according to Gordon-Taylor equation; whereas the T_g of the 50% drug loaded extrudates (H50) is in the same region of the amorphous CBZ, which is around 56 °C, indicating the presence of a significant amount of amorphous drug. The PXRD results confirm that 30% drug loaded extrudates are largely amorphous and 50% drug loaded extrudates contain a significant amount of crystalline CBZ. These results indicate that 30% drug loading approaches the saturation of the solubility of the drug in HPMCAS and 50% binary extrudates are supersaturated with crystalline drug. In

a way similar to the dried phase separated additives, these un-dissolved drug particles could act as the nuclei of the gas bubbles and facilitate the formation of the voids. Therefore, in the case of 50% drug loaded binary extrudates, viscosity is not the sole factor causing the voids.

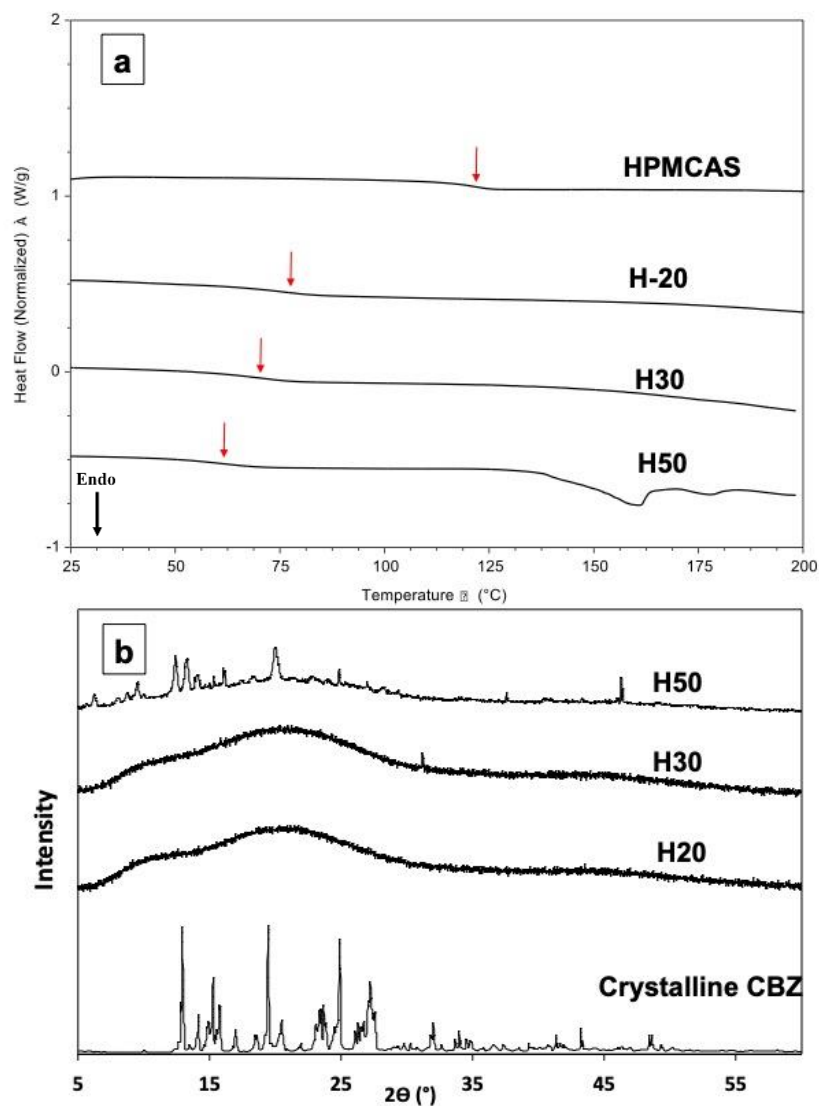


Figure 4.9: (a) DSC and (b) PXRD results of the binary extrudates with the drug loading ranging from 20-50% w/w.

As seen in Figure 4.6a, the addition of 5% (w/w) particulate additives of CNa, NaSG, LM, and MD resulted in further significant reductions of the viscosity and subsequently the torque values of the extrusion process in comparison to the binary extrudates of H2O. This was not the case for H-CP. As discussed earlier, H-CP forms a single-phase dispersion because CP is miscible with HPMCAS and CBZ at the proportion used in the formulation. CP was homogeneously mixed and formed a single-phase molecular dispersion with HPMCAS and CBZ. We speculate that any moisture carried by the additive would be homogeneously distributed and there are no nucleating sites for bubble formation. In the case of the other phase-separate particulate additives, water is concentrated locally in the particle and the release of a relatively large amount in a small region causes bubble formation. When the moisture turns to steam, it generates a significant volume of gas around each particle (approximately 1 cm³ of gas per g of matrix depending on the details of temperature and pressure).

A significant further reduction of the torque was observed when Gelucire 50/13 was added to the binary and ternary formulations, as shown in Figure 5b. This may contribute to the remarked reductions on both the void size and void density seen in Figure 4.4c. Gelucire 50/13 is a semi-crystalline lipid-based additive that is not miscible with HPMCAS. This is confirmed by the measurable melting of Gelucire in the DSC results of the extrudates [75]. At the extrusion temperature used in this study, the melt viscosities of fats and lipids are typically much lower in comparison to polymers, such as HPMCAS. As the molten Gelucire 50/13 is phase separated from HPMCAS, during the thermal extrusion, Gelucire acts as a ‘lubricant’ of the molten mixture and reduces the overall melt viscosity of the system in the extrusion. This facilitates the escape/collapse of entrapped gas bubbles and leads to fewer and smaller voids. The possibility of molten Gelucire coating the additive particles may also reduce the number of the nucleus sites of the gas bubbles which may have contributed to the significantly fewer voids with smaller diameters in the Gelucire containing extrudates seen in Figure 4.4c.

With the model particulate additives, 5% NaSG (w/w), increasing the drug loading should lead to reduced viscosity during extrusion due to the drug’s plasticisation effect on HPMCAS. We observed a reduction of the size of the voids, but this coincided with increased density of the voids (Figure 4.7e). This could be attributed to the break-up of each large void into a number of small satellite voids when the viscosity is low (but still sufficient to entrap the bubbles). Therefore, the results suggest that there is a critical

minimal viscosity of the mixture that above this viscosity the mixture would be able to retain the bubbles and allow the shape deformation, but without collapse of the bubble. The H-NaSG50 extrudates (with 5% NaSG and 50% drug load) are a much more complex case. The 50% mixture is saturated since 30% drug is the solubility limit. Hence the viscosity of the mixture should be similar to that of the 30% mixture which can form voids. However there are more particles in the 50% mixture due to un-dissolved drug. Nucleation from these particles results in more gas bubbles formed hence the 50% extrudates show a larger number of voids.

In order to eliminate the possibility that the formation of voids in the extrudates is drug specific, another model drug, felodipine (FND), that has a slightly lower T_g than CBZ, was tested. As seen in Figure 4.7g, interior voids in H-FDN extrudates are still clearly visible. Solid particulates can be seen at the interface of the voids. This confirms that the void formation is not drug specific and the presence of phase separated solid particulates is essential for void-forming.

To further confirm that the void-forming is not polymer specific and to prove that the viscosity of the mixture in the extruder is one of the key factors determining the formation of the voids, two different polymers with different reported melt viscosity were used. Binary extrudates of CBZ with Soluplus and Eudragit[®] E PO, two widely used HME polymers, were prepared without NaSG. At the HME temperature used in this study (150 °C) the complex viscosity measured is in the order of Eudragit[®] E PO ($10^{3.1}$ Pa.s) \approx Soluplus ($10^{3.8}$ Pa.s) $<$ HPMCAS ($10^{5.2}$ Pa.s) [213-215]. The extrudate diameters of H30 and H50 are significantly higher than the Eudragit[®] E PO and Soluplus based extrudates Figure 4.12. As seen in Figure 4.10, both Sol-30 and EPO-30 show either no void or very low numbers of small voids compared to the ones observed in H30 extrudates, despite the clear observation of the presence of recrystallized drug particles (highlighted by the red arrow). The DSC and PXRD data shown in Figure 4.11 confirmed these being recrystallized drug particles. From the melting point and the PXRD diffraction patterns, it is clear that the recrystallized drug particles are in different polymorphic form (form I) from the starting material which is CBZ form III [100, 108, 216]. This indicates that 30 and 50% drug loadings formed supersaturated solid dispersions for both Soluplus and Eudragit EPO. This confirms that a sufficient level of viscosity is important for the void formation and that when the viscosity is below the critical minimal viscosity void formation can be eliminated altogether even the presence of solid particles.

With increasing the drug loading to 50%, a significant amount of recrystallized drug particles can be observed in all formulations. Consequently, voids are observed in both H50 and EPO-50 extrudates. However, it is interesting to see that the Sol-50 shows no voids, despite the recrystallized drug particles being visible. We speculate that this may be due to the low interfacial tension between Soluplus and the drug particles. Soluplus is a surface-active polymer that may be easier to be spread and ‘wet’ the surface of the drug particles. However, this is speculative and further experiments are required which are out of the scope of this study.

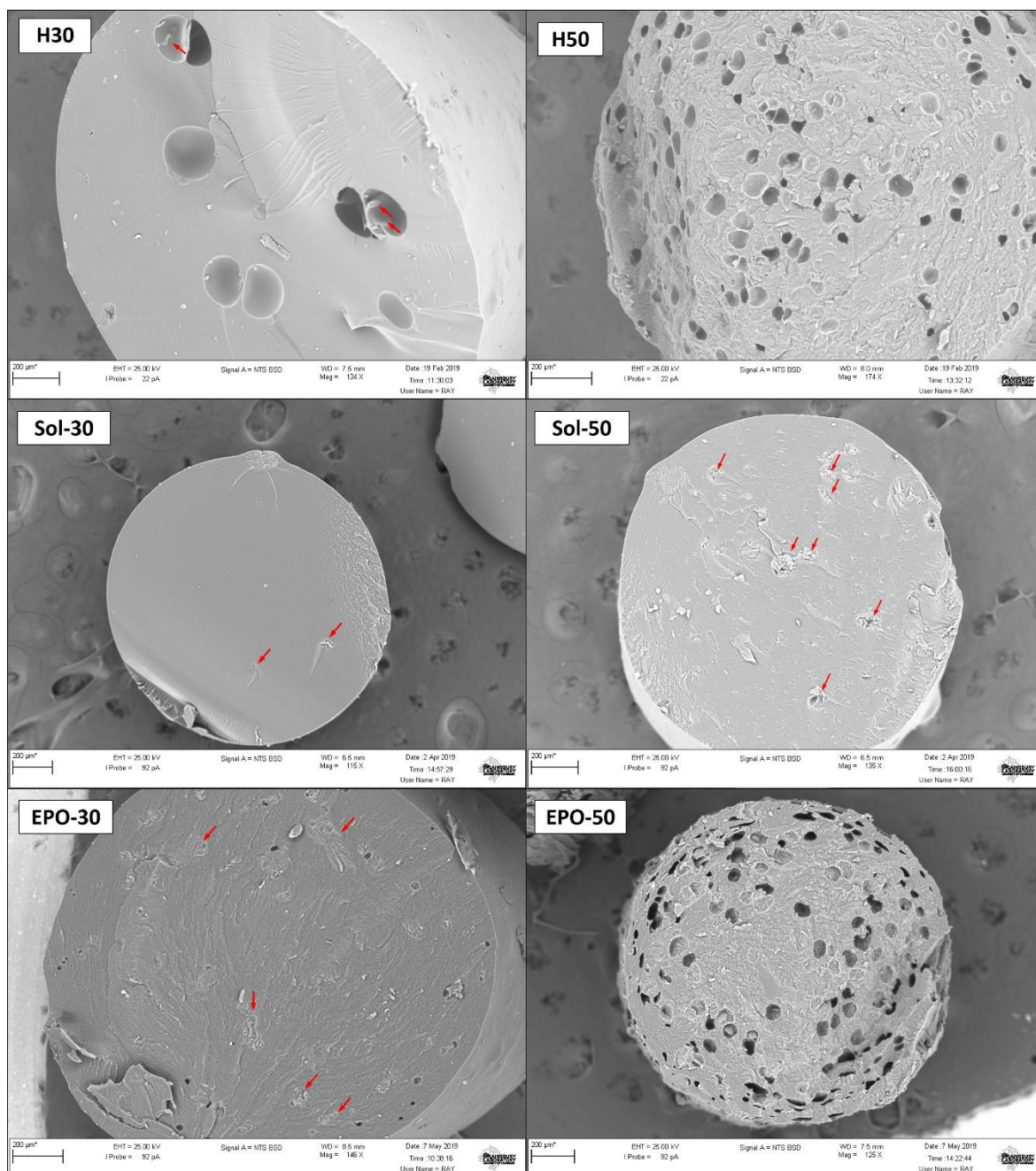


Figure 4.10: SEM images of the cross-sections of the extrudates showing the effect of matrix polymer type and drug loading on the void formation. All formulations were additive-free (red arrows indicate the presence of possible recrystallized drug particles).

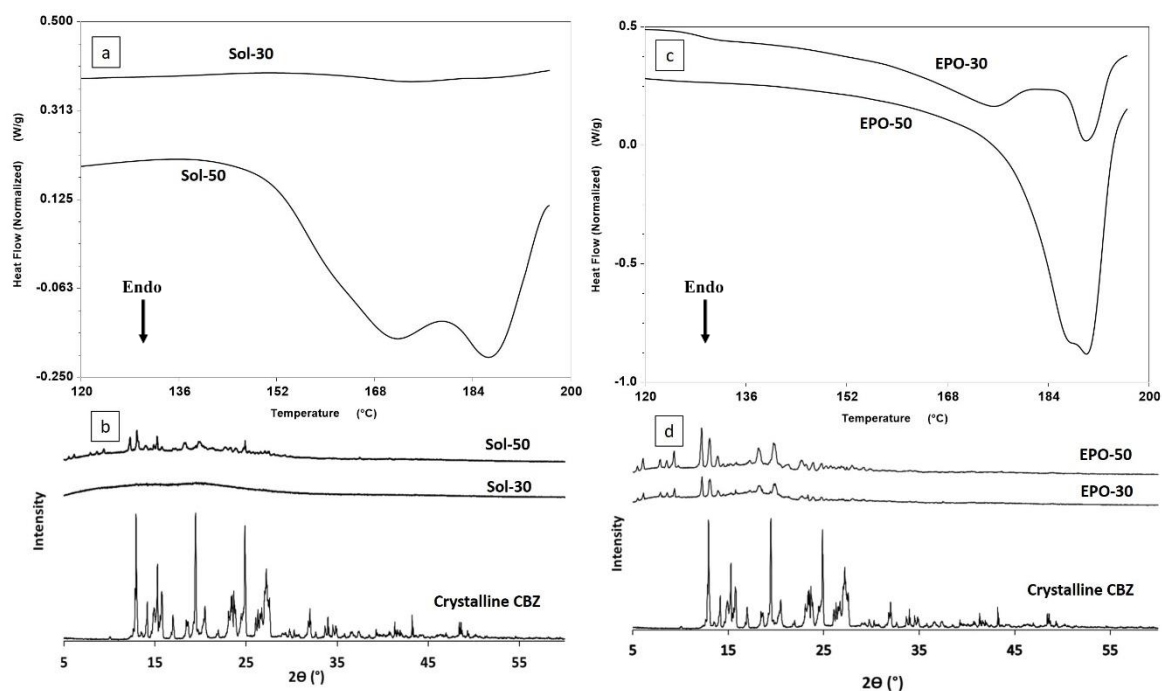


Figure 4.11: DSC (a and c) and PXRD (b and d) data of Sol-30, Sol-50 and EPO-30 and EPO-50.

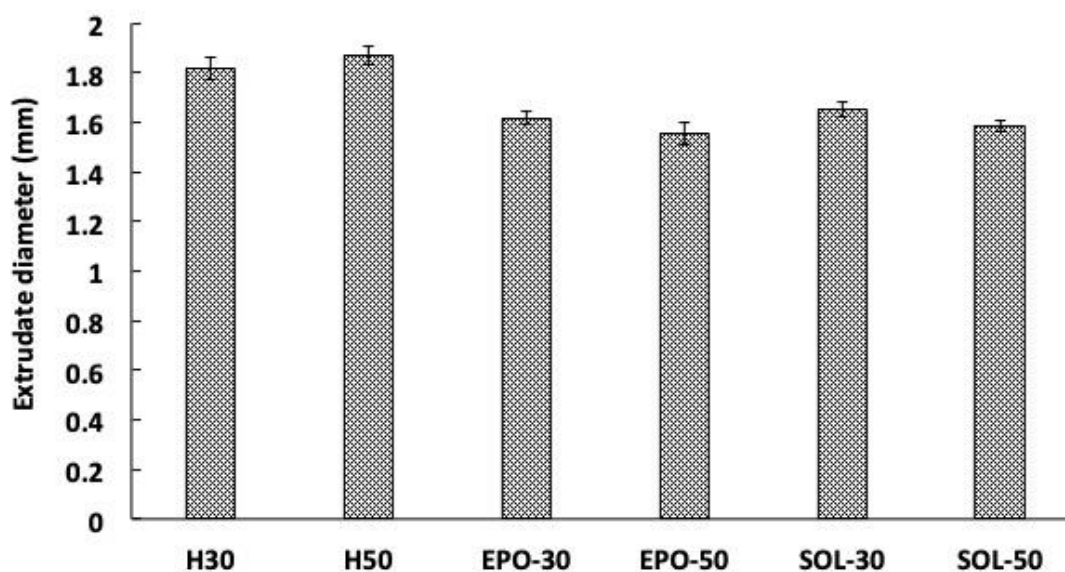


Figure 4.12: Extrudate diameters of the H30, H50, EPO 30, EPO 50, Sol-30 and Sol-50.

4.3.4 Effect of process parameters

As the formation of the voids is a result of the extrusion process, it is important to examine the effect of extrusion operation on the void formation. The bubble entrapment and collapse in the viscous polymer-drug mixture during the extrusion can be affected by the external perturbations experienced by the bubbles. Similar to complex multi-phase fluid flow, such sources of perturbations include the shock generated by the collapse of a

neighbour bubble, shape deformation caused by the large fluctuations of longitudinal and transverse velocity of the mixture that the bubbles are embedded in during the high shear movement of the extrusion, and uneven shear experienced by the mixture closer to the surface and beneath the surface of the rotating screws [217]. Based on this, we hypothesise that different levels of surface shear would influence the void formation. On the basis of this hypothesis, we employed a range of screw speeds to investigate the effect of the combination of the flow velocity and shear on the formation of voids. Unfortunately, for a manufacturing process such as HME, it is impossible to separately investigate a single factor in isolation, as increasing shear would also lead to a change in fluid velocity. Nevertheless, it should provide new insights into the control strategy of the void formation.

As seen in Figure 4.13, the screw speeds used during HME show a clear effect on the void diameter and the void density. At slower screw speeds, fewer voids were generated (Figure 4.13a). These voids were much smaller in diameter in comparison to the voids that were observed in the extrudates manufactured at 100 rpm screw speed. It is also noted that most of the well-defined voids (30-50 μm in diameter) are mainly located close to the edge of the extrudates. The small voids (10-20 μm in diameter) were scattered across the interior of the extrudates often showed a furrow tail. All these furrows are oriented in the same direction, which could well coincide with the rotation direction of the screw. Increasing the screw speed from 100 to 150 rpm resulted in a reduction of the void diameter by about half and an approximate 200% increase of the void density (Figure 4.13c). If the viscosity of the mixture was sufficient to hold the bubbles, the faster screw rotation could cause the deformation of the void shape and the breakage of a large void into smaller voids. This could explain the observed increased density and reduced void size. The differences between the mean void diameters of the extrudates processed by the three screw speeds are significantly different (Figure 4.13e), indicating the screw speed has a profound impact on the void formation. The results suggest that a slow screw speed needs to be selected to avoid void formation during extrusion.

Often lab scale bench top extruders are built with much shorter screws in comparison to industrial scale extruders. Therefore, the same formulation (H-NaSG) was prepared using a larger extruder (H-NaSG (EL)), EuroLab 16, to ensure that void formation is not an artefact of the small lab scale extruder. As seen in Figure 4.13d, although the overall diameters of the extrudates are larger than the extrudates produced by the bench top

extruder, the void diameters are not statistically significantly different from the ones produced by the small bench top extruder (Figure 4.13f). The difference in the diameter of the extrudates is due to the different size of die used on the large and bench top extruder. This result confirms the porosity is intrinsic to the formulation and the process, but not the scale of the extrusion instrument.

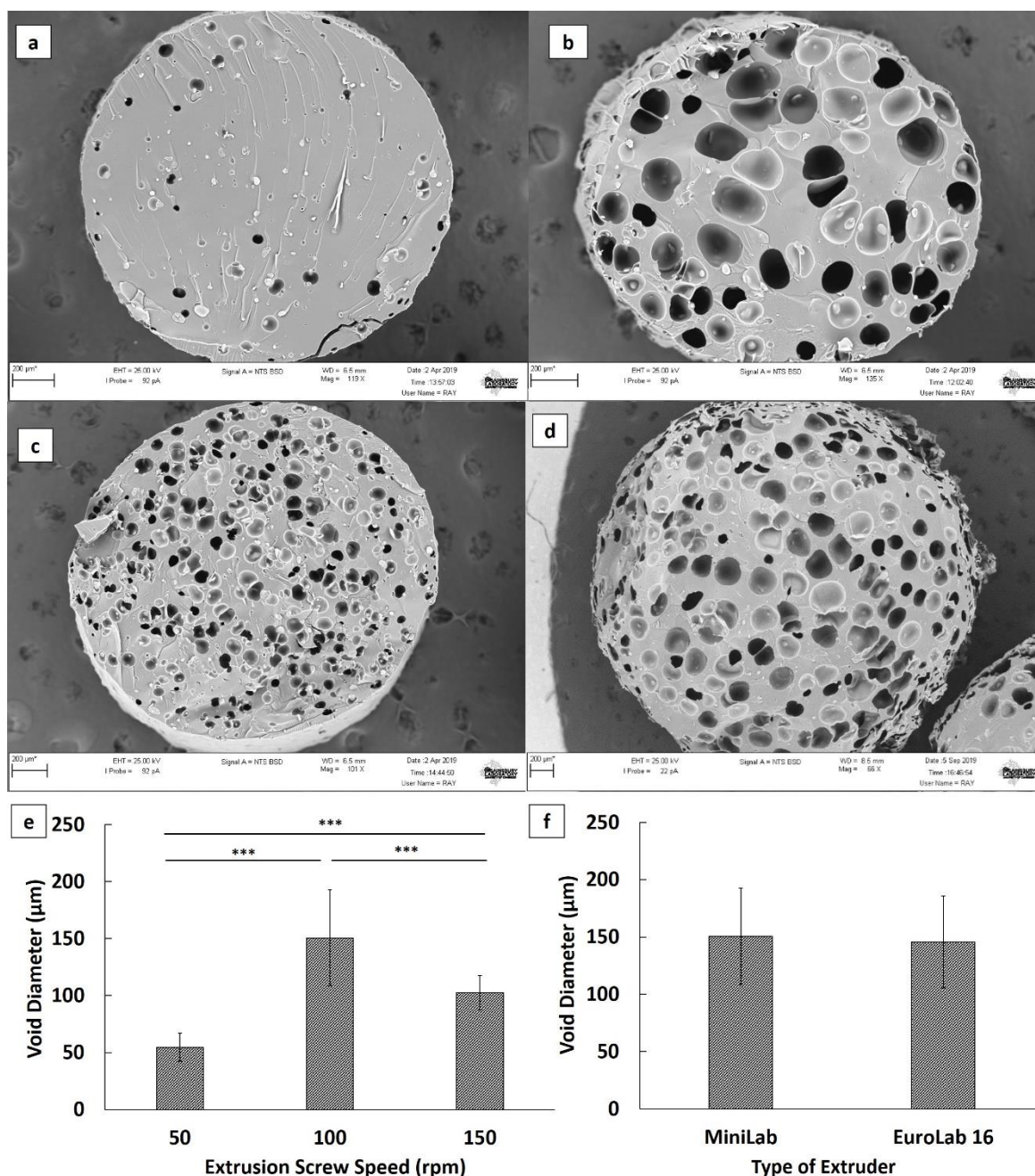


Figure 4.13: SEM images of the cross-sections of the interior structures of H-NaSG extrudates produced using a) 50 rpm; b) 100 rpm; c) 150 rpm screw speed on a Mini-lab twin screw extruder and d) H-NaSG (EL) produced by a EuroLab-16 Extruder at 100 rpm screw speed. The data are represented as the mean \pm SD, $n = 3$ (*) $P < 0.001$.**

4.3.5 Effect of porosity on drug release

If the extrudates were to be used as the dosage form (such as strands or short pellets), it is important to understand the impact of the interior voids on the drug release behaviour of the formulations. As seen in Figure 4.14, whatever the method used to induce void formation (either by changing the loading of the particulate additives, or the drug loading or the screw speed), a clear trend of higher relative void volume leading to a faster dissolution is observed. Drug loading shows the most profound impact on the drug release rate with shortening the T_{50} from 15 hours to 3.6 hours when changing the drug load from 20% to 50% (w/w). As seen in Figure 4.7, the extrudates with 50% drug loading have almost a honeycomb structure. Due to their high relative void volume, the material density per unit volume of H50 is significantly lower than the ones of H20. This may explain the rapid dissolution data. The changes in release rates due to changes in screw speed and NaSG loading were less dramatic than that the effects of changes in drug loading reflecting the smaller changes in relative void volume.

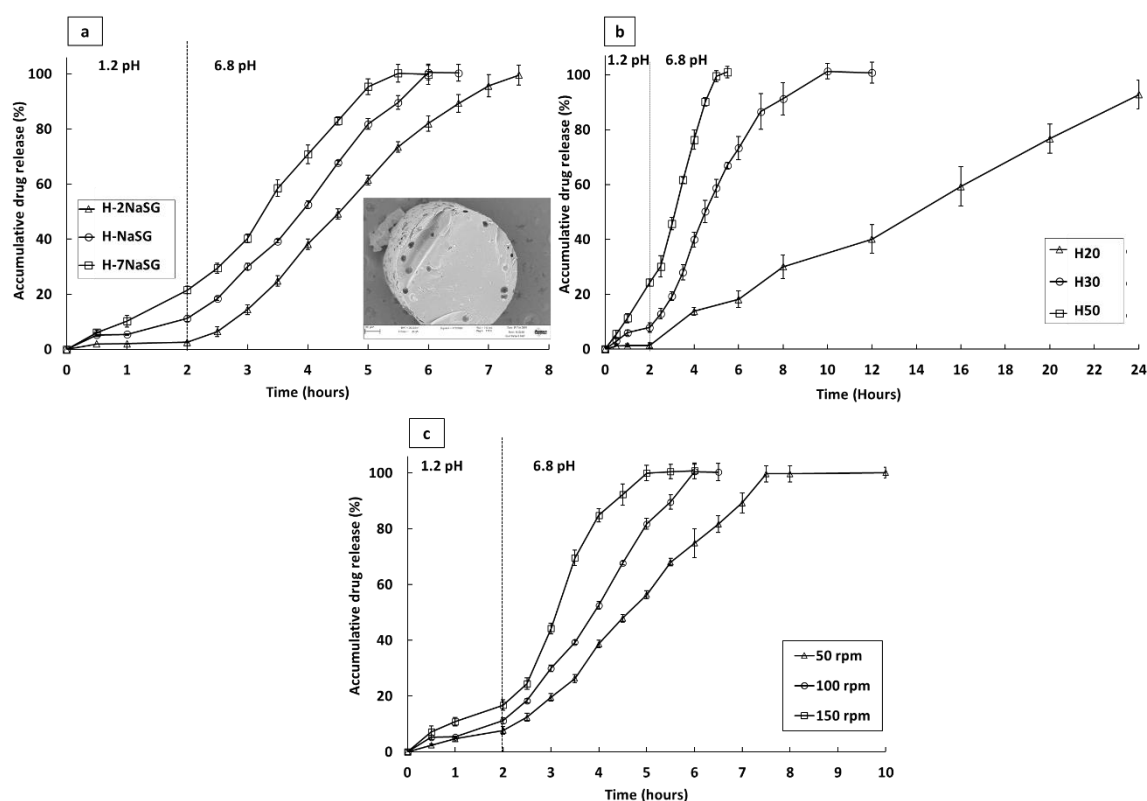


Figure 4.14: The in vitro drug release (0-2 hours in pH 1.2 simulated gastric pH followed by replacement of pH 6.8 PBS as the dissolution media) data of a) extrudates with a loading of NaSG ranging from 2-7% w/w (with the insert being the SEM images of 2% NaSG extrudates with a lower void density than others) (H-2NaSG, H-NaSG, H-7NaSG); b) binary extrudates with a drug loading ranging from 20-50% w/w (H20, H30, H50); c) H-NaSG extrudates processed using screw speed ranging from 50-150 rpm.

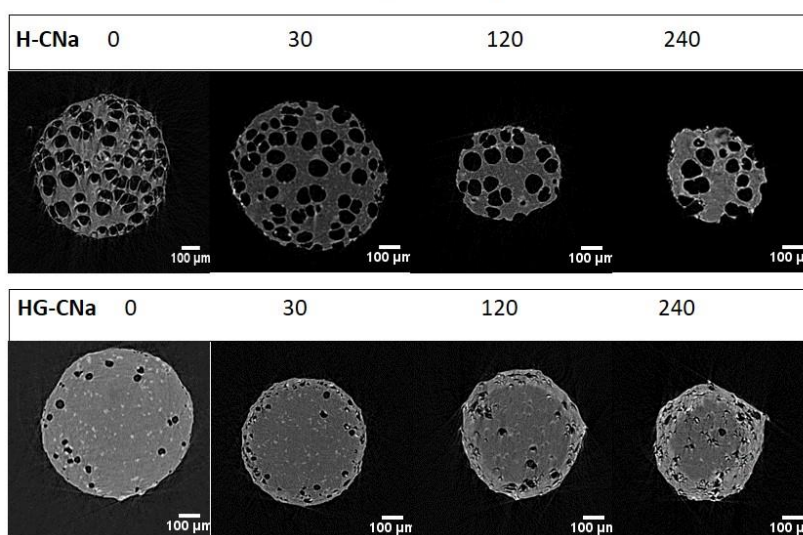
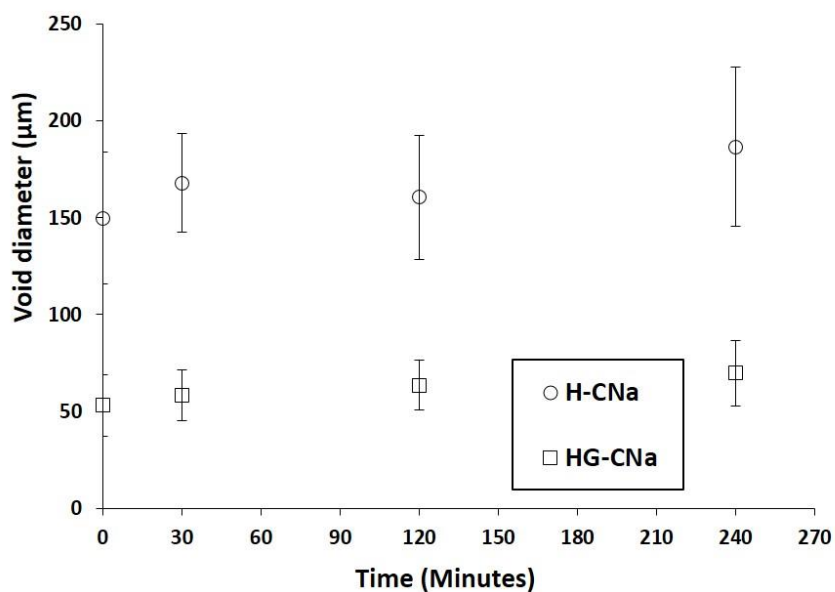


Figure 4.15: Void diameter change of H-CNa and HG-CNa during the dissolution process with the bottom panel showing the representative reconstructed cross-section images of the X μ CT data of the H-CNa and HG-CNa extrudates taken at different time intervals during the dissolution test.

In order to further confirm the role of the voids playing in facilitating the dissolution process, the void size and distribution were monitored during the dissolution process. As seen in Figure 4.15, despite with or without Gelucire 50/13, the void diameters of the extrudates with the particulate additives are fairly consistent throughout the dissolution process. This indicates that a surface erosion process dominates the dissolution process. This is confirmed by the SEM results of the extrudates. As seen in Figure 4.16, after 2 hours of the dissolution, the surface of the extrudates with interior voids all show the full exposure of open voids at the surfaces. The cross-section images of the extrudates show little visible changes in comparison to the fresh samples (Figure 4.1). This is good evidence suggesting the surface erosion is the main mechanism of the dissolution process.

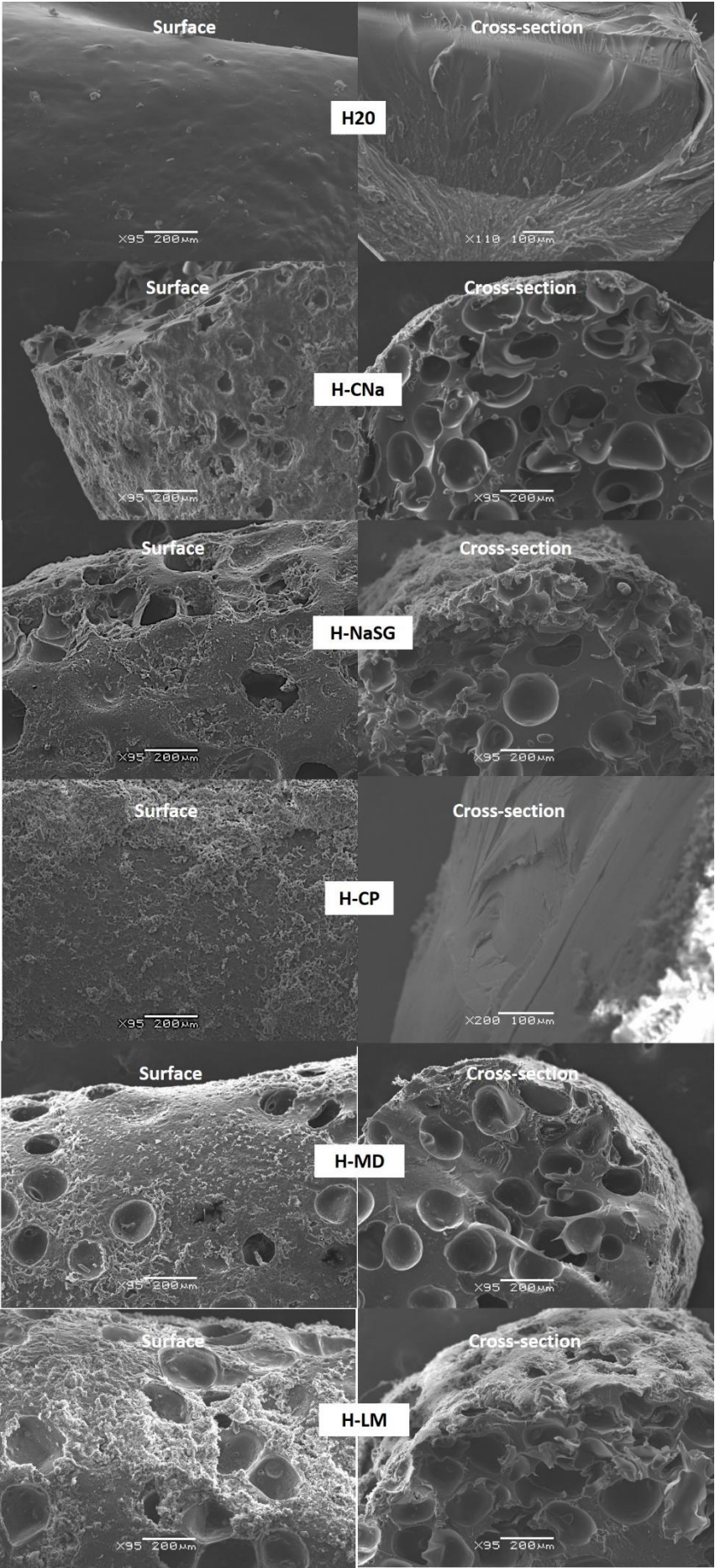


Figure 4.16: SEM images of the surfaces and the cross sections of the extrudates after 2 hours of the dissolution tests in pH 6.8 PBS followed by drying (the crusty texture of the surfaces is a results of salt crystallisation of the dissolution media used during drying).

4.4 Conclusion

This study explored the origin of the void formation in HME extrudates primarily produced by lab scale hot melt extruders and investigated the factors that can be used to manipulate the size and number density of such voids. The results indicated that the viscosity and the presence of phase-separated particulates are essential for the formation of the voids. It is likely that the particulates act as nuclei for bubbles forming from entrapped air and, if they contain moisture, steam formed from the moisture released during processing. A threshold level of the viscosity of the mixture controls the collapse/escape of the bubbles. Therefore, in order to minimise void formation, the results of this study indicate that low moisture content of the raw materials, low proportion of particulates and the addition of lubricants, such as low melting lipid excipients, could be beneficial. Slow screw speed is also preferred for reducing the formation of the voids. This study systematically reported the mechanism of void formation in HME extrudates and generated new insights into the strategies that can be used to manage such void formations.

**An investigation into the use of mesoporous
silica for improving physical stability of
amorphous solid dispersion with high drug
loading**

Chapter 5

5.1 Introduction

Amorphous solid dispersions (ASD) have been intensively studied for their ability to improve the dissolution of poorly soluble drugs and the physical stability of amorphous state of the drug [13, 16, 218]. One of the processing methods that have been widely reported for the industrial scale manufacturing of ASD is hot melt extrusion (HME). HME has been used by the pharmaceutical industry as an approach to improve the dissolution rate and maintain the supersaturation of poorly soluble drugs as well as producing controlled release formulations [75, 219]. Functional excipients are often required as additives in pharmaceutical HME to facilitate the extrusion process (such as plasticizers) and modulating the drug release profile (disintegrants or fillers) [49]. Recently, a number of studies explored the capability of HME, with the aid of amorphous polymeric excipients, to produce ASD with high drug loading to reduce the dosage size with the attempt to reduce pill burden and improve the patient's compliance [98, 219-221]. However, for the ASD with high drug loading, physical instability manifested by phase separation and drug recrystallisation is a challenging issue to overcome [15, 221, 222].

Mesoporous silica (MPS) is considered as one of the multifunctional additives that widely used in pharmaceutical manufacturing [223]. Moreover, loading poorly soluble APIs onto mesoporous silica as a carrier has been investigated intensively in the literature as one of the strategies that can enhance the bioavailability due to their distinctive features such as high surface area and pore volume, small pore diameter and biocompatibility [80-85, 224, 225]. In addition, researchers stated that the ability of mesoporous silica to stabilise the amorphous form of APIs through two mechanisms: surface adsorption and molecular interactions [16, 226-228]. Another advantage of MPS was found that once the amorphous drug adsorbed to the surfaces of the pores with confined inner pore space, the molecular mobility of the amorphous form was reduced, thus hindering the crystal nucleation and growth process [16, 229]. Drug recrystallisation could occur in MPS when the drug loading exceeded the limits of the number of drug molecules that the total surface areas and volume of the mesopores could accommodate [230-232]. Therefore, MPS presents as an alternative carrier for formulating and stabilising amorphous drug to polymeric based ASD. For polymeric based ASD, high drug loading, exceeding the saturated solubility of drug in the polymer matrix, often lead to the increased risks associated with phase separation [16, 233-235]. It was found that to form ASD with good long-term stability and exceed 30% w/w drug loading using ASD are extremely challenging [98, 220, 221].

Considering the pros and cons of both ASD and MPS, it is reasonable to experiment on combining the uses of MPS and polymeric based ASD to formulate and deliver stable amorphous drugs. Few recent studies prepared polymeric ASD containing MPS particles that were loaded with poorly soluble drug by hot melt extrusion (HME) [82, 228, 236]. Their results showed the notable improvement in the drug dissolution rate and the absence of APIs crystals. The purpose of this study is to systematically investigate the formulation principle of forming stable ASD with high drug loading by the aid of MPS. We hypothesise that the stabilisation mechanism is mainly due to the hybrid nature of the matrix containing two sources of capabilities for stabilising the amorphous drugs, mesopores and drug solubility in the polymer. The polymeric binary extrudates without MPS was used as the control for comparison and validation. The polymeric-MPS matrix demonstrates the ability to improve the physical stability of the amorphous drug at high drug loading (>30% w/w). In addition, the modulation of drug release kinetics was explored by size reduction of the formulation to demonstrate the possibility of controlled release of poorly soluble model drug, tolbutamide.

5.2 Materials and methods

5.2.1 Materials

Crystalline tolbutamide (TBA; $M_w=270.3\text{g/mol}$, form I) was purchased from Sigma Aldrich (Gillingham, UK). Poly(vinyl)caprolactam–poly(vinyl)acetate–poly(ethylene)glycol graft co-polymer (Soluplus[®]) was kindly donated by BASF (Ludwigshafen, Germany). MPS used in this study was Syloid[®] XDP 3050 which was kindly donated by Grace GmbH & Company KG (Worms, Germany). Syloid[®] XDP 3050 is amorphous mesoporous silica with average particle size of 50 μm , average surface area of 300 m^2/g , average pore diameter of 22 nm and average pore volume of 1.8 cm^3/g . Tween 80 was purchased from Sigma Aldrich (Gillingham, UK). Size 3 hard gelatine capsule were purchased from Capsuline (Florida, USA).

5.2.2 TBA loading by MPS alone

Melt loading method was used to load TBA into MPS. Crystalline TBA and MPS were mixed together in a glass vial for 5 min using a spatula. The powder mixture was transferred into aluminum sample dish and heated to 135 °C above T_m of TBA

(128°C)[104, 237]. Once the drug was completely melted, the mixing was continued with a spatula for further 5 min. Subsequently, the samples were cooled to room temperature, then to be further analyzed or to be mixed and extruded with Soluplus-Tween 80 for HME.

5.2.3 Preparation of ASD using HME

The ASD formulations investigated in this study are summarised in Table 5.1. All ASD samples were prepared using a co-rotating twin screw Haake Minilab extruder (Thermo Fisher, Karlsruhe, Germany). All formulations were extruded at 130 °C with 5 min retention time and at 30 rpm screw speed. 10 grams of the materials were accurately weighed and premixed using mortar and pestle for 5 minutes prior to HME. For LD1-4 formulations, TBA was pre-loaded into MPS and TBA-MPS powder was mixed with polymeric excipients for HME. For HD1, 30% (w/w) TBA was mixed with polymeric excipients prior to HME and no MPS was used in this formulation. For HD2, HD3 and HD4 formulations, 12% TBA was loaded into MPS using the method described earlier, and the remaining 18, 23 and 28% (w/w) of crystalline TBA were added to the Soluplus-Tween mixtures, respectively. The TBA loaded MPS and the powder mixes of TBA with polymer were then mixed and used for HME. The high drug loading formulations HD2, HD3 and HD4 were stored under 75% relative humidity (RH) at ambient temperature for 1 and 3 months for stability study.

Table 5.1: List of ingredients of the ASD formulations prepared by HME.

Formulation code	Soluplus (% w/w)	Tween 80 (%w/w)	TBA (% w/w)	MPS (% w/w)	Total Weight (mg)
TBA20			20	80	50
TBA40			40	60	25
TBA60			60	40	16.5
TBA80			80	20	12.5
LD1	75	5	4	16	250
LD2	75	5	8	12	125
LD3	75	5	12	8	84
LD4	75	5	16	4	62.5
HD1	65	5	30	0	33.3
HD2	57	5	30 *	8	33.3

HD3	52	5	35 **	8	28.5
HD4	47	5	40 ***	8	25

*12% TBA was loaded in MPS, 18% crystalline TBA was mixed with polymer.

** 12% TBA was loaded in MPS, 23% crystalline TBA was mixed with polymer.

***12% TBA was loaded in MPS, 28% crystalline TBA was mixed with polymer.

5.2.4 Materials characterisation

5.2.4.1 Powder X-ray diffraction (PXRD)

PXRD was performed to measure the crystallinity of raw materials and extruded formulations using a D5005 X-ray diffractometer (Siemens, Munich, Germany) with monochromatic CuK α radiation (wavelength = 1.54056 Å). The samples were scanned from a 2 θ angle of 5° to 60°, with a step size of 0.02° and 2°/min scanning speed.

5.2.4.2 Differential scanning calorimetry (DSC)

A TA Universal Q2500 Discovery series DSC (TA Instruments, Newcastle, DE, United States) was used to characterise the thermal properties of the raw materials and HME extrudates. The instrument was thoroughly calibrated prior to sample testing. TA standard crimped pans and lids were used for all measurements. For all standard DSC experiments, a heating rate of 20 °C/min was used with 50 ml/min nitrogen purge flow. For modulated temperature DSC (MTDSC) experiment, a 2 °C/min heating rate 60 s period and 0.31 °C amplitude was used. TA Trios software was used for data analysis. All formulations were tested in triplicate.

5.2.4.3 Scanning electron microscopy (SEM)

A Zeiss Gemini SEM 300 Field Emission Scanning Electron Microscope built with Schottky field emitter electron source (Denka Company Limited) was used to study the surface microstructure of the formulation extrudates. The elemental analysis was performed with an Oxford Instruments Ultim Max 170 EDS system. The samples were coated with gold using a Polaron SC7640 sputter gold coater (Quorum Technologies, Laughton, UK) prior to imaging.

5.2.5 *In vitro* drug release studies

All *in vitro* drug release studies were carried out using a Erweka DT126 light USP I basket dissolution apparatus (Erweka GmbH., Langen, Germany) under sink condition. They were operated in 900 mL dissolution media of pH 6.8 phosphate buffer saline (PBS) with

100 rpm rotation speed and maintained at 37 ± 0.5 °C for each test. The ASD in the forms of HME extrudate strands (within range of 13 ± 4 mm in length and 1.85 ± 0.3 mm in width) and milled extrudates filled in hard gelatine capsules were tested, containing equivalently 10 mg to maintain the sink condition of TBA (TBA Solubility: 109 mg/L) [111]. In terms of the capsule preparations, the HME extrudates of HD2, HD3 and HD4 were milled using pestle and mortar. The obtained powders were further screened to $250\mu\text{m}$ undersize to be filled into size 3 hard gelatine capsules. 3 ml aliquots were withdrawn from each dissolution vessel and filtered through $0.45\ \mu\text{m}$ filters (Minisart Sartorius, Goettingen, Germany) at predetermined time intervals. After each sampling, 3 ml of fresh preheated fresh media were replenished to the dissolution vessel. The concentration of drug determined by HPLC (Jasco PU-1580 Series HPLC system, Jasco Ltd, UK) with Symmetry® C18 (4.6 x 250mm (Waters, USA) maintained at 40°C . The injected volume was $20\ \mu\text{l}$. The mobile phase consisted of a 50:50 v/v mixture of acetonitrile and water containing 0.1% v/v formic acid. 7.2 min is the retention time, the flow rate was 1 mL/min, and the UV detection was set at 229 nm. The measured peak area values at different time intervals were converted to concentration values using the calibration curves shown in Figure 5.1b. All measurements were performed in triplicate.

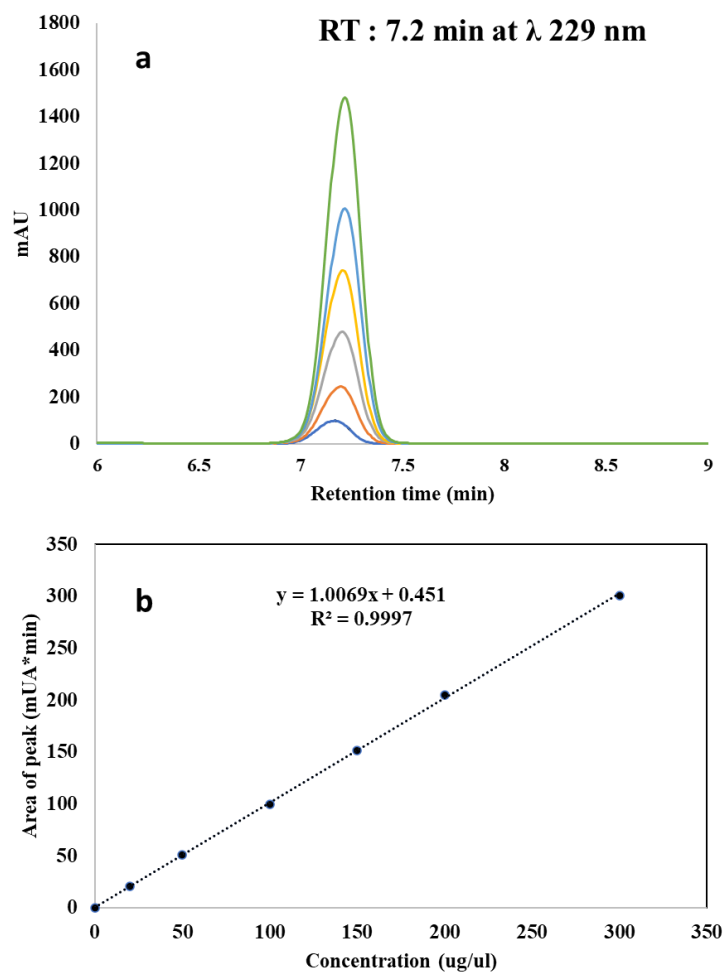


Figure 5.1: (a) Representative HPLC chromatograms of tolbutamide at different concentrations and (b) Calibration curve of tolbutamide in phosphate buffer solution (pH = 6.8).

5.3 Results and discussion

5.3.1 Investigation into MPS loading capacity of amorphous TBA

In this study, the crystalline TBA melted in the presence of MPS was used as the means of loading TBA into the mesopores of MPS. If most of the TBA was held inside the pores of MPS, there should be little TBA on the surface of the MPS particles. In order to confirm this, elemental analysis was used with SEM to examine the surfaces of the MPS particles after drug loading at two different TBA: MPS ratios, 20: 80 and 40: 60 (w/w) (with formulation code of TBA20 and TBA40, respectively). As seen in Figure 5.2, no morphological differences of TBA 20 and TBA 40 can be seen from the SEM results. The elemental analysis results of TBA20 showed complete absence of sulphur which is used as a marker for the presence of TBA on the surfaces of the TBA loaded MPS particles. However, the results of TBA40, TBA 60 and TBA 80 confirmed the detection of a low quantity of sulphur at the surfaces of these TBA-loaded MPS particles. The PXRD results, shown in Figure 5.3a, also confirmed that TBA20 is fully amorphous, but detectable

amounts of crystalline TBA are in TBA 40, TBA60 and TBA80 formulations. This result indicates that at a drug loading between 20 and 40% w/w, the inner surfaces of the mesopores within MPS particles are fully saturated with the adsorbed TBA molecules. This led to the surface adsorption of TBA that was detected in TBA40, TBA60 and TBA80. In order to ensure no excess amount of unloaded TBA, MPS loaded with 20% TBA was in this study for the following ASD studies.

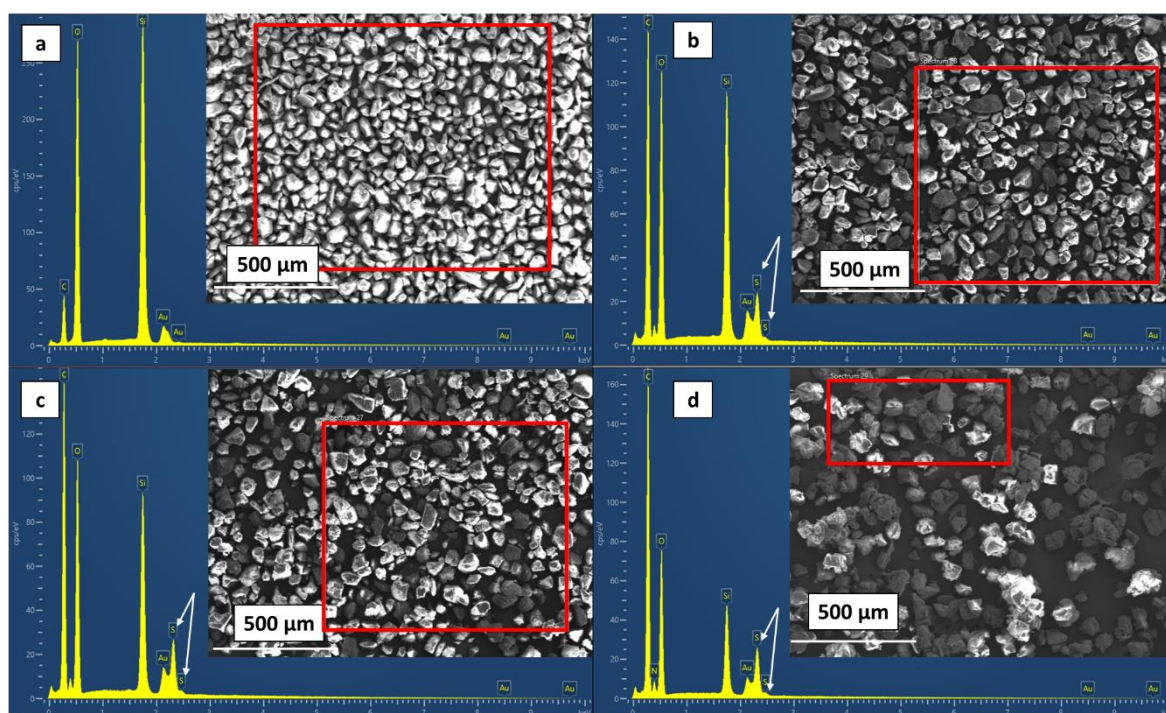


Figure 5.2: SEM with elemental analysis results of (a) TBA20, (b) TBA40, (c) TBA60 and (d) TBA80. The Sulphur peak is used as the indicator of excess TBA adsorbed on the surfaces of MPS particles. The elemental analysis spectra are the average values of the selected areas highlighted in red squares.

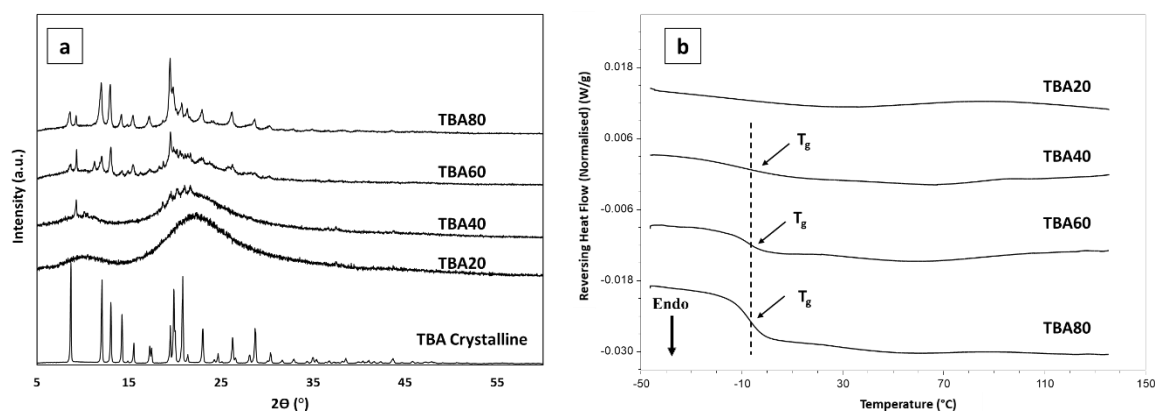


Figure 5.3: (a) PXRD and (b) MTDSC results of TBA20, TBA40, TBA60 and TBA80 formulations with the detectable T_g highlighted by the arrows.

An attempt to further quantify the loading of TBA in the mesopores of MPS particles, MTDSC was used to measure the T_g of the amorphous TBA in TBA20-80 samples. As reported in the literature, if drug molecules were successfully adsorbed and held within the mesopores of MPS, there should be no detectable T_g signalling no presence of amorphous drug clusters [227, 238, 239]. If any T_g of amorphous drug is detected, this is likely to be the drug unsuccessfully loaded within pores but adsorbed on the outer surfaces of the MPS particles. Using the heat capacity change at the glass transition of the amorphous TBA, the loading of amorphous TBA in MPS was quantified. As seen in Figure 5.3, no melting of crystalline TBA is present in the MTDSC results of all samples. No detectable T_g is present in TBA20 samples, while clear T_g 's are observed in TBA40-80 samples. The heat capacity change (ΔC_p) of pure amorphous TBA at T_g was 0.502 J/(g·°C). As the ΔC_p is proportional to the quantity of the amorphous material, the ΔC_p values at the T_g of the TBA 40-80 were measured and divided by the ΔC_p values of pure amorphous TBA to obtain the amorphous contents within TBA40-80 samples. 23±4, 38±3 and 54±6 % (w/w) of TBA were detected being amorphous in TBA40, TBA60 and TBA80, respectively. If these proportions are drug on the outer surface of the silica and not absorbed in the pores, with the total TBA used being 40, 60, and 80% (w/w) in these formulations, this result indicated that 17, 22 and 26% (w/w) of the loaded TBA are within the mesopores. This largely agrees with the mesopore loading limit of TBA being between 20-40% w/w.

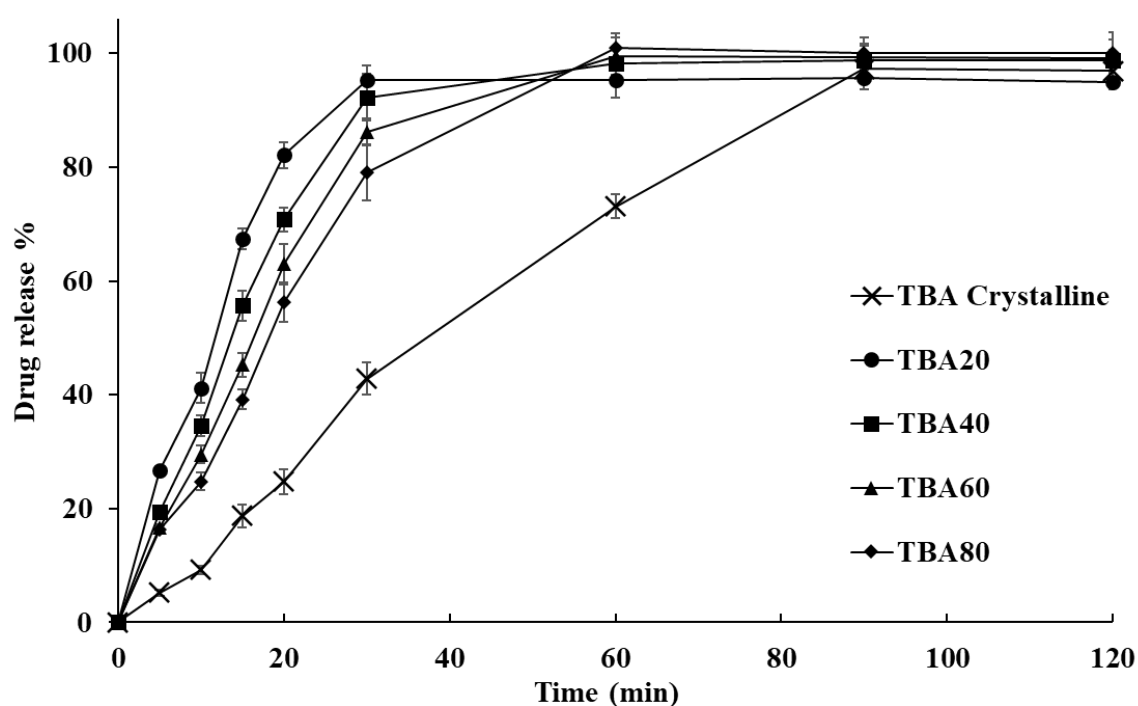


Figure 5.4: The in vitro TBA release profiles of TBA20, TBA40, TBA60 and TBA80 formulations in pH 6.8 PBS.

The in-vitro drug release data of the TBA loaded MPS formulations are shown in Figure 5.4. All formulations demonstrated improvement in the TBA release rate in comparison to crystalline TBA. This indicates that MPS possess significant ability to speed up the drug release. Moreover, the lower drug loading (TBA20) sample shows a slightly faster release rate than TBA40-80 samples in the first 30 minutes. As TBA20 has no detected amorphous drug on the outer surfaces of the MPS particles, the fastest drug release observed in TBA20 is likely to be attributed to the complete molecular adsorption within the pores of MPS. For TBA 40, 60 and 80, some of the TBA that were on the outside of the pores of MPS might block the pores and led to reduced surface area for dissolution. This faster drug release of TBA40-80 samples than crystalline TBA may arise from a combination of the amorphous phase and the high surface area of the MPS particles. The pure crystalline drug will have low surface area and a lower solubility than the amorphous phase.

5.3.2 Low drug loading ASDs (LD) containing TBA-MPS prepared by HME

The LD1-4 formulations were prepared with different proportion of TBA being pre-loaded into MPS to investigate the effects of polymeric matrix on the physical stability and in vitro drug release performance of the formulations. To ensure TBA was fully loaded into the mesopores of MPS, and no excess drug adsorbed on the outer surfaces of MPS, relatively low drug loadings between 4-16% (w/w) (well below the saturation loading limit identified previously) were used.

To confirm that there is no TBA leakage from the MPS into the polymer matrix after HME, elemental analysis was used with SEM. As seen in Figure 5.5, MPS particles can be clearly identified in the SEM images of the cross-sections of the HME extrudates containing TBA-MPS. The targeted tested areas of elemental analysis are both on the surfaces of MPS particles (S) and the polymer areas (P) that are free from MPS particles. If sulphur signal is identified within the polymer areas, it indicates that TBA is leaked from MPS into Soluplus. As seen in Figure 5.5, sulphur peak from TBA was absent from the elemental analysis performed on both MPS particles embedded in the Soluplus-Tween matrix and the polymer areas that are free from MPS particles for LD1 and LD2 formulations. However, sulphur peaks are detectable for both types of areas in LD3 and

LD4 formulations. This indicates that TBA did not leak from MPS into the polymeric matrices during HME process for LD1 and LD2 formulations but leaked for LD3 and LD4 formulations. LD3 and LD4 have higher drug loads than LD1 and LD2 and this may contribute to the observed TBA leakage.

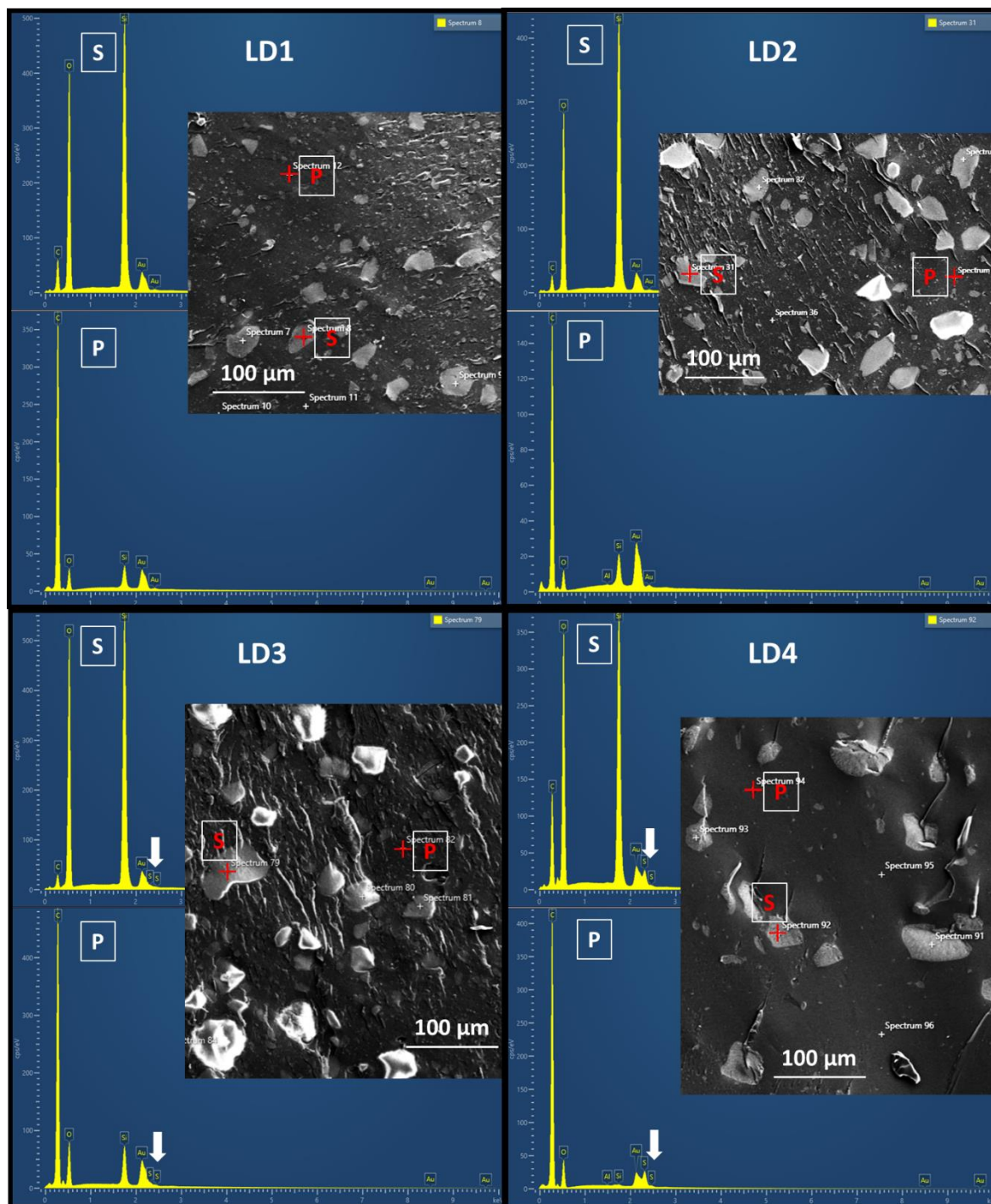


Figure 5.5: SEM and elemental analysis of LD1, LD2, LD3 and LD4 showing the absence of sulphur signal in LD1 and LD2 and the presence of the sulphur peak in LD3 and LD4 (sulphur signals are highlighted with the white arrows. The crosses are the tested points of elemental analysis and S stands for the surfaces of MPS particles and P stands for polymer areas free from MPS particles.

To further characterise the LD formulations, DSC and PXRD were used. As shown in Figure 5.6a, no crystalline TBA is detected by PXRD for all the LD formulations. If there is no significant TBA leakage from MPS into the Soluplus matrices of the formulations, the T_g of the LD formulations should be consistent with the T_g of placebo Soluplus-Tween extrudates which is approximately 48.5 °C. The same T_g values were detected for LD1, LD2 and LD3 formulations, as seen in Figure 5.6b. However, for LD4, the T_g of the formulation is lower than the one of the placebo extrudates. As amorphous TBA has a T_g of 4 °C [240], it is reasonable to suggest that the leakage of TBA into the polymeric matrices that further plasticised and depressed the T_g of the formulation. This result agrees well with the findings of the elemental analysis for LD4. For LD3, DSC did not detect any shift in T_g of the formulation, this may be due to the low quantity of TBA leaked into the polymer matrices which did not induce DSC-detectable shift of the T_g . From the physicochemical characterisation results, it can be concluded that when being co-processed with Soluplus-Tween via HME the maximal TBA loading in MPS with minimal leakage is 12% (w/w). This loading of TBA in MPS is further used in the next section of investigations into the high drug loading ASD formulations.

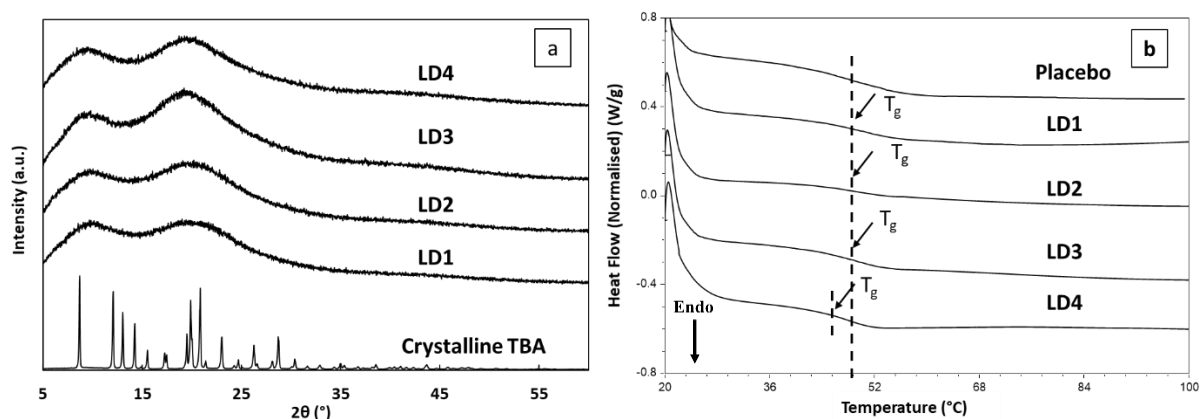


Figure 5.6: (a) PXRD patterns and (b) DSC data of LD1-4 formulations.

With the characterisation results in mind, it is reasonable to predict that fast TBA release may be observed in LD3 and LD4 in which amorphous TBA is readily to be released from the polymer matrices. In the case of LD1 and LD2, the erosion of polymer matrices needs to occur prior to the release of the MPS particles and the release of TBA incorporated inside the mesopores of MPS. As seen in Figure 5.7, LD1-4 formulations all achieved nearly zero-order controlled release of TBA over 12 hours. As predicted previously, LD4 shows a slightly faster release rate than the rest of the formulations and reached 100% by 10 hours. LD3 shows a slightly faster release rate than LD1 and LD2 between 2-6 hours, but no significant difference before 2 hour and after 6 hours.

Therefore, it is reasonable to conclude that when most drug molecules are hosted in MPS, the drug release rate is independent to the drug loading. This can be advantageous when developing controlled release oral dosage forms of a drug with predetermined release rate but requiring a range of products with different strengths of doses for different patients' needs.

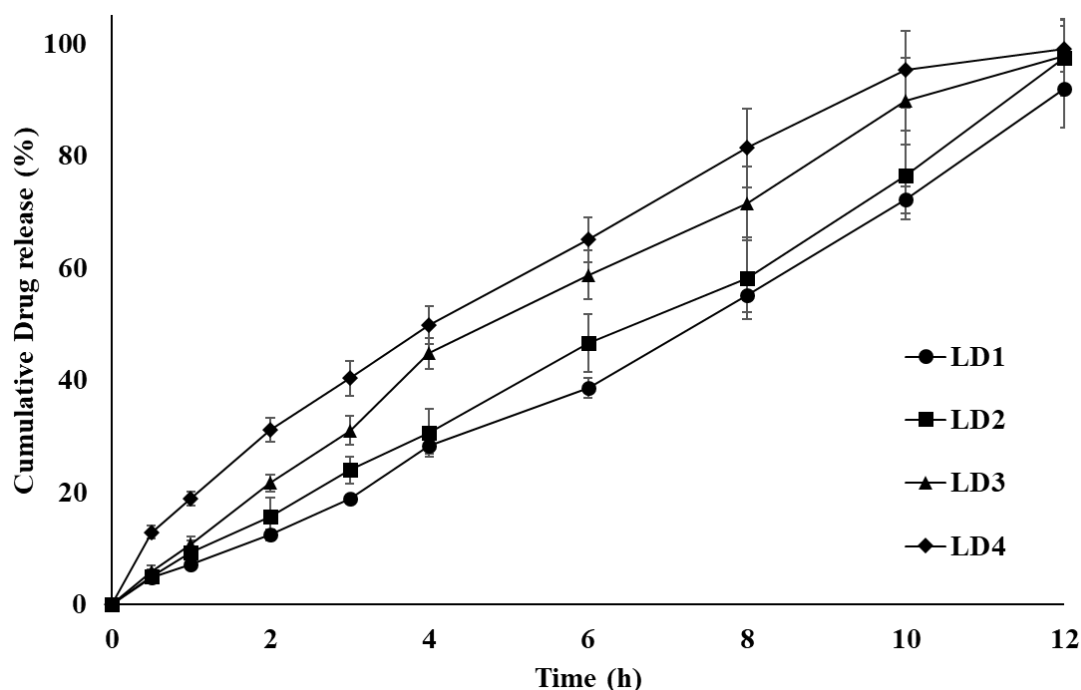


Figure 5.7: The in vitro drug release of the HME extrudates of LD1, LD2, LD3 and LD4 formulations in pH 6.8 PBS.

5.3.3 High drug loading ASD containing TBA-MPS and free TBA

From the study of the HME formulations of TBA loaded MPS in Soluplus-Tween, it was concluded that 12% (w/w) TBA in MPS is the maximal TBA loading to avoid significant TBA leakage during the extrusion process. In this part of the investigation, free TBA was added into the Soluplus-Tween mix in addition to the TBA-MPS with 12% (w/w) TBA loading in order to increase the overall drug loading of the formulations. HD1 was used as the control sample that contain no TBA-MPS, but only 30% (w/w) free TBA that was extruded with Soluplus-Tween. The SEM image of the cross-sections of the HD1 (placebo) extrudates revealed the even distribution of MPS particles in the polymer matrix (Figure 5.8). Similarly, for HD2-4 extrudates, the MPS particles embedded and dispersed in the polymeric matrix can be clearly identified. Air pockets with 100-200 μm in diameter can be clearly seen in HD4. Similar features were observed in other ASD prepared by HME and the formation of the air pockets were attributed to high drug loading with the presence of un-dissolved particulate drug within the extrudates [241].

The physical states of the drug in the MPS loaded ASD were further investigated using PXRD and MTDSC.

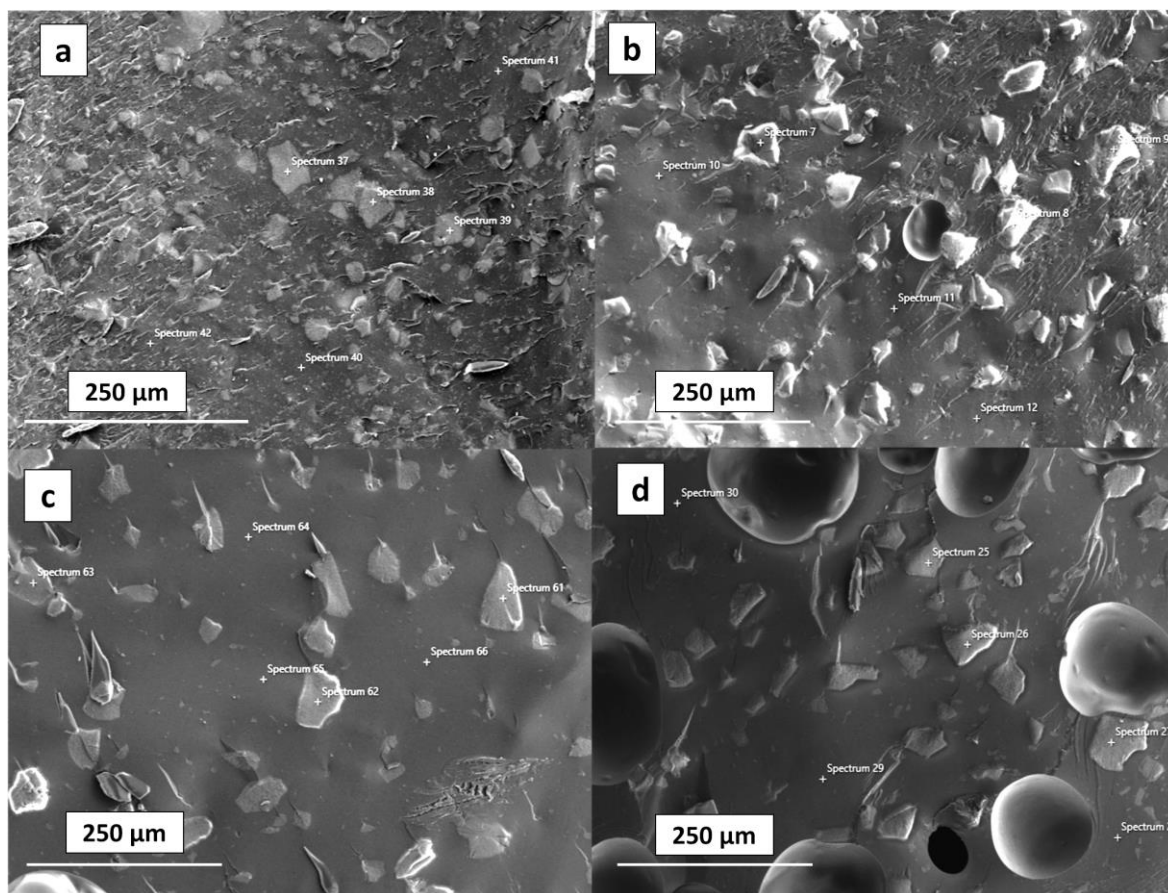


Figure 5.8: SEM images of the cross-sections of the interior structures of (a) HD1, (b) HD2, (c) HD3 and (d) HD4 form extrudates.

As seen in Figure 5.9a, PXRD diffraction patterns of HD1 shows multiple peaks of crystalline TBA, indicating rapid recrystallisation of TBA in the solid dispersions prepared by HME with Soluplus-Tween at 30% TBA loading without the use of MPS. In contrast, the freshly prepared HD2 and HD3 samples show no sign of crystalline TBA. HD4 samples displayed some diffraction peaks of crystalline TBA, but the intensity is much lower than HD1. The MTDSC results (Figure 5.9b) of placebo HD1 shows a T_g with a relaxation peak at 40 ± 1.02 °C. For HD2 and HD3 samples, no relaxation peak was detected, but only a broad T_g at 41 ± 0.6 and 35 ± 0.73 °C with no crystalline TBA melting, confirming the fully amorphous natures of the ASD. However, the DSC result of HD4 shows the T_g at 40 ± 0.6 °C, similar to HD2 and HD3, but is accompanied by a relaxation peak and a depressed crystalline TBA melting at 123 °C, indicating the presence of crystalline TBA in the matrix. The PXRD and DSC data confirmed that 30% (w/w) drug loading without the use MPS reached supersaturation in Soluplus-Tween matrix, led to rapid drug recrystallisation. The use of free TBA and MPS hosting 12%

(w/w) amorphous drug allowed the total loading of up to 35% (w/w) TBA in the ASD, with 12% in the MPS and 23% free TBA in Soluplus-Tween matrices.

When further increasing the free TBA loading in the polymer matrices to 28% (w/w) (HD4), drug recrystallisation was observed.

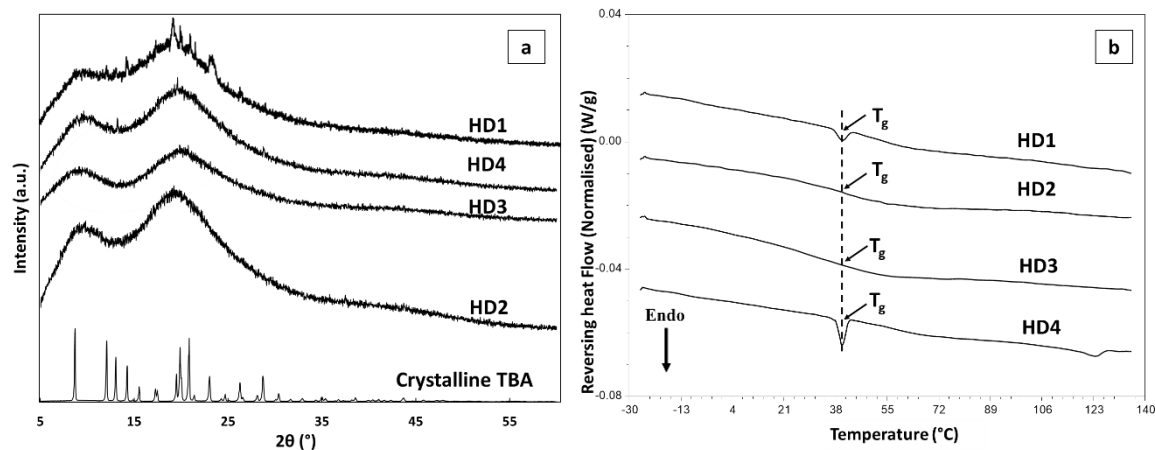


Figure 5.9: (a) PXRD patterns of freshly prepared HD1, HD2, HD3 and HD4 formulations, with crystalline TBA as reference and (b) MDSC thermograms of them.

To investigate the stability of the ASD with high drug loadings, stability studies at room temperature and 75% RH were conducted for one and three months. As seen in Figure 5.10, the PXRD results show the fully amorphous halos of HD2 and HD3 formulations after being stored 1 and 3 months. On the contrary, the halo associated with the amorphous fraction of TBA reduced and the intensity of the diffraction peaks of crystalline TBA increased with increasing the aging time from 1 month to 3 months for HD4 formulation, indicating the continuous TBA recrystallisation during aging.

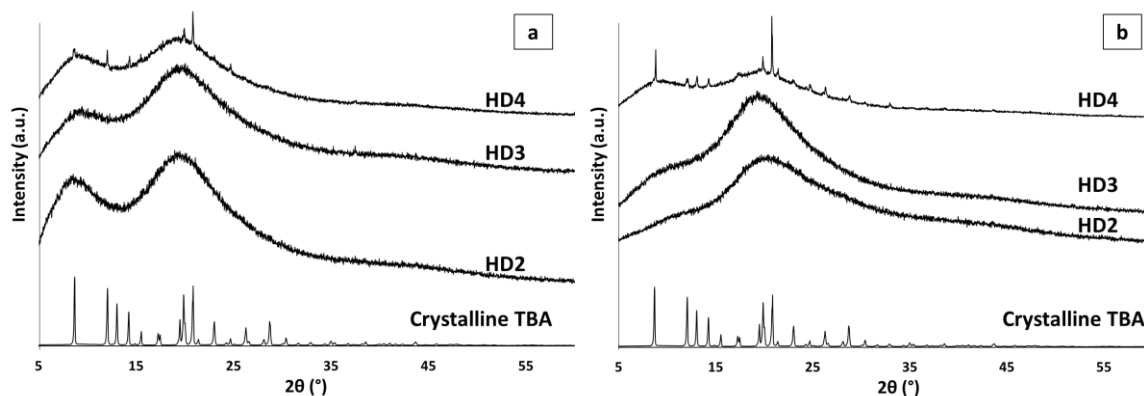


Figure 5.10: PXRD data of HD2, HD3 and HD4 aged under 75% RH for (a) 1 month and (b) 3 months.

The impact on *in vitro* drug release of ASDs containing MPS with the aim to increase the drug loading was examined. The *in vitro* drug release of the formulations in the forms of intact extrudates were first examined. As seen in Figure 5.11a, the control sample, HD1 with 30% free TBA loading but no MPS, shows a zero-order release profile with 31% drug release at 6 hours and 78% by 12 hours. This drug release rate is significantly slower than the rest of HD formulations, and is slower than the LD1 extrudates, which is the ASD formulation containing MPS with lowest drug loading (4% w/w) and which also displayed the slowest drug release rate among LD formulations. For the ASD formulations containing MPS with 12% TBA and different amounts of free TBA, higher the total drug loading resulted in faster the drug release rate... HD2 and HD3 reached 100% drug release by 10 hours, whereas HD4 reached complete drug release by 8 hours. Prior to reaching 100% drug release, near zero-order TBA release was achieved by all three formulations. The faster drug release of HD4 in comparison to HD2 and HD3 is likely to be due to the higher drug loading acting as the thermodynamic driving force of passive diffusion of the free TBA incorporated in the polymeric matrices. Although small amount of recrystallised TBA was detected in the freshly prepared HD4, the presence of surfactant, Tween 80, in the polymeric matrices may act as the solubilising enhancer of the crystalline drug during the dissolution. Collectively, if one compares the release rate of the HME extrudates with low drug loading (LD formulations) and high drug loading (HD formulations) with MPS, the differences in release rate are small with total release occurring in the 10 to 12 hour time span. However, as HD4 showed rapid drug recrystallisation, it is considered to be an unstable formulation with poor storage stability. The control sample with 30% free TBA with no MPS showed the slowest drug release rate. Therefore, it is reasonable to summarise that the HME extrudates of ASDs containing MPS-TBA can be used for controlled release of TBA with near zero-order drug release kinetics that is only weakly dependent on the drug loading.

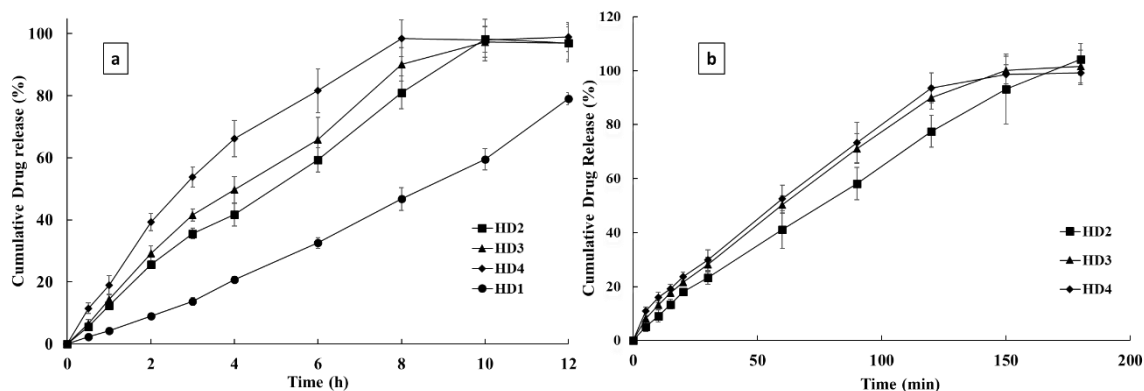


Figure 5.11: The *in vitro* drug release of freshly prepared HD2, HD3 and HD4 formulations in pH 6.8 PBS a) being tested as intact HME extrudates and b) being tested as hard gelatine capsules filled with milled extrudates.

It is well known that the dimensions of the ASDs may affect the drug release behaviour of the formulations [242, 243]. In order to explore the impacts of particle size reduction on the drug release kinetics of the MPS loaded formulations with high drug loading, the HD formulations were milled into powder form and filled in hard gelatine capsules. As seen Figure 5.11b, the 100% drug release was achieved within 3 hours for HD2, HD3 and HD4. No significant difference in drug release rate was observed between the three ASDs with MPS-TBA. Again, this result confirms that using MPS as an amorphous host to increase the overall drug loading can lead to formulations with drug release kinetics that is only weakly dependent on the drug loading. The biggest advantage of this is allowing the rapid development of solid dosage forms using a single template formulation with a fixed drug release kinetics but with a range of dosages for patients with different dose requirement.

5.4 Conclusion

This study explored the use of MPS as a functional excipient to increase the overall drug loading for forming stable amorphous solid dispersions of poorly soluble drug for not only improving apparent drug dissolution but also maintain the supersaturation data during controlled drug release. The saturated drug loading of TBA in MPS was confirmed as being approximately 20% (w/w). The TBA loaded MPS showed improved dissolution rate in comparison to crystalline TBA. The MPSs pre-loaded with a range of low quantities of TBA, between 4-16% (w/w), were further incorporated into Soluplus-Tween matrices via HME. Free TBA was detected in the LD formulations with 16% TBA pre-loaded in MPS, indicating drug leakage during HME from MPS into the polymeric matrices. Thus, the MPS pre-loaded with 12% (w/w) TBA was further studied for their

capabilities to produce ASDs with high drug loading. The MPS-TBA was used with free TBA in the ASDs with high drug loadings. The results confirmed that without MPS, the ASDs with 30% drug loading was unstable with rapid drug recrystallisation, whereas with MPS-TBA the total drug loading can be increased to 35% with no stability issues. More importantly, not only controlled release kinetics was achieved with MPS-TBA containing formulations, but it was also observed that the drug release rate of the MPS containing ASDs is independent of the drug loading. This will enable rapid product development using a single formulation template to produce a product line with a range of strengths of targeted API.

Conclusion and Future Outlook

Chapter 6

6.1 General Conclusion

Overall, this thesis provides an understanding of the use of functional additives as an advantageous part in ASD prepared via HME processing. It has four primary focuses: drug release rate, internal microstructure, physical stability and performance of formulations.

6.1.1 Using functional additives as strategy to manipulate drug release from hot melt extruded solid dispersions

This study proposed the use of HME as a single-step and solvent-free technique to directly manufacture controlled release oral formulations. The selected polymer (HPMCAS-LF) showed great potential as a matrix excipient for monolithic controlled release formulations. As shown in Chapter 3, the DSC results confirmed the formation of molecular dispersion of 20 % CBZ –HPMCAS, as well as PXRD with the amorphous nature of the binary extrudate. The CBZ-HPMCAS binary extrudates demonstrated zero-order controlled release of CBZ over 24 hours. The intermolecular interactions (most likely to be either van der Waals or hydrophobic interactions not detected by IR) between CBZ and HPMCAS and the microenvironments are responsible for the sustained release of CBZ. Also, another reason for sustained release is the polymer matrix itself, which acts as a diffusion barrier, hence delaying the diffusion of the drug. To accelerate the complete drug release from the extrudates from 24 hours to 12 hours, several additives (CNa, NaSG, CP, MD and LM) with 5% (w/w) loading were mixed into the formulation during HME. Furthermore, DSC and PXRD show the amorphous nature of all the ternary extrudates. ATR-FTIR results confirm that the addition of additives had no effect on the intermolecular interaction between CBZ and HPMCAS. Regarding the release profile, all ternary extrudates demonstrate a faster drug release rate than CBZ-HPMCAS binary formulation due to the existence of internal porosity, which led to rapid water penetration, matrix erosion and breakdown.

As a result of interior porosity, formulations containing CNa, NaSG, LM and MD follow zero order release kinetics and super case II transport, which led to quicker erosion and rapid drug release. In addition, the release rate of the HME extrudates could be sustained further by incorporating lipid excipient (Gelucire 50/13) during the HME process. The DSC data show the melting point of Gelucire, beside the crystalline peaks in PXRD,

indicating that Gelucire remains phase-separated from the polymeric matrix. Except for the HG-LM, all samples containing Gelucire have zero-order kinetics and are slower to release than samples without Gelucire. In contrast to the ternary extrudates without Gelucire, the dissolution behaviour of Gelucire containing extrudates involved continuous swelling and gel formation at similar rates. In addition, SEM images of Gelucire containing extrudates shows a less internal porosity than samples without Gelucire. The gel-forming ability of Gelucire, which is also phase-separated in the extrudates, allowed for the substantial swelling of the extrudates and the further prolongation of drug release. UV imaging was able to provide a direct visualisation and a deeper understanding of the simultaneous drug release and swelling/erosion phenomena. This study details clear formulation strategies for modulating the drug release rate from controlled release formulation prepared directly by HME, as represented in Figure 6.1.

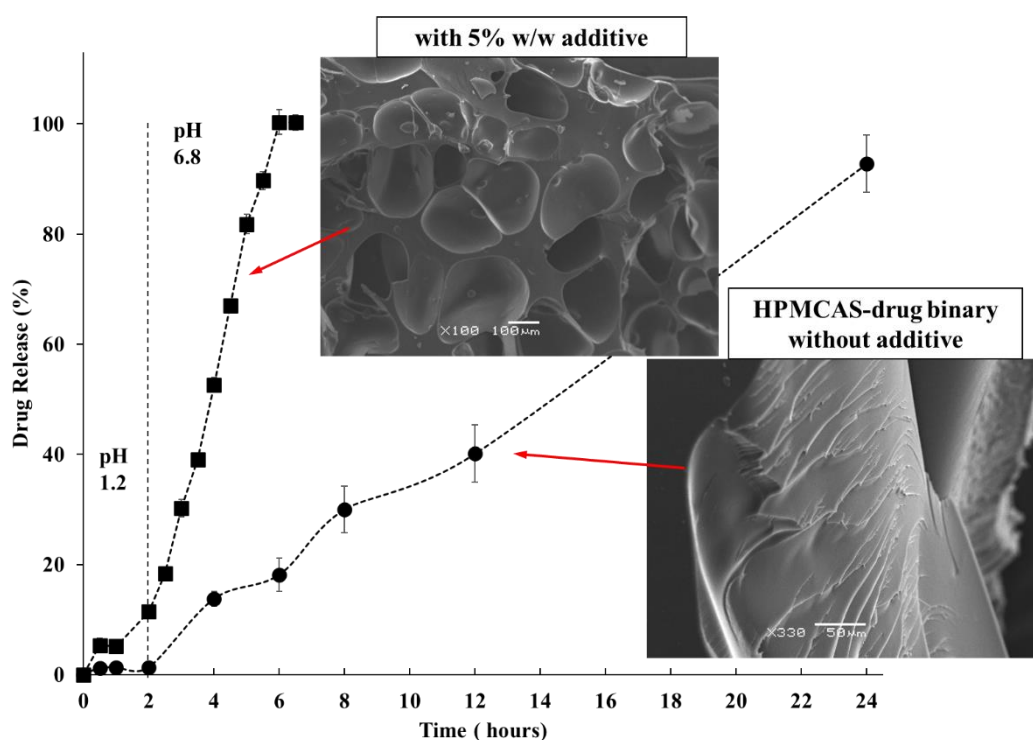


Figure 6.1: An illustration showing the potential of using functional additives to control drug release from HME formulations.

6.1.2 Investigating the parameters that control and adjust void formations

This study made a detailed investigation into the factors that affect the formation of the voids using lab-scale hot melt extruders. These factors include the types of materials (i.e. drug, polymer and additive) used in the formulation, the quantity of the drug and the additives used, the key extrusion processing parameters, the type of extruder and the drying of raw materials prior to extrusion. As shown in Chapter 4, both SEM and X μ CT results confirmed that the additive particles are mostly located at the surface of the voids and that the voids are not interconnected, which indicates that the co-existence of the drug and the additives are essential for the formation of the voids inside the extrudates. There is no clear correlation between moisture content and void diameter. Hence, this indicates that the moisture content of the additives is not the sole cause of the formation of the voids. However, there is a clear reduction in void size and density when the raw materials of the additives were dried for six hours at 105 °C.

Furthermore, additives particles generate some voids. It is likely that they act as nuclei for dissolved air. These gas bubbles are entrapped, meaning they cannot escape, due to the high viscosity of the mix. Thus, they remain as voids that can be observed in the extrudates after cooling. In terms of viscosity, both polymer type and drug loading may affect the viscosity of the molten mixture in the extruder. Both may also affect cavity formation by changing the viscosity. If the viscosity is too high, bubbles will not grow, whereas if it is too low, bubbles will burst or escape to the surface. By increasing the drug load from 20% to 50% w/w, the density of the voids and the diameter of the extrudates increase. Gelucire is a lipid-based additive that acts as a ‘lubricant’ of the molten mixture and reduces the overall melt viscosity of the system in the extrusion. As shown in Chapter 4, Gelucire accelerates the escape/collapse of entrapped gas bubbles and coats the additive particles, leading to a reduced number of nucleus sites and smaller voids. The study confirms that void formation is not drug- or polymer-specific, and the presence of phase-separated solid particulates is essential for void-forming.

According to screw speed data, faster screw rotation could cause the deformation of the void’s shape and break a large void into smaller voids. Drug release results demonstrate that high relative void volume leads to faster dissolution. The changes in release rates due to changes in screw speed and additive particle loading were less dramatic than the effects

of changes in drug loading that reflect smaller changes in relative void volume. Therefore, in order to minimise void formation, the results of this study indicate that low moisture content of the raw materials, low proportion of particulates and the addition of lubricants, such as low melting lipid excipients, could be beneficial. Slow screw speed is also preferred to reduce the formation of the voids. This study systematically reported the mechanism of void formation in HME extrudates and generated new insights into the parameters that control and adjust void formation and manipulate drug release, as shown in Figure 6.2.

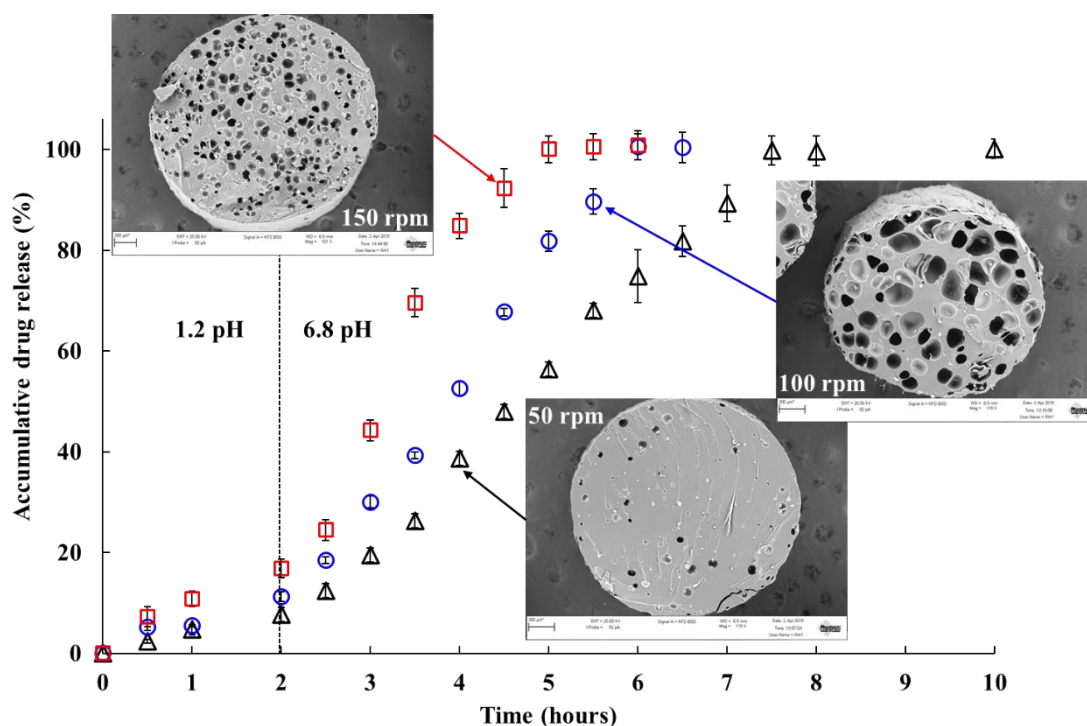


Figure 6.2: A graphic illustration showing the impact of internal microstructure on the drug release of HME solid dispersion.

6.1.3 Using mesoporous silica to improve the stability of amorphous solid dispersion with high drug loading

As shown in Chapter 5, four different proportions of crystalline TBA melted in the presence of MPS as a loading method into the mesopore to investigate the MPS loading capacity of TBA. The elemental analysis results of TBA20 confirmed the complete absence of sulphur, which is typically used as a marker for the presence of TBA on the surfaces of the TBA loaded MPS particles. However, a low quantity of sulphur was detected at the surfaces of TBA40, TBA60 and TBA80. Moreover, PXRD confirmed that TBA20 is fully amorphous, but detectable amounts of crystalline TBA were found in TBA 40, TBA60 and TBA80 formulations. Therefore, at a drug loading of between 20 and 40% w/w, the inner surfaces of the mesopores within MPS particles are fully saturated with the adsorbed TBA molecules. This led to the surface adsorption of the TBA that was detected in TBA40, TBA60 and TBA80. Moreover, the MTDSC were used to quantify the loading of TBA in the mesopores of MPS by measuring the T_g of the amorphous TBA in TBA20-80 samples. The results showed that 17%, 22% and 26% (w/w) of the loaded TBA were within the mesopores in TBA40, TBA60 and TBA80, respectively. This largely agrees with the idea that the mesopore loading limit of TBA is between 20–40% w/w. In terms of drug release results, there was an improvement in TBA release rate in all formulations compared to crystalline TBA. The rapid drug release observed is likely due to the complete molecular adsorption within the pores of MPS, the amorphous phase and the high surface area of MPS particles.

The LD1-4 formulations were extruded with different proportion of TBA being pre-loaded into MPS to investigate the effects of a polymeric matrix on the physical stability and the in-vitro drug release performance of the formulations. Elemental analysis was conducted with SEM to confirm the TBA leakage from the MPS into the polymer matrix after HME. A sulphur peak from TBA was absent from the elemental analysis performed on both MPS particles embedded in the Soluplus–Tween matrix and the polymer areas free from MPS particles for LD1 and LD2 formulations. For LD3 and LD4, the sulphur sign was present. This indicates that TBA did not leak from MPS into the polymeric matrices during the HME process in LD1 and LD2 formulations, but did leak in LD3 and LD4 formulations. LD3 and LD4 have higher drug loads than LD1 and LD2, which may have contributed to the observed TBA leakages. PXRD confirmed that no crystalline TBA was detected for all LD formulations. DSC results showed the depression of T_g in

LD4 in comparison to a placebo as an indication of TBA leakage, which concurs with prior elemental analysis of TBA leakage into the matrix. LD1-4 formulations all achieved nearly zero-order controlled release of TBA over 12 hours. LD4 shows a slightly faster release rate than the rest of the formulations and reached 100% after ten hours. Therefore, it is reasonable to conclude that when most drug molecules are hosted in MPS, the drug release rate is independent to the drug loading.

This study investigated increasing the overall drug loading and stability enhancement. It was hypothesised that the hybrid nature of the matrix, which makes it capable of stabilising the amorphous drugs, mesopores and drug solubility in the polymer, could improve the stabilisation of high drug loaded formulation, as represented in Figure 6.3. As shown in Chapter 5, the SEM images of the cross-sections of the HD1-4 extrudates clearly show the MPS particles embedded and dispersed in the polymeric matrix. Air pockets 100–200 μm in diameter can be clearly seen in HD4 due to high drug loading, with an un-dissolved particulate drug within the extrudates. PXRD diffraction patterns of HD1 and HD4 show some diffraction peaks of crystalline TBA, indicating rapid recrystallisation of TBA in the solid dispersions. In contrast, the freshly prepared HD2 and HD3 samples show no sign of crystalline TBA. MTDSC confirmed the fully amorphous natures of HD2 and HD3. Therefore, PXRD and DSC data confirmed that 30% (w/w) drug loading without MPS reached supersaturation in the Soluplus–Tween matrix, which led to rapid drug recrystallisation. The use of the free TBA and MPS hosting 12% (w/w) amorphous drug allowed for a total loading of up to 35% (w/w) TBA in the ASD, 12% in the MPS and 23% free TBA in Soluplus–Tween matrices. In terms of stability, PXRD results show the fully amorphous halos of HD2 and HD3 formulations after being stored for 1–3 months following stressed stability test. On the contrary, the halo associated with the amorphous fraction of TBA reduced and the intensity of the diffraction peaks of crystalline TBA increased with age from one month to three months for the HD4 formulation. This proves the continuous TBA recrystallisation during aging. The HD2-4 formulation reached 100%, whereas HD1 reached 78% drug release by 12 hours.

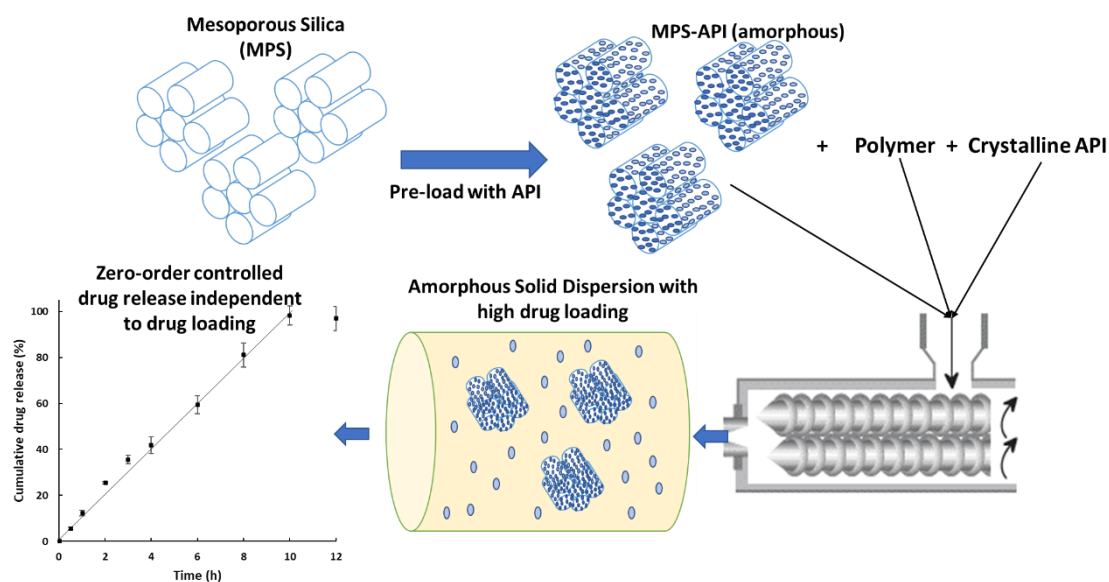


Figure 6.3: schematic illustration of using MPS to produce ASD with high drug loading.

6.2 Future outlook

Considering the results obtained in this thesis, it would be important to explore further several areas. It is recommended to expand the study to include a larger number of HME-based polymers or polymer blends, such as Eudragit and PVP-based polymers. This thesis explores the drug release behaviour, internal microstructure and stability needed to achieve the most promising formulation. It is also recommended to study different model drugs, including freely and poorly soluble drugs. Further studies must scale up the formulations from the lab to the industrial level. In addition, studying the effects of the particle size of the additives in the void formation may be beneficial. Conducting long-term stability monitoring (9–12 months) is highly recommended to make sure that their physicochemical properties and structures are comparable to fresh samples and not subject to change and degradation during storage and transport. Further in-vitro and in-vivo (pharmacokinetics) studies on solid dosage forms (e.g. tablets, pellets) obtained from CBZ amorphous solid dispersions could provide useful information about bioavailability improvement by comparing this to products on the market. Regarding ICH guidelines, the introduction of QbD principles is important for drug product development by controlling the quality the pharmaceutical product for the intermediate to the final stage of production. In-line NIR could be an advantageous tool for providing real-time measurements of the HME process by attaching an NIR probe to the end part of the die, which is highly sensitive to changes in H-bonding, the presence of water and chemical change in groups such as NH and OH during the extrusion process.

Bibliography

1. Hanada, M., S.V. Jermain, and R.O. Williams, *Enhanced Dissolution of a Porous Carrier-Containing Ternary Amorphous Solid Dispersion System Prepared by a Hot Melt Method*. Journal of Pharmaceutical Sciences, 2018. **107**(1): p. 362-371.
2. Stegemann, S., et al., *When poor solubility becomes an issue: from early stage to proof of concept*. European journal of pharmaceutical sciences, 2007. **31**(5): p. 249-261.
3. Amidon, G.L., et al., *A theoretical basis for a biopharmaceutical drug classification: the correlation of in vitro drug product dissolution and in vivo bioavailability*. Pharmaceutical research, 1995. **12**(3): p. 413-420.
4. Janssens, S. and G. Van den Mooter, *Review: physical chemistry of solid dispersions*. J Pharm Pharmacol, 2009. **61**(12): p. 1571-86.
5. Vo, C.L., C. Park, and B.J. Lee, *Current trends and future perspectives of solid dispersions containing poorly water-soluble drugs*. Eur J Pharm Biopharm, 2013. **85**(3 Pt B): p. 799-813.
6. Baghel, S., H. Cathcart, and N.J. O'Reilly, *Polymeric Amorphous Solid Dispersions: A Review of Amorphization, Crystallization, Stabilization, Solid-State Characterization, and Aqueous Solubilization of Biopharmaceutical Classification System Class II Drugs*. J Pharm Sci, 2016. **105**(9): p. 2527-44.
7. Rabinow, B.E., *Nanosuspensions in drug delivery*. Nature reviews. Drug discovery, 2004. **3**(9): p. 785.
8. Martena, V., et al., *Effect of four different size reduction methods on the particle size, solubility enhancement and physical stability of nicergoline nanocrystals*. Drug Development and Industrial Pharmacy, 2014. **40**(9): p. 1199-1205.
9. Berge, S.M., L.D. Bighley, and D.C. Monkhouse, *Pharmaceutical Salts*. Journal of Pharmaceutical Sciences, 1977. **66**(1): p. 1-19.
10. Stella, V.J. and K.W. Nti-Addae, *Prodrug strategies to overcome poor water solubility*. Advanced drug delivery reviews, 2007. **59**(7): p. 677-694.
11. Müller, R.H. and K. Peters, *Nanosuspensions for the formulation of poorly soluble drugs*. International Journal of Pharmaceutics, 1998. **160**(2): p. 229-237.
12. Rodríguez-Spong, B., et al., *General principles of pharmaceutical solid polymorphism: a supramolecular perspective*. Advanced drug delivery reviews, 2004. **56**(3): p. 241-274.
13. Newman, A., *Pharmaceutical amorphous solid dispersions*. 2015: John Wiley & Sons.
14. Williams, M., et al., *Hot-melt extrusion technology: optimizing drug delivery*. European Journal of Parenteral Sciences and Pharmaceutical Sciences, 2010. **15**(2): p. 61.
15. Pandi, P., et al., *Amorphous solid dispersions: An update for preparation, characterization, mechanism on bioavailability, stability, regulatory considerations and marketed products*. International Journal of Pharmaceutics, 2020. **586**: p. 119560.
16. Shah, N., et al., *Amorphous solid dispersions. Theory and practice*: Springer, 2014.
17. Lapuk, S.E., et al., *Kinetic stability of amorphous dipyridamole: A fast scanning calorimetry investigation*. International Journal of Pharmaceutics, 2020. **574**: p. 118890.
18. Hallouard, F., et al., *Solid Dispersions for Oral Administration: An Overview of the Methods for their Preparation*. Current Pharmaceutical Design, 2016. **22**(32): p. 4942-4958.
19. Chiou, W.L. and S. Riegelman, *Pharmaceutical Applications of Solid Dispersion Systems*. Journal of Pharmaceutical Sciences, 1971. **60**(9): p. 1281-1302.
20. Meng, F., U. Gala, and H. Chauhan, *Classification of solid dispersions: correlation to (i) stability and solubility (ii) preparation and characterization techniques*. Drug Dev Ind Pharm, 2015. **41**(9): p. 1401-15.
21. Goud, N.R., et al., *Fast dissolving eutectic compositions of curcumin*. Int J Pharm, 2012. **439**(1-2): p. 63-72.

22. Zajc, N., et al., *Physical properties and dissolution behaviour of nifedipine/mannitol solid dispersions prepared by hot melt method*. International Journal of Pharmaceutics, 2005. **291**(1): p. 51-58.
23. Law, D., et al., *Properties of rapidly dissolving eutectic mixtures of poly(ethylene glycol) and fenofibrate: the eutectic microstructure*. J Pharm Sci, 2003. **92**(3): p. 505-15.
24. Baird, J.A. and L.S. Taylor, *Evaluation of amorphous solid dispersion properties using thermal analysis techniques*. Adv Drug Deliv Rev, 2012. **64**(5): p. 396-421.
25. Qian, K., et al., *Drug-Rich Phases Induced by Amorphous Solid Dispersion: Arbitrary or Intentional Goal in Oral Drug Delivery?* Pharmaceutics, 2021. **13**(6): p. 889.
26. Solanki, N.G., et al., *Effects of Surfactants on Itraconazole-Hydroxypropyl Methylcellulose Acetate Succinate Solid Dispersion Prepared by Hot Melt Extrusion. II: Rheological Analysis and Extrudability Testing*. Journal of Pharmaceutical Sciences, 2019. **108**(9): p. 3063-3073.
27. Tran, P., et al., *Overview of the Manufacturing Methods of Solid Dispersion Technology for Improving the Solubility of Poorly Water-Soluble Drugs and Application to Anticancer Drugs*. Pharmaceutics, 2019. **11**(3): p. 132.
28. Kumar, V., *Solid dispersions of opioid antagonists*. 2011, Google Patents.
29. Ziaee, A., et al., *Spray drying of pharmaceuticals and biopharmaceuticals: Critical parameters and experimental process optimization approaches*. European Journal of Pharmaceutical Sciences, 2019. **127**: p. 300-318.
30. van Drooge, D.J., et al., *Characterization of the molecular distribution of drugs in glassy solid dispersions at the nano-meter scale, using differential scanning calorimetry and gravimetric water vapour sorption techniques*. Int J Pharm, 2006. **310**(1-2): p. 220-9.
31. Vishali, D.A., et al., *Spray freeze drying: Emerging applications in drug delivery*. Journal of Controlled Release, 2019. **300**: p. 93-101.
32. Hu, J., et al., *Improvement of Dissolution Rates of Poorly Water Soluble APIs Using Novel Spray Freezing into Liquid Technology*. Pharmaceutical Research, 2002. **19**(9): p. 1278-1284.
33. Hur, S. and W.D. Kim. *The electrospinning process and mechanical properties of nanofiber mats under vacuum conditions*. in *Key Engineering materials*. 2006. Trans Tech Publ.
34. Verreck, G., et al., *Preparation and characterization of nanofibers containing amorphous drug dispersions generated by electrostatic spinning*. Pharmaceutical research, 2003. **20**(5): p. 810-817.
35. Kawakami, K., *Miscibility analysis of particulate solid dispersions prepared by electrospray deposition*. International Journal of Pharmaceutics, 2012. **433**(1): p. 71-78.
36. Kaassis, A.Y., et al., *Pulsatile drug release from electrospun poly (ethylene oxide)–sodium alginate blend nanofibres*. Journal of materials chemistry B, 2014. **2**(10): p. 1400-1407.
37. El-Egakey, M.A., M. Soliva, and P. Speiser, *Hot extruded dosage forms. I. Technology and dissolution kinetics of polymeric matrices*. Pharmaceutica Acta Helvetiae, 1971. **46**(1): p. 31-52.
38. Follonier, N., E. Doelker, and E.T. Cole, *Evaluation of hot-melt extrusion as a new technique for the production of polymer-based pellets for sustained release capsules containing high loadings of freely soluble drugs*. Drug Development and Industrial Pharmacy, 1994. **20**(8): p. 1323-1339.
39. Maniruzzaman, M., et al., *A review of hot-melt extrusion: process technology to pharmaceutical products*. ISRN Pharm, 2012. **2012**: p. 436763.
40. Thiry, J., F. Krier, and B. Evrard, *A review of pharmaceutical extrusion: Critical process parameters and scaling-up*. International Journal of Pharmaceutics, 2015. **479**(1): p. 227-240.
41. Mishra, M., *Handbook of encapsulation and controlled release*. 2015: CRC Press.

42. Shah, S., et al., *Melt extrusion with poorly soluble drugs*. International journal of pharmaceutics, 2013. **453**(1): p. 233-252.
43. Patil, H., R.V. Tiwari, and M.A. Repka, *Hot-Melt Extrusion: from Theory to Application in Pharmaceutical Formulation*. AAPS PharmSciTech, 2016. **17**(1): p. 20-42.
44. Repka, M.A., N. Langley, and J. DiNunzio, *Melt extrusion*. Materials, Technology and Drug Product Design, 2013. **4**: p. 5.
45. Crowley, M.M., et al., *Pharmaceutical applications of hot-melt extrusion: part I*. Drug Dev Ind Pharm, 2007. **33**(9): p. 909-26.
46. Ghebre-Sellassie, I., et al., *Pharmaceutical extrusion technology*. 2003: CRC Press.
47. Jani, R. and D. Patel, *Hot melt extrusion: An industrially feasible approach for casting orodispersible film*. asian journal of pharmaceutical sciences, 2015. **10**(4): p. 292-305.
48. Lang, B., J.W. McGinity, and R.O. Williams III, *Hot-melt extrusion—basic principles and pharmaceutical applications*. Drug development and industrial pharmacy, 2014. **40**(9): p. 1133-1155.
49. Repka, M.A., et al., *Pharmaceutical applications of hot-melt extrusion: Part II*. Drug Dev Ind Pharm, 2007. **33**(10): p. 1043-57.
50. Tran, P.H.L., B.-J. Lee, and T.T.D. Tran, *Recent studies on the processes and formulation impacts in the development of solid dispersions by hot-melt extrusion*. European Journal of Pharmaceutics and Biopharmaceutics, 2021. **164**: p. 13-19.
51. Douroumis, D., *Hot-melt extrusion: Pharmaceutical applications*. 2012: John Wiley & Sons.
52. Zhu, Y., et al., *Controlled release of a poorly water-soluble drug from hot-melt extrudates containing acrylic polymers*. Drug Dev Ind Pharm, 2006. **32**(5): p. 569-83.
53. Bruce, C., et al., *Crystal growth formation in melt extrudates*. Int J Pharm, 2007. **341**(1-2): p. 162-72.
54. Ozguney, I., D. Shuwisitkul, and R. Bodmeier, *Development and characterization of extended release Kollidon SR mini-matrices prepared by hot-melt extrusion*. Eur J Pharm Biopharm, 2009. **73**(1): p. 140-5.
55. Aharoni, S.M., *Increased glass transition temperature in motionally constrained semicrystalline polymers*. Polymers for Advanced Technologies, 1998. **9**(3): p. 169-201.
56. Zhu, Y., K.A. Mehta, and J.W. McGinity, *Influence of Plasticizer Level on the Drug Release from Sustained Release Film Coated and Hot-Melt Extruded Dosage Forms*. Pharmaceutical Development and Technology, 2006. **11**(3): p. 285-294.
57. Ghebremeskel, A.N., C. Vemavarapu, and M. Lodaya, *Use of surfactants as plasticizers in preparing solid dispersions of poorly soluble API: Selection of polymer–surfactant combinations using solubility parameters and testing the processability*. International Journal of Pharmaceutics, 2007. **328**(2): p. 119-129.
58. Shah, N., et al., *Amorphous solid dispersions*. Advances in Delivery Science and Technology, Springer, 2014.
59. Melocchi, A., et al., *Evaluation of Hot-Melt Extrusion and Injection Molding for Continuous Manufacturing of Immediate-Release Tablets*. Journal of Pharmaceutical Sciences, 2015. **104**(6): p. 1971-1980.
60. Puri, V., et al., *Development of Maltodextrin-Based Immediate-Release Tablets Using an Integrated Twin-Screw Hot-Melt Extrusion and Injection-Molding Continuous Manufacturing Process*. Journal of Pharmaceutical Sciences, 2017. **106**(11): p. 3328-3336.
61. Bhagurkar, A.M., et al., *Development of an ointment formulation using hot-melt extrusion technology*. AAPS PharmSciTech, 2016. **17**(1): p. 158-166.
62. Mendonsa, N.S., et al., *Development of poloxamer gel formulations via hot-melt extrusion technology*. International journal of pharmaceutics, 2018. **537**(1-2): p. 122-131.
63. Thommes, M., et al., *Improvement of the dissolution rate of poorly soluble drugs by solid crystal suspensions*. Molecular pharmaceutics, 2011. **8**(3): p. 727-735.

64. Liu, X., et al., *Improving the chemical stability of amorphous solid dispersion with cocrystal technique by hot melt extrusion*. *Pharmaceutical research*, 2012. **29**(3): p. 806-817.
65. Sherry, R., *Granules comprising a NSAID and a sugar alcohol made by melt extrusion*. 2007, Google Patents.
66. Sun, Y., et al., *Nimodipine semi-solid capsules containing solid dispersion for improving dissolution*. *International journal of pharmaceutics*, 2008. **359**(1-2): p. 144-149.
67. Fan, W., et al., *The Preparation of Curcumin Sustained-Release Solid Dispersion by Hot-Melt Extrusion—II. Optimization of Preparation Process and Evaluation In Vitro and In Vivo*. *Journal of Pharmaceutical Sciences*, 2020. **109**(3): p. 1253-1260.
68. Alshetaili, A., et al., *Development and Characterization of Sustained-Released Donepezil Hydrochloride Solid Dispersions Using Hot Melt Extrusion Technology*. *Pharmaceutics*, 2021. **13**(2): p. 213.
69. Ijaz, Q.A., et al., *Preparation and Characterization of pH-Independent Sustained-Release Tablets Containing Hot Melt Extruded Solid Dispersions of Clarithromycin*. *AAPS PharmSciTech*, 2021. **22**(8): p. 275.
70. Maniruzzaman, M., et al., *Novel Controlled Release Polymer-Lipid Formulations Processed by Hot Melt Extrusion*. *AAPS PharmSciTech*, 2016. **17**(1): p. 191-199.
71. Kapote, D.N. and K.G. Wagner, *Shellac- a natural carrier for colon targeting of indomethacin using hot melt extrusion*. *Drug Development and Industrial Pharmacy*, 2021. **47**(5): p. 748-757.
72. Vo, A.Q., et al., *Continuous Manufacturing of Ketoprofen Delayed Release Pellets Using Melt Extrusion Technology: Application of QbD Design Space, Inline Near Infrared, and Inline Pellet Size Analysis*. *Journal of Pharmaceutical Sciences*, 2020. **109**(12): p. 3598-3607.
73. Dierickx, L., et al., *Co-extrusion as manufacturing technique for fixed-dose combination mini-matrices*. *European Journal of Pharmaceutics and Biopharmaceutics*, 2012. **81**(3): p. 683-689.
74. Sarode, A.L., et al., *Stability assessment of hypromellose acetate succinate (HPMCAS) NF for application in hot melt extrusion (HME)*. *Carbohydrate Polymers*, 2014. **101**: p. 146-153.
75. Alqahtani, F., et al., *An investigation into the use of low quantities of functional additives to control drug release from hot melt extruded solid dispersions for poorly soluble drug delivery*. *International Journal of Pharmaceutics*, 2020. **579**: p. 119172.
76. Pimparade, M.B., et al., *Development of taste masked caffeine citrate formulations utilizing hot melt extrusion technology and in vitro–in vivo evaluations*. *International journal of pharmaceutics*, 2015. **487**(1-2): p. 167-176.
77. Yang, K., R. Glemza, and C. Jarowski, *Effects of amorphous silicon dioxides on drug dissolution*. *Journal of pharmaceutical sciences*, 1979. **68**(5): p. 560-565.
78. Monkhouse, D.C. and J.L. Lach, *Use of adsorbents in enhancement of drug dissolution II*. *Journal of pharmaceutical sciences*, 1972. **61**(9): p. 1435-1441.
79. Takeuchi, H., et al., *Solid dispersion particles of amorphous indomethacin with fine porous silica particles by using spray-drying method*. *International Journal of Pharmaceutics*, 2005. **293**(1-2): p. 155-164.
80. Genina, N., B. Hadi, and K. Löbmann, *Hot Melt Extrusion as Solvent-Free Technique for a Continuous Manufacturing of Drug-Loaded Mesoporous Silica*. *Journal of Pharmaceutical Sciences*, 2018. **107**(1): p. 149-155.
81. Limnell, T., et al., *Physicochemical stability of high indomethacin payload ordered mesoporous silica MCM-41 and SBA-15 microparticles*. *International journal of pharmaceutics*, 2011. **416**(1): p. 242-251.
82. Solomon, S., J. Iqbal, and A.B. Albadarin, *Insights into the ameliorating ability of mesoporous silica in modulating drug release in ternary amorphous solid dispersion prepared by hot melt extrusion*. *European Journal of Pharmaceutics and Biopharmaceutics*, 2021. **165**: p. 244-258.

83. Baumgartner, A. and O. Planinšek, *Application of commercially available mesoporous silica for drug dissolution enhancement in oral drug delivery*. European Journal of Pharmaceutical Sciences, 2021. **167**: p. 106015.
84. Maleki, A., et al., *Mesoporous silica materials: From physico-chemical properties to enhanced dissolution of poorly water-soluble drugs*. Journal of Controlled Release, 2017. **262**: p. 329-347.
85. Mellaerts, R., et al., *Increasing the oral bioavailability of the poorly water soluble drug itraconazole with ordered mesoporous silica*. European Journal of Pharmaceutics and Biopharmaceutics, 2008. **69**(1): p. 223-230.
86. Kinnari, P., et al., *Comparison of mesoporous silicon and non-ordered mesoporous silica materials as drug carriers for itraconazole*. International journal of pharmaceutics, 2011. **414**(1-2): p. 148-156.
87. Poostforooshan, J., et al., *Aerosol-Assisted Synthesis of Tailor-Made Hollow Mesoporous Silica Microspheres for Controlled Release of Antibacterial and Anticancer Agents*. ACS Applied Materials & Interfaces, 2020. **12**(6): p. 6885-6898.
88. Zheng, J., et al., *pH-sensitive poly (glutamic acid) grafted mesoporous silica nanoparticles for drug delivery*. International journal of pharmaceutics, 2013. **450**(1-2): p. 296-303.
89. Sun, Y., et al., *Nanoassemblies constructed from mesoporous silica nanoparticles and surface-coated multilayer polyelectrolytes for controlled drug delivery*. Microporous and mesoporous materials, 2014. **185**: p. 245-253.
90. Moritz, M. and M. Łaniecki, *Application of SBA-15 mesoporous material as the carrier for drug formulation systems. Papaverine hydrochloride adsorption and release study*. Powder technology, 2012. **230**: p. 106-111.
91. Park, S.-Y. and P. Pendleton, *Mesoporous silica SBA-15 for natural antimicrobial delivery*. Powder technology, 2012. **223**: p. 77-82.
92. Tang, Q., et al., *Drug delivery from hydrophobic-modified mesoporous silicas: control via modification level and site-selective modification*. Journal of Solid State Chemistry, 2010. **183**(1): p. 76-83.
93. Kovačič, B., F. Vrečer, and O. Planinšek, *Solid dispersions of carvedilol with porous silica*. Chemical and Pharmaceutical Bulletin, 2011. **59**(4): p. 427-433.
94. Howland, R.D., et al., *Lippincott's illustrated reviews: Pharmacology*. 2006: Lippincott Williams & Wilkins Philadelphia.
95. Steffens, K.E. and K.G. Wagner, *Dissolution enhancement of carbamazepine using twin-screw melt granulation*. European Journal of Pharmaceutics and Biopharmaceutics, 2020. **148**: p. 77-87.
96. Sathisaran, I. and S.V. Dalvi, *Investigating cocrystallization of carbamazepine with structurally compatible cofomers: new cocrystal and eutectic phases with enhanced dissolution*. AAPS PharmSciTech, 2021. **22**(1): p. 1-14.
97. Abou-Taleb, H.A., Z. Fathalla, and H. Abdelkader, *Comparative studies of the effects of novel excipients amino acids with cyclodextrins on enhancement of dissolution and oral bioavailability of the non-ionizable drug carbamazepine*. European Journal of Pharmaceutical Sciences, 2020. **155**: p. 105562.
98. Alshahrani, S.M., et al., *Stability-enhanced hot-melt extruded amorphous solid dispersions via combinations of Soluplus(R) and HPMCAS-HF*. AAPS PharmSciTech, 2015. **16**(4): p. 824-34.
99. Dołęga, A., P.M. Zieliński, and N. Osiecka-Drewniak, *New Insight Into Thermodynamical Stability of Carbamazepine*. Journal of Pharmaceutical Sciences, 2019. **108**(8): p. 2654-2660.
100. Grzesiak, A.L., et al., *Comparison of the Four Anhydrous Polymorphs of Carbamazepine and the Crystal Structure of Form I**Supplementary material: X-ray crystallographic information file (CIF) of triclinic CBZ (form I) is available*. Journal of Pharmaceutical Sciences, 2003. **92**(11): p. 2260-2271.

101. Liu, W., L. Dang, and H. Wei, *Thermal, phase transition, and thermal kinetics studies of carbamazepine*. Journal of thermal analysis and calorimetry, 2013. **111**(3): p. 1999-2004.
102. Bertoni, S., B. Albertini, and N. Passerini, *Different BCS Class II Drug-Gelucire Solid Dispersions Prepared by Spray Congealing: Evaluation of Solid State Properties and In Vitro Performances*. Pharmaceutics, 2020. **12**(6): p. 548.
103. McGinityx, J.W., P. Maincent, and H. Steinfink, *Crystallinity and dissolution rate of tolbutamide solid dispersions prepared by the melt method*. Journal of pharmaceutical sciences, 1984. **73**(10): p. 1441-1444.
104. Svärd, M., et al., *Thermodynamic Stability Analysis of Tolbutamide Polymorphs and Solubility in Organic Solvents*. Journal of Pharmaceutical Sciences, 2016. **105**(6): p. 1901-1906.
105. Destri, G.L., et al., *Crystal Morphologies and Polymorphs in Tolbutamide Microcrystalline Powder*. Journal of Pharmaceutical Sciences, 2013. **102**(1): p. 73-83.
106. Zeng, L., Å.C. Rasmuson, and M. Svärd, *Solubility of Two Polymorphs of Tolbutamide in n-Propanol: Comparison of Methods*. Journal of Pharmaceutical Sciences, 2020. **109**(10): p. 3021-3026.
107. Naima, Z., et al., *Interactions between carbamazepine and polyethylene glycol (PEG) 6000: characterisations of the physical, solid dispersed and eutectic mixtures*. European Journal of Pharmaceutical Sciences, 2001. **12**(4): p. 395-404.
108. Gosselin, P.M., et al., *Polymorphic properties of micronized carbamazepine produced by RESS*. International Journal of Pharmaceutics, 2003. **252**(1): p. 225-233.
109. Ng, Y.C., et al., *Stabilisation of amorphous drugs under high humidity using pharmaceutical thin films*. European Journal of Pharmaceutics and Biopharmaceutics, 2013. **84**(3): p. 555-565.
110. Deng, J., et al., *Degradation of the antiepileptic drug carbamazepine upon different UV-based advanced oxidation processes in water*. Chemical Engineering Journal, 2013. **222**: p. 150-158.
111. Dannenfelser, R.-M. and S.H. Yalkowsky, *Data base of aqueous solubility for organic non-electrolytes*. Science of The Total Environment, 1991. **109-110**: p. 625-628.
112. Curatolo, W., J.A. Nightingale, and S.M. Herbig, *Utility of Hydroxypropylmethylcellulose Acetate Succinate (HPMCAS) for Initiation and Maintenance of Drug Supersaturation in the GI Milieu*. Pharmaceutical Research, 2009. **26**(6): p. 1419-1431.
113. Friesen, D.T., et al., *Hydroxypropyl Methylcellulose Acetate Succinate-Based Spray-Dried Dispersions: An Overview*. Molecular Pharmaceutics, 2008. **5**(6): p. 1003-1019.
114. Pinto, J.M.O., et al., *HPMCAS as an effective precipitation inhibitor in amorphous solid dispersions of the poorly soluble drug candesartan cilexetil*. Carbohydrate Polymers, 2018. **184**: p. 199-206.
115. Solanki, N.G., et al., *Effects of Surfactants on Itraconazole-HPMCAS Solid Dispersion Prepared by Hot-Melt Extrusion I: Miscibility and Drug Release*. Journal of Pharmaceutical Sciences, 2019. **108**(4): p. 1453-1465.
116. Ueda, K., et al., *Inhibitory Effect of Hydroxypropyl Methylcellulose Acetate Succinate on Drug Recrystallization from a Supersaturated Solution Assessed Using Nuclear Magnetic Resonance Measurements*. Molecular Pharmaceutics, 2013. **10**(10): p. 3801-3811.
117. Ueda, K., et al., *The effect of HPMCAS functional groups on drug crystallization from the supersaturated state and dissolution improvement*. International Journal of Pharmaceutics, 2014. **464**(1): p. 205-213.
118. Shamma, R.N. and M. Basha, *Soluplus®: A novel polymeric solubilizer for optimization of Carvedilol solid dispersions: Formulation design and effect of method of preparation*. Powder Technology, 2013. **237**: p. 406-414.
119. Djuris, J., et al., *Preparation of carbamazepine-Soluplus solid dispersions by hot-melt extrusion, and prediction of drug-polymer miscibility by thermodynamic model fitting*. Eur J Pharm Biopharm, 2013. **84**(1): p. 228-37.

120. Basha, M., A. Salama, and S.H. Noshi, *Soluplus® based solid dispersion as fast disintegrating tablets: a combined experimental approach for enhancing the dissolution and antiulcer efficacy of famotidine*. Drug development and industrial pharmacy, 2020. **46**(2): p. 253-263.
121. Zi, P., et al., *Solubility and bioavailability enhancement study of lopinavir solid dispersion matrixed with a polymeric surfactant-Soluplus*. European Journal of Pharmaceutical Sciences, 2019. **134**: p. 233-245.
122. Albadarin, A.B., et al., *Development of stability-enhanced ternary solid dispersions via combinations of HPMCP and Soluplus® processed by hot melt extrusion*. International journal of pharmaceutics, 2017. **532**(1): p. 603-611.
123. Anwer, M.K., et al., *Preparation of spray dried amorphous solid dispersion of diosmin in soluplus with improved hepato-reno-protective activity: In vitro anti-oxidant and in-vivo safety studies*. Journal of Drug Delivery Science and Technology, 2020. **60**: p. 102101.
124. Yang, H., et al., *Investigation of a nanosuspension stabilized by Soluplus® to improve bioavailability*. International Journal of Pharmaceutics, 2014. **477**(1): p. 88-95.
125. Rowe, R.C., P. Sheskey, and M. Quinn, *Handbook of pharmaceutical excipients*. 2009: Libros Digitales-Pharmaceutical Press.
126. Quodbach, J. and P. Kleinebudde, *Systematic classification of tablet disintegrants by water uptake and force development kinetics*. Journal of Pharmacy and Pharmacology, 2014. **66**(10): p. 1429-1438.
127. Bolhuis, G.K., K. Zuurman, and G.H.P. te Wierik, *Improvement of dissolution of poorly soluble drugs by solid deposition on a super disintegrant. II. The choice of super disintegrants and effect of granulation*. European Journal of Pharmaceutical Sciences, 1997. **5**(2): p. 63-69.
128. Desai, P.M., C.V. Liew, and P.W.S. Heng, *Understanding Disintegrant Action by Visualization*. Journal of Pharmaceutical Sciences, 2012. **101**(6): p. 2155-2164.
129. Karataş, A., N. Yüksel, and T. Baykara, *Improved solubility and dissolution rate of piroxicam using gelucire 44/14 and labrasol*. Il Farmaco, 2005. **60**(9): p. 777-782.
130. Yüksel, N., et al., *Enhanced bioavailability of piroxicam using Gelucire 44/14 and Labrasol: in vitro and in vivo evaluation*. European Journal of Pharmaceutics and Biopharmaceutics, 2003. **56**(3): p. 453-459.
131. Barker, S.A., et al., *An investigation into the structure and bioavailability of α -tocopherol dispersions in Gelucire 44/14*. Journal of Controlled Release, 2003. **91**(3): p. 477-488.
132. El-Badry, M., G. Fetih, and M. Fathy, *Improvement of solubility and dissolution rate of indomethacin by solid dispersions in Gelucire 50/13 and PEG4000*. Saudi Pharmaceutical Journal, 2009. **17**(3): p. 217-225.
133. Shinde, U.K., D.G. Suryawanshi, and P.D. Amin, *Development of Gelucire® 48/16 and TPGS Mixed Micelles and Its Pellet Formulation by Extrusion Spheronization Technique for Dissolution Rate Enhancement of Curcumin*. AAPS PharmSciTech, 2021. **22**(5): p. 182.
134. Qi, S., D. Marchaud, and D.Q. Craig, *An investigation into the mechanism of dissolution rate enhancement of poorly water-soluble drugs from spray chilled gelucire 50/13 microspheres*. Journal of pharmaceutical sciences, 2010. **99**(1): p. 262-274.
135. Real, J.P., et al., *Design of novel oral ribobendazole formulation applying melting solidification printing process (MESO-PP): An innovative solvent-free alternative method for 3D printing using a simplified concept and low temperature*. International Journal of Pharmaceutics, 2020. **587**: p. 119653.
136. Siepmann, F., et al., *Controlled drug release from Gelucire-based matrix pellets: Experiment and theory*. International Journal of Pharmaceutics, 2006. **317**(2): p. 136-143.
137. Sinchaipanid, N., V. Junyaprasert, and A. Mitrevej, *Application of hot-melt coating for controlled release of propranolol hydrochloride pellets*. Powder Technology, 2004. **141**(3): p. 203-209.

138. Banerjee, S., et al., *Lipids for Taste masking and Taste assessment in pharmaceutical formulations*. Chemistry and Physics of Lipids, 2021. **235**: p. 105031.
139. Madgulkar, A.R., M.R. Bhalekar, and R.R. Padalkar, *Formulation design and optimization of novel taste masked mouth-dissolving tablets of tramadol having adequate mechanical strength*. AAPS PharmSciTech, 2009. **10**(2): p. 574-581.
140. Tabriz, A.G., et al., *Personalised Tasted Masked Chewable 3D Printed Fruit-Chews for Paediatric Patients*. Pharmaceutics, 2021. **13**(8): p. 1301.
141. Favaro-Trindade, C.S., et al., *Encapsulation of active pharmaceutical ingredients in lipid micro/nanoparticles for oral administration by spray-cooling*. Pharmaceutics, 2021. **13**(8): p. 1186.
142. Tran, L.T.C., et al., *Erythromycin encapsulation in nanoemulsion-based delivery systems for treatment of Helicobacter pylori infection: Protection and synergy*. Biochemical and Biophysical Research Communications, 2017. **493**(1): p. 146-151.
143. Panigrahi, K.C., et al., *Gelucire: A versatile polymer for modified release drug delivery system*. Future Journal of Pharmaceutical Sciences, 2018. **4**(1): p. 102-108.
144. Mehuys, E., C. Vervaet, and J.P. Remon, *Hot-melt extruded ethylcellulose cylinders containing a HPMC–Gelucire® core for sustained drug delivery*. Journal of Controlled Release, 2004. **94**(2): p. 273-280.
145. Jiménez de los Santos, C.J., et al., *Enhancement of albendazole dissolution properties using solid dispersions with Gelucire 50/13 and PEG 15000*. Journal of Drug Delivery Science and Technology, 2017. **42**: p. 261-272.
146. Hülsmann, S., et al., *Melt extrusion – an alternative method for enhancing the dissolution rate of 17 β -estradiol hemihydrate*. European Journal of Pharmaceutics and Biopharmaceutics, 2000. **49**(3): p. 237-242.
147. Yu, J.Y., S.H. Roh, and H.J. Park, *Characterization of ferulic acid encapsulation complexes with maltodextrin and hydroxypropyl methylcellulose*. Food Hydrocolloids, 2021. **111**: p. 106390.
148. Lai, F., et al., *Formulation strategy and evaluation of nanocrystal piroxicam orally disintegrating tablets manufacturing by freeze-drying*. International Journal of Pharmaceutics, 2014. **467**(1): p. 27-33.
149. Ziyani, L. and N. Fatah, *Use of experimental designs to optimize fluidized bed granulation of maltodextrin*. Advanced Powder Technology, 2014. **25**(3): p. 1069-1075.
150. Kolter, K. and D. Flick, *Structure and Dry Binding Activity of Different Polymers, Including Kollidon® VA 64*. Drug Development and Industrial Pharmacy, 2000. **26**(11): p. 1159-1165.
151. Potes, N., J.P. Kerry, and Y.H. Roos, *Additivity of water sorption, alpha-relaxations and crystallization inhibition in lactose–maltodextrin systems*. Carbohydrate Polymers, 2012. **89**(4): p. 1050-1059.
152. Ilić, I., et al., *The compressibility and compactibility of different types of lactose*. Drug Development and Industrial Pharmacy, 2009. **35**(10): p. 1271-1280.
153. Hebbink, G.A. and B.H.J. Dickhoff, *Chapter 5 - Application of lactose in the pharmaceutical industry*, in *Lactose*, M. Paques and C. Lindner, Editors. 2019, Academic Press. p. 175-229.
154. Zhou, Q., et al., *Effect of mechanical dry particle coating on the improvement of powder flowability for lactose monohydrate: A model cohesive pharmaceutical powder*. Powder Technology, 2011. **207**(1): p. 414-421.
155. Kelly, G.M., et al., *Effect of hydrolyzed whey protein on surface morphology, water sorption, and glass transition temperature of a model infant formula*. Journal of Dairy Science, 2016. **99**(9): p. 6961-6972.
156. Franks, F. and T. Auffret, *Freeze-drying of Pharmaceuticals and Biopharmaceuticals*. 2008: royal Society of Chemistry.
157. Ando, M., et al., *Evaluation of a novel sugar coating method for moisture protective tablets*. International Journal of Pharmaceutics, 2007. **336**(2): p. 319-328.

158. Van Speybroeck, M., et al., *Ordered mesoporous silica material SBA-15: a broad-spectrum formulation platform for poorly soluble drugs*. Journal of pharmaceutical sciences, 2009. **98**(8): p. 2648-2658.
159. Azaïs, T., et al., *Solid-state NMR study of ibuprofen confined in MCM-41 material*. Chemistry of Materials, 2006. **18**(26): p. 6382-6390.
160. Bremmell, K.E. and C.A. Prestidge, *Enhancing oral bioavailability of poorly soluble drugs with mesoporous silica based systems: opportunities and challenges*. Drug development and industrial pharmacy, 2019. **45**(3): p. 349-358.
161. Waters, L.J., et al., *Enhancing the dissolution of phenylbutazone using Syloid® based mesoporous silicas for oral equine applications*. Journal of pharmaceutical analysis, 2018. **8**(3): p. 181-186.
162. Bukara, K., et al., *Ordered mesoporous silica to enhance the bioavailability of poorly water-soluble drugs: Proof of concept in man*. European Journal of Pharmaceutics and Biopharmaceutics, 2016. **108**: p. 220-225.
163. Jambhrunkar, S., et al., *Modulating in vitro release and solubility of griseofulvin using functionalized mesoporous silica nanoparticles*. Journal of Colloid and Interface Science, 2014. **434**: p. 218-225.
164. Lizoňová, D., et al., *Molecular-level insight into hot-melt loading and drug release from mesoporous silica carriers*. European Journal of Pharmaceutics and Biopharmaceutics, 2018. **130**: p. 327-335.
165. Charnay, C., et al., *Inclusion of ibuprofen in mesoporous templated silica: drug loading and release property*. European Journal of Pharmaceutics and Biopharmaceutics, 2004. **57**(3): p. 533-540.
166. Maderuelo, C., A. Zarzuelo, and J.M. Lanao, *Critical factors in the release of drugs from sustained release hydrophilic matrices*. Journal of Controlled Release, 2011. **154**(1): p. 2-19.
167. Nokhodchi, A., et al., *The Role of Oral Controlled Release Matrix Tablets in Drug Delivery Systems*. BioImpacts : BI, 2012. **2**(4): p. 175-187.
168. Bouman, J., et al., *The Development of Direct Extrusion-Injection Moulded Zein Matrices as Novel Oral Controlled Drug Delivery Systems*. Pharmaceutical Research, 2015. **32**(8): p. 2775-2786.
169. Chen, Y., et al., *Polymer-Mediated Drug Supersaturation Controlled by Drug–Polymer Interactions Persisting in an Aqueous Environment*. Molecular Pharmaceutics, 2019. **16**(1): p. 205-213.
170. Fang, Y., et al., *Eudragit L/HPMCAS blend enteric-coated lansoprazole pellets: enhanced drug stability and oral bioavailability*. AAPS PharmSciTech, 2014. **15**(3): p. 513-521.
171. Rumondor, A.C., L.A. Stanford, and L.S. Taylor, *Effects of polymer type and storage relative humidity on the kinetics of felodipine crystallization from amorphous solid dispersions*. Pharm Res, 2009. **26**(12): p. 2599-606.
172. Rumondor, A.C.F., M.J. Jackson, and L.S. Taylor, *Effects of Moisture on the Growth Rate of Felodipine Crystals in the Presence and Absence of Polymers*. Crystal Growth & Design, 2010. **10**(2): p. 747-753.
173. Helms, R.A. and D.J. Quan, *Textbook of therapeutics: drug and disease management*. 2006: Lippincott Williams & Wilkins.
174. Koda-Kimble, M.A., *Koda-Kimble and Young's applied therapeutics: the clinical use of drugs*. 2012: Lippincott Williams & Wilkins.
175. Weisler, R.H., *Carbamazepine extended-release capsules in bipolar disorder*. Neuropsychiatric Disease and Treatment, 2006. **2**(1): p. 3-11.
176. Powell, G., et al., *Immediate-release versus controlled-release carbamazepine in the treatment of epilepsy*. Cochrane Database of Systematic Reviews, 2016(12).
177. Hulse, W.L., J. Gray, and R.T. Forbes, *A discriminatory intrinsic dissolution study using UV area imaging analysis to gain additional insights into the dissolution behaviour of active pharmaceutical ingredients*. Int J Pharm, 2012. **434**(1-2): p. 133-9.

178. Ward, A., et al., *Variable-focus microscopy and UV surface dissolution imaging as complementary techniques in intrinsic dissolution rate determination*. Int J Pharm, 2017. **530**(1-2): p. 139-144.
179. Boetker, J.P., et al., *A new approach to dissolution testing by UV imaging and finite element simulations*. Pharm Res, 2013. **30**(5): p. 1328-37.
180. Pajander, J., et al., *Behaviour of HPMC compacts investigated using UV-imaging*. Int J Pharm, 2012. **427**(2): p. 345-53.
181. Asare-Addo, K., et al., *Direct imaging of the dissolution of salt forms of a carboxylic acid drug*. Int J Pharm, 2018. **551**(1-2): p. 290-299.
182. Asare-Addo, K., et al., *Effect of preparation method on the surface properties and UV imaging of indomethacin solid dispersions*. Eur J Pharm Biopharm, 2019. **137**: p. 148-163.
183. Ward, A., et al., *Development of a novel method utilising dissolution imaging for the measurement of swelling behaviour in hydrophilic matrices*. International Journal of Pharmaceutics: X, 2019. **1**: p. 100013.
184. Chen, J., et al., *Thermal and X-ray Diffraction Analysis of Lactose Polymorph*. Procedia Engineering, 2015. **102**: p. 372-378.
185. Borisover, M., M. Sela, and B. Chefetz, *Enhancement effect of water associated with natural organic matter (NOM) on organic compound–NOM interactions: A case study with carbamazepine*. Chemosphere, 2011. **82**(10): p. 1454-1460.
186. Ritger, P.L. and N.A. Peppas, *A simple equation for description of solute release II. Fickian and anomalous release from swellable devices*. Journal of Controlled Release, 1987. **5**(1): p. 37-42.
187. Peppas, N.A. and B. Narasimhan, *Mathematical models in drug delivery: How modeling has shaped the way we design new drug delivery systems*. Journal of Controlled Release, 2014. **190**: p. 75-81.
188. Korsmeyer, R.W., et al., *Mechanisms of solute release from porous hydrophilic polymers*. International Journal of Pharmaceutics, 1983. **15**(1): p. 25-35.
189. Bruschi, M.L., *5 - Mathematical models of drug release*, in *Strategies to Modify the Drug Release from Pharmaceutical Systems*, M.L. Bruschi, Editor. 2015, Woodhead Publishing. p. 63-86.
190. Siepmann, J. and N.A. Peppas, *Modeling of drug release from delivery systems based on hydroxypropyl methylcellulose (HPMC)*. Advanced Drug Delivery Reviews, 2001. **48**(2): p. 139-157.
191. Fosca, M., J.V. Rau, and V. Uskoković, *Factors influencing the drug release from calcium phosphate cements*. Bioactive Materials, 2022. **7**: p. 341-363.
192. Maity, S. and B. Sa, *Ca-carboxymethyl xanthan gum mini-matrices: Swelling, erosion and their impact on drug release mechanism*. International Journal of Biological Macromolecules, 2014. **68**: p. 78-85.
193. Adam, S.H., *The Gordon-Taylor equation. Additivity and interaction in compatible polymer blends*. Die Makromolekulare Chemie, 1988. **189**(8): p. 1941-1955.
194. Skrdla, P.J., P.D. Floyd, and P.C. Dell'Orco, *The amorphous state: first-principles derivation of the Gordon-Taylor equation for direct prediction of the glass transition temperature of mixtures; estimation of the crossover temperature of fragile glass formers; physical basis of the "Rule of 2/3"*. Physical Chemistry Chemical Physics, 2017. **19**(31): p. 20523-20532.
195. Lu, X. and R.A. Weiss, *Relationship between the glass transition temperature and the interaction parameter of miscible binary polymer blends*. Macromolecules, 1992. **25**(12): p. 3242-3246.
196. Tajarobi, F., et al., *The influence of crystallization inhibition of HPMC and HPMCAS on model substance dissolution and release in swellable matrix tablets*. Eur J Pharm Biopharm, 2011. **78**(1): p. 125-33.
197. Qi, S., D. Marchaud, and D.Q.M. Craig, *An investigation into the mechanism of dissolution rate enhancement of poorly water-soluble drugs from spray chilled gelucire 50/13 microspheres*. Journal of Pharmaceutical Sciences, 2010. **99**(1): p. 262-274.

198. Maniruzzaman, M., et al., *A review on the taste masking of bitter APIs: hot-melt extrusion (HME) evaluation*. Drug Development and Industrial Pharmacy, 2014. **40**(2): p. 145-156.
199. Snejdrova, E. and M. Dittrich, *Pharmaceutical applications of plasticized polymers*. Recent advances in plasticizers, 2012. **159**: p. 23-34.
200. Balogh, A., et al., *Plasticized Drug-Loaded Melt Electrospun Polymer Mats: Characterization, Thermal Degradation, and Release Kinetics*. Journal of Pharmaceutical Sciences, 2014. **103**(4): p. 1278-1287.
201. Maru, S.M., et al., *Characterization of thermal and rheological properties of zidovudine, lamivudine and plasticizer blends with ethyl cellulose to assess their suitability for hot melt extrusion*. European Journal of Pharmaceutical Sciences, 2011. **44**(4): p. 471-478.
202. Fukuda, M., N.A. Peppas, and J.W. McGinity, *Floating hot-melt extruded tablets for gastroretentive controlled drug release system*. Journal of Controlled Release, 2006. **115**(2): p. 121-129.
203. Deng, W., et al., *Stabilization of fenofibrate in low molecular weight hydroxypropylcellulose matrices produced by hot-melt extrusion*. Drug Dev Ind Pharm, 2013. **39**(2): p. 290-8.
204. Krupa, A., et al., *In vitro and in vivo behavior of ground tadalafil hot-melt extrudates: How the carrier material can effectively assure rapid or controlled drug release*. International Journal of Pharmaceutics, 2017. **528**(1): p. 498-510.
205. Sadia, M., et al., *Channelled tablets: An innovative approach to accelerating drug release from 3D printed tablets*. Journal of Controlled Release, 2018. **269**: p. 355-363.
206. Sadia, M., et al., *Adaptation of pharmaceutical excipients to FDM 3D printing for the fabrication of patient-tailored immediate release tablets*. International journal of pharmaceutics, 2016. **513**(1-2): p. 659-668.
207. Crowley, M.M., et al., *Physicochemical properties and mechanism of drug release from ethyl cellulose matrix tablets prepared by direct compression and hot-melt extrusion*. International Journal of Pharmaceutics, 2004. **269**(2): p. 509-522.
208. Alshafiee, M., et al., *Hot-melt extrusion process impact on polymer choice of glyburide solid dispersions: The effect of wettability and dissolution*. International Journal of Pharmaceutics, 2019. **559**: p. 245-254.
209. Martinez-Marcos, L., et al., *A novel hot-melt extrusion formulation of albendazole for increasing dissolution properties*. International Journal of Pharmaceutics, 2016. **499**(1): p. 175-185.
210. Almeida, A., et al., *Ethylene vinyl acetate as matrix for oral sustained release dosage forms produced via hot-melt extrusion*. European Journal of Pharmaceutics and Biopharmaceutics, 2011. **77**(2): p. 297-305.
211. Smirnov, B.M. and R.S. Berry, *Growth of bubbles in liquid*. Chemistry Central Journal, 2015. **9**(1): p. 48.
212. Landau, L. and E. Lifshitz, *Theoretical Physics, vol. 6, Fluid Mechanics*. 1987, Pergamon, London.
213. Parikh, T., et al., *Investigation of thermal and viscoelastic properties of polymers relevant to hot melt extrusion-III: Polymethacrylates and polymethacrylic acid based polymers*. Journal of Excipients and Food Chemicals, 2016. **5**(1): p. 1003.
214. Meena, A., et al., *Investigation of thermal and viscoelastic properties of polymers relevant to hot melt extrusion-II: cellulosic polymers*. Journal of Excipients and Food Chemicals, 2016. **5**(1): p. 1002.
215. Gupta, S.S., et al., *Investigation of thermal and viscoelastic properties of polymers relevant to hot melt extrusion-I: Polyvinylpyrrolidone and related polymers*. Journal of Excipients and Food Chemicals, 2016. **5**(1): p. 1001.
216. Caliandro, R., G. Di Profio, and O. Nicolotti, *Multivariate analysis of quaternary carbamazepine-saccharin mixtures by X-ray diffraction and infrared spectroscopy*. Journal of Pharmaceutical and Biomedical Analysis, 2013. **78-79**: p. 269-279.

217. Hann, D.B., A.V. Cherdantsev, and B.J. Azzopardi, *Study of bubbles entrapped into a gas-sheared liquid film*. International Journal of Multiphase Flow, 2018. **108**: p. 181-201.
218. Le, T.-T., et al., *Delivery of Poorly Soluble Drugs via Mesoporous Silica: Impact of Drug Overloading on Release and Thermal Profiles*. Pharmaceutics, 2019. **11**(6): p. 269.
219. Nashed, N., M. Lam, and A. Nokhodchi, *A comprehensive overview of extended release oral dosage forms manufactured through hot melt extrusion and its combination with 3D printing*. International Journal of Pharmaceutics, 2021. **596**: p. 120237.
220. Dedroog, S., C. Huygens, and G. Van den Mooter, *Chemically identical but physically different: A comparison of spray drying, hot melt extrusion and cryo-milling for the formulation of high drug loaded amorphous solid dispersions of naproxen*. European Journal of Pharmaceutics and Biopharmaceutics, 2019. **135**: p. 1-12.
221. Tian, Y., et al., *The design and development of high drug loading amorphous solid dispersion for hot-melt extrusion platform*. International Journal of Pharmaceutics, 2020. **586**: p. 119545.
222. Bhujbal, S.V., et al., *Pharmaceutical amorphous solid dispersion: A review of manufacturing strategies*. Acta Pharmaceutica Sinica B, 2021. **11**(8): p. 2505-2536.
223. Farjadian, F., et al., *Mesoporous silica nanoparticles: Synthesis, pharmaceutical applications, biodistribution, and biosafety assessment*. Chemical Engineering Journal, 2019. **359**: p. 684-705.
224. Zhang, H., et al., *Synthesis of novel mesoporous silica nanoparticles for loading and release of ibuprofen*. Journal of Controlled Release, 2011. **152**.
225. McCarthy, C.A., et al., *Mesoporous silica formulation strategies for drug dissolution enhancement: a review*. Expert opinion on drug delivery, 2016. **13**(1): p. 93-108.
226. Ditzinger, F., et al., *Opportunities for Successful Stabilization of Poor Glass-Forming Drugs: A Stability-Based Comparison of Mesoporous Silica Versus Hot Melt Extrusion Technologies*. Pharmaceutics, 2019. **11**(11): p. 577.
227. Knapik-Kowalczyk, J., et al., *Importance of Mesoporous Silica Particle Size in the Stabilization of Amorphous Pharmaceuticals-The Case of Simvastatin*. Pharmaceutics, 2020. **12**(4).
228. Hanada, M., et al., *Ternary Amorphous Solid Dispersions Containing a High-Viscosity Polymer and Mesoporous Silica Enhance Dissolution Performance*. Molecular Pharmaceutics, 2021. **18**(1): p. 198-213.
229. Brás, A.R., et al., *Influence of Nanoscale Confinement on the Molecular Mobility of Ibuprofen*. The Journal of Physical Chemistry C, 2014. **118**(25): p. 13857-13868.
230. Antonino, R.S.C.M.Q., et al., *Impact of drug loading in mesoporous silica-amorphous formulations on the physical stability of drugs with high recrystallization tendency*. International Journal of Pharmaceutics: X, 2019. **1**: p. 100026.
231. Geng, H., et al., *Hollow mesoporous silica as a high drug loading carrier for regulation insoluble drug release*. International Journal of Pharmaceutics, 2016. **510**(1): p. 184-194.
232. Wei, Q., C.M. Keck, and R.H. Müller, *Oral hesperidin—Amorphization and improved dissolution properties by controlled loading onto porous silica*. International journal of pharmaceutics, 2017. **518**(1-2): p. 253-263.
233. Tipduangta, P., et al., *The use of polymer blends to improve stability and performance of electrospun solid dispersions: The role of miscibility and phase separation*. International Journal of Pharmaceutics, 2021. **602**: p. 120637.
234. Kawakami, K., et al., *Time-dependent phase separation of amorphous solid dispersions: Implications for accelerated stability studies*. Journal of Drug Delivery Science and Technology, 2018. **46**: p. 197-206.
235. Singh, A., et al., *Effect of Compression on the Molecular Arrangement of Itraconazole–Soluplus Solid Dispersions: Induction of Liquid Crystals or Exacerbation of Phase Separation?* Molecular Pharmaceutics, 2016. **13**(6): p. 1879-1893.
236. Prinderre, P., *Mesoporous dosage forms for poorly soluble drugs*. 2018, Google Patents.

237. Thirunahari, S., et al., *Conformational Polymorphism of Tolbutamide: A Structural, Spectroscopic, and Thermodynamic Characterization of Burger's Forms I–IV*. *Journal of Pharmaceutical Sciences*, 2010. **99**(7): p. 2975-2990.
238. Hempel, N.-J., et al., *A fast and reliable DSC-based method to determine the monomolecular loading capacity of drugs with good glass-forming ability in mesoporous silica*. *International Journal of Pharmaceutics*, 2018. **544**(1): p. 153-157.
239. Mellaerts, R., et al., *Enhanced release of itraconazole from ordered mesoporous SBA-15 silica materials*. *Chemical Communications*, 2007(13): p. 1375-1377.
240. Nartowski, K.P., et al., *Nanocrystallization of Rare Tolbutamide Form V in Mesoporous MCM-41 Silica*. *Molecular Pharmaceutics*, 2018. **15**(11): p. 4926-4932.
241. Alqahtani, F., et al., *An investigation into the formations of the internal microstructures of solid dispersions prepared by hot melt extrusion*. *European Journal of Pharmaceutics and Biopharmaceutics*, 2020. **155**: p. 147-161.
242. Zhang, B., et al., *Effects of porosity on drug release kinetics of swellable and erodible porous pharmaceutical solid dosage forms fabricated by hot melt droplet deposition 3D printing*. *International Journal of Pharmaceutics*, 2021. **604**: p. 120626.
243. Chen, W., et al., *Effect of Particle Size on Drug Loading and Release Kinetics of Gefitinib-Loaded PLGA Microspheres*. *Molecular Pharmaceutics*, 2017. **14**(2): p. 459-467.